In vivo analysis of the mitochondrial protein frataxin in *Drosophila melanogaster*

DISSERTATION ZUR ERLANGUNG
DES DOKTORGRADES DER NATURWISSENSCHAFTEN (DR. RER. NAT.)
DER FAKULTÄT FÜR BIOLOGIE UND VORKLINISCHE MEDIZIN
DER UNIVERSITÄT REGENSBURG

vorgelegt von
Oliver Manfred Edenharter
aus Burglengenfeld
im Jahr 2017

Das Promotionsgesuch wurde eingereicht am:

Die Arbeit wurde angeleitet von:
Prof. Dr. Stephan Schneuwly

Unterschrift:

Table of contents

Abstract

Friedreich's ataxia is the most common recessive ataxia in the Caucasian population. It is caused by a defect in the expression of the mitochondrial protein frataxin and leads to neurodegeneration. The main role of frataxin lies in iron-sulphur cluster biosynthesis and loss of the protein results in mitochondrial iron accumulation and diminished energy production within the cell. Although mitochondrial function is severely affected, little is known about the influence of frataxin deficiency on mitochondrial dynamics and homeostasis.

In this work, I utilized previously established *Drosophila melanogaster* RNAi models of Friedreich's ataxia. To unravel the effects of frataxin depletion on the mitochondrial network, I focused on glia and muscle tissue, since these RNAi lines are not very efficient in neurons. I could show that mitochondrial morphology is disturbed, in agreement with the compromised membrane potential and energy production. Through the use of autophagy markers like p62, GFP-Atg8a and the newly established mtRosella, I performed a detailed analysis of mitochondrial degradation in frataxin deficient flies. I could demonstrate that damaged mitochondria are successfully targeted for degradation via mitophagy and promoting autophagy slightly improves Friedreich's ataxia phenotypes.

To analyse potential genetic interactions between frataxin and genes involved in mitochondrial homeostasis, I carried out a forward genetic screen. This screen identified knockdown of Marf, the *Drosophila* homologue of Mitofusin, as a suppressor of Friedreich's ataxia phenotypes in glia. Since Marf has been described to play a pivotal role in mitochondrial fusion, mitophagy and the interface between mitochondria and the ER, I examined how Marf silencing affects all three pathways in a frataxin deficient background. Interestingly, I could show that loss of frataxin triggers the ER stress response and identified ER stress as a key factor in the disease. Whereas mitochondrial morphology and degradation were unaffected by Marf silencing, it suppressed ER stress in frataxin-deficient cells and this was sufficient to improve locomotion, brain degeneration and lipid dyshomeostasis. Furthermore, application of the chemical TUDCA, a known attenuator of ER stress, was also able to partially rescue Friedreich's ataxia phenotypes.

These results suggest that the protection mediated by Marf knockdown is linked to its role in mitochondrial-ER contacts instead of mitochondrial fusion or degradation. Furthermore, ER stress appears to play a crucial role in the aetiology of the disease.

1. Introduction

1.1. Friedreich's ataxia

Friedreich's ataxia (FRDA) is a recessive neurodegenerative disorder that was first described by Nikolaus Friedreich in the 19th century (Friedreich, 1863) and is the most common hereditary ataxia in the Caucasian population (Cossee et al, 1997).

The disease commonly manifests at adolescence and progresses with age (Harding, 1981). Based on available data from studies in several European countries, prevalence in Europe occurs in a gradient from southwest (Spain) to northeast (Scandinavia), ranging from 1:20.000 to 1:250.000 (Vankan, 2013).

FRDA patients show several typical symptoms that can be categorized into neurological and non-neurological. Neurological symptoms include: gait ataxia; severe proprioceptive and superficial sensory loss; weakness and atrophy of the extremities; loss of muscle tone or spasticity; depressed reflexes; visual loss and hearing deficit. All patients require wheelchairs eventually. The following hallmarks comprise the neuropathology: degeneration of large sensory neurons in dorsal root ganglia; progressive degeneration of pyramidal tracts; major lesions in the dentate nucleus and demyelination of nerve fibers (Koeppen & Mazurkiewicz, 2013).

The most important non-neurological symptom is hypertrophic cardiomyopathy. Indeed, heart failure is the main cause of death among patients (Dürr et al, 1996). In addition, about 25% of patients also suffer from diabetes mellitus (Filla et al, 1996).

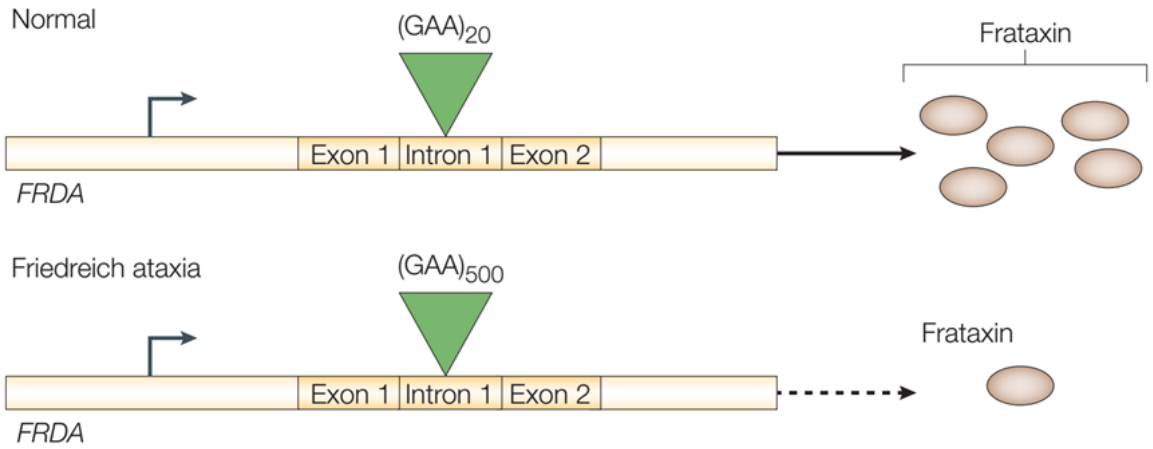

Figure 1: GAA triplet repeat in the FXN gene reduces frataxin levels

GAA triplet repeat expansion in the first intron of frataxin results in decreased levels of frataxin. Most patients have expansions in both alleles (adapted from Gatchel & Zoghbi, 2005).

The disease is caused by mutations in the frataxin (FXN) gene, most commonly an expansion of a GAA triplet repeat in the first intron (Campuzano et al, 1997). The number of

triplets in heathy people ranges from 10-40, while FRDA patients usually have over 500 repeats (Figure 1). Age of onset normally correlates inversely with triplet repeat length and patients with more repeats often suffer from faster progression (Montermini et al, 1997; Patel et al, 2016). How the GAA triplet repeat facilitates loss of protein is still a matter of debate. One proposed mechanism is the formation of an intramolecular triple DNA helix called 'sticky DNA' in the repeat region, inhibiting transcription elongation (Potaman et al, 2004). Alternatively, inhibition of transcription initiation via epigenetic modifications at the FXN locus has been suggested (Greene et al, 2007; Sandi et al, 2013). Recent advancements imply that both factors may play a role in transcription inhibition (Li et al, 2015). Other mutations such as deletions or point mutations have been reported but are rare and always associated with a triplet repeat expansion in the other allele. These compound heterozygotes account for about 2 - 4% of all cases (Cossee et al, 1999).

All FRDA patients show a basal level of the frataxin protein and patients with a complete loss of frataxin have not been documented. In this sense, complete knockout of frataxin results in embryonic lethality in mouse and *Drosophila* (Cossee et al, 2000; Anderson et al, 2005). At present, no effective therapy for FRDA has been developed so far.

1.2. The frataxin protein

1.2.1. Frataxin structure

The primary product of the FXN gene is a precursor protein of 210 amino acid length and 23 kilodalton (kDa) size. It is then processed in a two-step maturation process into mature frataxin, constituting a 14.2 kDa mitochondrial protein composed of 130 amino acids (Schmucker et al, 2008).

Crystal structure analysis revealed that frataxin forms an α-β sandwich and consists of two nearly parallel α helices and seven β strands (Dhe-Paganon et al, 2000).

Frataxins are highly conserved among species, with homologues not only in animals, but also in plants, fungi and bacteria (Gibson et al, 1996; Campuzano et al, 1996; Koutnikova et al, 1997). In agreement, their crystal structures are also nearly identical (Cho et al, 2000; He et al, 2004). Eukaryotic frataxins share two highly conserved domains in their structure: An N-terminal tail region containing a mitochondrial import signal (Gibson et al, 1996) and a C-terminal region responsible for protein stability (Faraj et al, 2016).

The high degree of homology among the molecular structure of different frataxins has allowed the establishment of many different models in order to elucidate the exact function of frataxin and its role in mediating FRDA. Such models include yeast (Foury & Cazzalini, 1997),

mouse (Puccio et al, 2001), *C.elegans* (Ventura et al, 2005; Vazquez-Manrique et al, 2006) and *Drosophila melanogaster* (Anderson et al, 2005; Llorens et al, 2007).

1.2.2. Frataxin function

Frataxin is present in all human cells, but expression levels differ depending on the tissue (Pandolfo, 2003). It is predominantly expressed in tissues with a high metabolic rate, including liver, kidney, neurons and heart. Not surprising, these are also the tissues where mitochondria are enriched (Koutnikova et al, 1997).

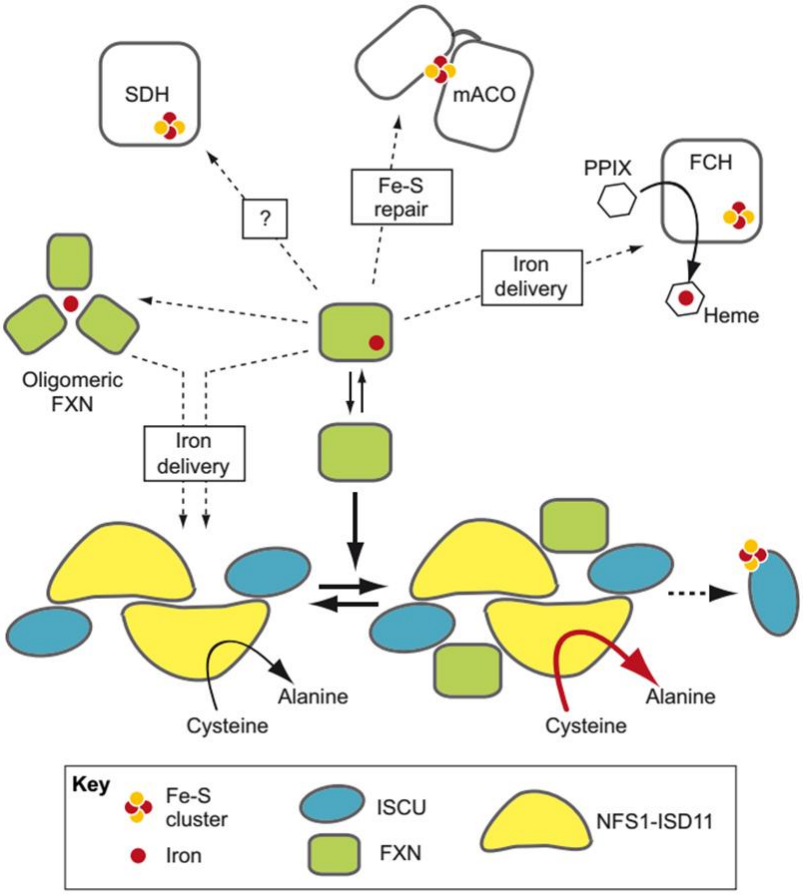

Figure 2: Frataxin has a key role in ISC biogenesis

The proposed main function of frataxin lies in ISC biogenesis, which involves the cysteine desulphurase NFS1-ISD11 and the scaffold protein ISCU. Frataxin can bind to this complex and increases the cysteine desulphurase activity, functioning as an allosteric activator (red arrow). In addition, frataxin has been proposed to supply iron to various mitochondrial proteins including succinate dehydrogenase (SDH), mitochondrial aconitase (mACO) and ferrochelatase (FCH). *In vitro*, frataxin also forms oligomeric structures that can store iron (from Martelli et al, 2012b).

The precise biological role of frataxin as a key regulator of iron-sulphur cluster (ISC) biogenesis has been well established (Tsai & Barondeau, 2010; Schmucker et al, 2011; Pandey et al, 2013). ISCs are small inorganic cofactors that are involved in many essential cellular pathways including energy metabolism and various enzymatic reactions (Lill, 2009). According to the current model, the following proteins are involved in the formation of ISCs: ISCU, which serves as the scaffold on which the cluster is assembled; NFS1-ISD11, a cysteine desulphurase that provides sulphur, and FXN, which increases the cysteine desulphurase activity, thus working as an allosteric activator (Figure 2). In bacteria, frataxin has instead been described as

a repressor of cluster formation (Adinolfi et al, 2009; Iannuzzi et al, 2011), but this anomaly seems to be restricted to bacteria, as no evidence of this in eukaryotes has been published.

Originally, it was thought that frataxin might provide iron for ISC formation due to its iron binding capacity, since frataxin was able to transfer iron to ISCU both *in vitro* and in bacteria (Yoon & Cowan, 2003; Layer et al, 2006). This model has been challenged by the works of Tsai & Barondeau and Schmucker et al, who used mammalian recombinant proteins to show that interaction of frataxin and the scaffold machinery is independent of iron, but increases the cysteine desulphurase activity of NFS1-ISD11. The physiological source of iron is still a disputed topic, as no conclusive evidence has been found for a particular donor. Therefore, it has been suggested there might me multiple sources of iron (Barupala et al, 2016).

Apart from this main function, frataxin has been proposed to be involved in other pathways, such as providing iron directly to succinate dehydrogenase, mitochondrial aconitase and ferrochelatase (Gonzalez-Cabo et al, 2005; Bulteau et al, 2004; Yoon & Cowan, 2004). However, different approaches failed to reproduce some of these interactions (Schmucker et al, 2011). Therefore, the relevance of these functions is still a matter of debate.

Additionally, frataxin in yeast is capable of forming oligomers when exposed to excess iron, which suggests an excess sequestration function (Adamec et al, 2000). However, this task seems to be restricted to yeast, likely because yeast lacks the common mitochondrial iron storage protein mitoferritin (Chiang et al, 2016).

1.2.3. Metabolic and cellular consequences of frataxin depletion

Even though it is still disputed which roles frataxin does ultimately perform *in vivo*, a common thread of all proposed functions is iron metabolism. Thus, it comes as no surprise that iron accumulation in the form of intracellular iron deposits was one of the first cellular symptoms of FRDA to be described (Lamarche et al, 1980).

Over the years, the following alterations have been established as the main consequences of frataxin deficiency: Impairment of ISC biogenesis, altered cellular iron metabolism, mitochondrial dysfunction resulting from iron overload, and increased oxidative stress (Pandolfo, 2012).

The scaffold machinery for ISC biogenesis is essentially in an off state when frataxin is absent and cannot synthesize new clusters (Tsai & Barondeau, 2010). This results in reduced activities of multiple proteins dependent on ISC clusters: Aconitase and complexes I, II, and III of the respiratory chain are among the prime enzymes affected (Rötig et al, 1997). In turn, this impacts the pathways these proteins are involved in, most importantly the citric acid cycle and

the electron transport chain in mitochondria, leading to loss of mitochondrial membrane potential and reduced ATP production (Shidara & Hollenbeck, 2010; Bolinches-Amoros et al, 2014).

A consequence of dysfunctional ISC biogenesis is enhanced activity of the cytosolic iron regulatory protein 2 (IRP2). It is involved in the control of iron metabolism by binding mRNA to repress translation or degradation (Eisenstein, 2000). IRP2 activation results in altered levels of proteins implicated in iron flux and distribution, altogether leading to a continuous iron transport into the mitochondria and accompanying cytosolic iron depletion. (Whitnall et al, 2008; Huang et al, 2009). If not used in a biosynthetic process, excess iron in mitochondria then can become oxidized and form insoluble precipitates (Koeppen, 2011). In particular, surplus iron in conjunction with reactive oxygen species (ROS), primarily hydrogen peroxide (H_2O_2), produces highly toxic free radicals in the so-called Fenton reaction ($Fe^{2+} + H_2O_2 \rightarrow Fe^{3+} + OH^- + OH^{\cdot}$). The hydroxyl radical $OH^{\cdot}$ produced by this reaction then damages many intracellular components such as proteins, DNA and membrane lipids (Delatycki et al, 2000). Heightened levels of oxidative stress markers have been found in patient samples (Emond et al, 2000; Schulz et al, 2000). Increased oxidative stress is also a hallmark of several FRDA models such as cell culture , *C.elegans* and *Drosophila* (Wong et al, 1999; Vazquez-Manrique et al, 2006; Llorens et al, 2007). Consequently, it has been shown that H_2O_2 detoxification protects frataxin deficient cells from oxidant damage (Pastore et al, 2003; Anderson et al, 2008). Likewise, sequestration of Fe^{2+} ions by overexpression of mitochondrial ferritin was able to reduce oxidative damage in FRDA fibroblasts (Campanella et al, 2009).

Unfortunately, clinical studies with the antioxidant idebenone revealed no significant effect on patients (Lagedrost et al, 2011; Meier et al, 2012). In similar fashion, the iron chelator deferiprone has been evaluated, but results remain inconclusive, even though some parameters showed encouraging trends (Pandolfo & Hausmann, 2013).

Another pathway affected in FRDA patients is lipid metabolism. In *Drosophila*, frataxin knockdown results in an increase in fatty acids metabolism and enhanced lipid peroxidation levels (Navarro et al, 2010). Similarly, lipid accumulation was observed in mouse models of frataxin deficient cardiomyocites and liver (Puccio et al, 2001; Martelli et al, 2012a; Obis et al, 2014). Signs of altered lipid metabolism have also been found in patients (Swarup et al, 2013). A possible mechanism is the differential regulation of PPARγ and its co-activator PGC1α found in a mouse model of FRDA. PPARs are nuclear receptors that serve as transcriptional sensors of fatty acids and play key roles in lipid regulation by repressing genes involved in lipogenesis. Interestingly, the exact response differed from tissue to tissue, likely because PGC1α is able to

activate tissue-specific transcription factors, triggering diverse metabolic programs in different tissues (Coppola et al, 2009).

Furthermore, it has been proposed that the prevalence of diabetes in FRDA patients might be connected to lipid metabolism dysfunctions. A clinical trial testing the drug pioglitazone, used for treating diabetes, has been completed but study results remain unpublished so far (Tamarit et al, 2016).

1.3. Glia and skeletal muscles in FRDA

1.3.1. The role of glial cells

Apart from neurons and the heart muscle, the primarily affected tissues, other cell types with an abundant expression of frataxin also display pathological manifestations. A premier example are glial cells. Glia are a class of non-neuronal cells that provide support and protection for neurons in the central and peripheral nervous systems. The main tasks of glia are to hold neurons in place and to supply nutrients and oxygen to neurons. It has recently been established that glia also play a crucial role in synapse formation and directly communicate with neurons (Stogsdill & Eroglu, 2017).

In FRDA, demyelination of the large axons has been reported in patients, along with abnormal Schwann cell morphology (Morral et al, 2010). In agreement, cultured Schwann cells were severely affected by lack of frataxin, leading to inflammation and ultimately cell death (Lu et al, 2009). Demyelination of large axons was also detected within the lumbar roots of a mouse model (Al-Mahdawi et al, 2006). Furthermore, targeted loss of frataxin in *Drosophila* glia caused defects in lipid metabolism, increased sensitivity to oxidative insult and impairment of locomotor activity (Navarro et al, 2010). More recently, a study of frataxin silencing in human astrocytes revealed detrimental effects not only cell-autonomously, but also for neuron-glia interactions (Loria & Diaz-Nido, 2015). In fact, lipid droplet accumulation in glia following mitochondrial dysfunction seems to be a key consequence of ROS in several neurodegenerative diseases (Liu et al, 2015).

1.3.2. The glial network of *Drosophila*

Unlike mammals, in which glia comprise almost 90% of brain cells, insect nervous systems have far fewer glial cells. Only 10% of the 90,000 cells estimated to occur in the adult central nervous system (CNS) of *Drosophila* can be identified as glial cells (Edwards & Meinertzhagen, 2010). Furthermore, even though Schwann cells and myelin sheaths cannot be found in insects, fly glia also generate multi-layered membrane protections around neurons and

axons. Not surprisingly, glia in the fruit fly are equally important as the ones found in mammals and share the same characteristics and are able to perform the same tasks as their mammalian counterparts (Stork et al, 2012).

In *Drosophila*, glia of the CNS can be divided into three major groups based on their location: Surface, cortex and neuropil glia (Figure 3).

Surface glia comprise the outermost glia of the brain and can further be subdivided into two categories, an outer layer (perineurial) and an inner layer (subperineurial). While the exact role of perineurial glia remains unclear, subperineurial glia form an effective blood-brain barrier which excludes molecules over a certain size over from entering the CNS (Stork et al, 2008).

Cortex or cell body glia envelop the somata of neurons in the outer layer of the brain (cortex). Cortex glia of the optic lobe are called satellite glia. They serve an important function in the maintenance of neurons, as well as in proper layering of neuronal cell bodies in the developing brain.

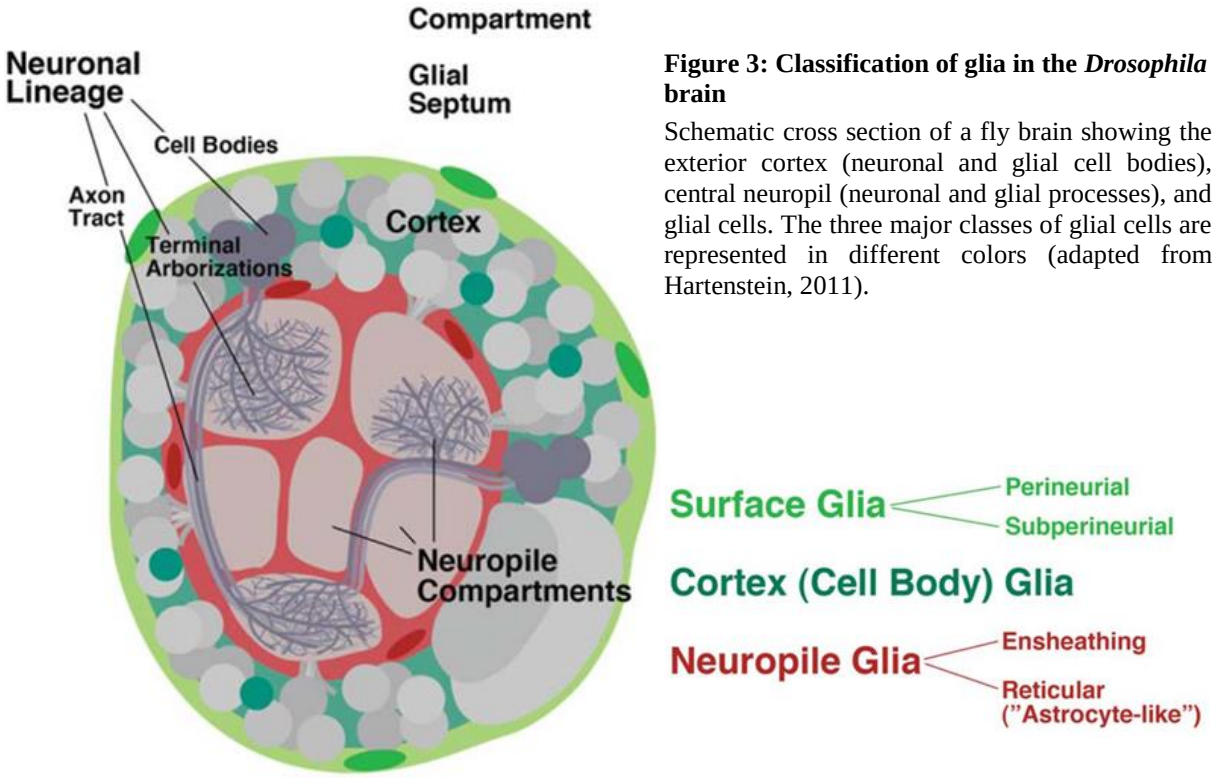

Figure 3: Classification of glia in the *Drosophila* brain

Schematic cross section of a fly brain showing the exterior cortex (neuronal and glial cell bodies), central neuropil (neuronal and glial processes), and glial cells. The three major classes of glial cells are represented in different colors (adapted from Hartenstein, 2011).

Neuropil glia surround the axons of neurons by extending sheath-like membranes around fibre bundles to form an isolation similar to myelin sheaths. They are the most diverse type of glia and can be broadly subdivided into two structurally distinct types: Ensheathing glia are lamellar and surround axons along the outer surface of the neuropil area. Reticular or astrocyte-like glia are widely branched, forming a network with terminal axons and synaptic regions (Awasaki et al, 2008). Neuropil glia fulfil several important tasks within the insect brain: They

serve as a guidance mechanism for axons, are involved in neuronal apoptosis and participate in synaptic transmission by taking up transmitters from the synaptic cleft (Hartenstein, 2011).

1.3.3. Involvement of skeletal muscle in FRDA

Although mitochondria are highly abundant in skeletal muscles because of their ample energy demands, muscle symptoms are overall less prominent than neurological ones. Nonetheless, FRDA patients display general muscle weakness, most prominent in the hip, and progressive loss of muscle strength in the distal limbs (Beauchamp et al, 1995; Dürr et al, 1996).

Because the symptoms are milder, the effect of frataxin depletion on skeletal muscles has been incompletely characterized. Magnetic resonance spectroscopy of calf muscles in FRDA patients revealed impaired mitochondrial respiration and ATP synthesis in addition to delayed recovery of tissue oxygenation after exercise (Lodi et al, 1999; Lynch et al, 2002; Nachbauer et al, 2012). However, a recent study that used the forearm instead of calf failed to reproduce these findings, though the authors could detect a correlation between reduced mitochondrial capacity and the severity of the disease (Bossie et al, 2016). Overall, involvement of skeletal muscle tissue in FRDA remains poorly understood.

1.4. Mitochondrial dynamics

1.4.1. FRDA is a mitochondriopathy

Frataxin is a mitochondrial protein and therefore FRDA at its core should be considered a mitochondrial disease. Indeed, due to its similarities to other mitochondrial diseases, it is classified as a member of the family of neurodegenerative mitochondriopathies (Swerdlow, 2009).

Mitochondria are self-dividing organelles responsible for generating cellular energy via ATP synthesis, regulating intracellular calcium levels, altering the redox potential of cells and regulating apoptosis. Increasing evidence suggests that alterations in these tasks play a central role in the development and progression of neurodegenerative diseases. Correspondingly, a common thread of mitochondriopathies are increased generation of free radicals, low production of cellular ATP, mitochondrial DNA damage and ultimately cell death. (Reddy, 2008).

1.4.2. The role of fusion and fission

Electron micrographs showing solitary, bean-shaped organelles have largely inspired the textbook appearance of mitochondria as singular structures within the cell. In the 1980s, live-

cell studies finally showed that mitochondria are actually highly dynamic organelles that are organized in large, intracellular networks (Bereiter-Hahn, 1990).

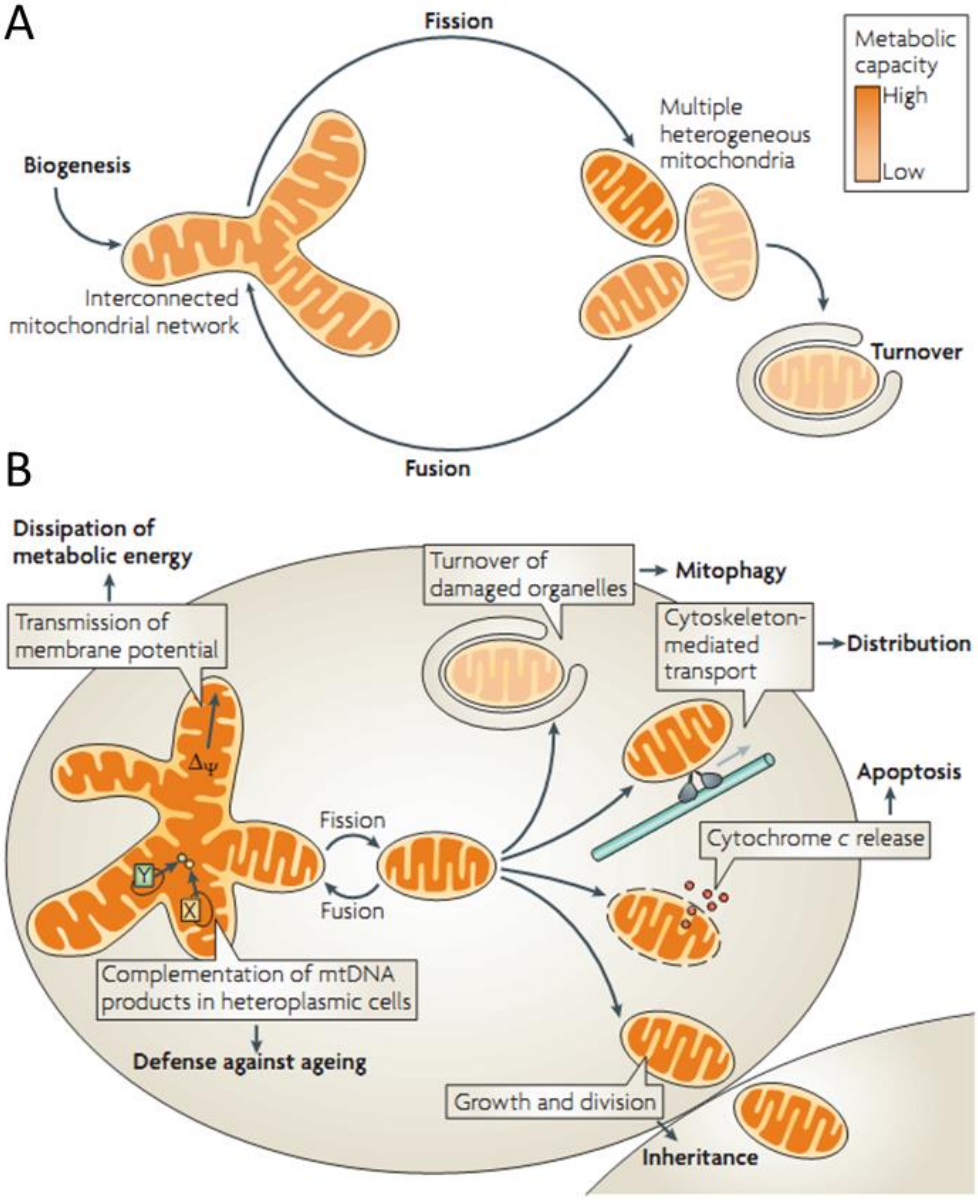

Figure 4: Biological functions of mitochondrial dynamics

(A) During their life cycle, mitochondria undergo many fission and fusion events, forming either interconnected mitochondrial networks or numerous heterogeneous mitochondria, depending on the physiological conditions. (B) Both interconnected networks and solitary mitochondria fulfil distinct and important roles in the cell (adapted from Westermann, 2010b).

Mitochondria frequently fuse and divide within the cell, depending on the physiological conditions. Fusion generates large networks of interconnected mitochondria, whereas fission results in multiple mitochondrial fragments (Figure 4A). Mitochondria themselves cannot be generated *de novo*. Instead, new mitochondria are formed by the growth and division of pre-existing organelles. This process involves the import of mitochondrial proteins encoded by the

nucleus, amplification of the mitochondrial DNA (mtDNA) and translation of proteins encoded by said DNA (Westermann, 2010b). During their life cycle, active mitochondria are transported through the cell via the actin cytoskeleton by myosin motor proteins (Altmann et al, 2008). Finally, surplus or damaged organelles are degraded through macroautophagy, in a process called mitophagy (Kim et al, 2007).

The structure of the mitochondrion is the key factor in determining the function it performs within the cell (Figure 4B). Mitochondrial networks can be found in metabolically active cells under conditions of high energy demand, such as neurons and muscles (Westermann, 2012). Large, interconnected networks show increased levels of mitochondrial respiration. In addition, they are responsible for the transmission of membrane potential along the cell, enabling the production of ATP in remote parts. Furthermore, mitochondrial fusion is required for the repair of mutations in the mtDNA via complementation, serving as defence mechanism against ageing. If two mitochondria, which carry mutations in different genes, fuse, the resulting organelle will feature an intact allele of both genes and therefore be able to bypass the defect (Ono et al, 2001).

Correspondingly, inhibition of mitochondrial fusion resulted in mitochondrial dysfunction, compensatory mitochondrial proliferation, accumulation of point mutations in the mitochondrial genome and depletion of mtDNA in mouse (Chen et al, 2010).

Mitochondrial fission also serves a variety of purposes. It is required for production of additional mitochondria and proper distribution of mitochondria to daughter cells. Moreover, fission is required for the generation of transportable mitochondria for movement along the cytoskeleton. Early during apoptosis, mitochondrial fragmentation triggers the release of pro-apoptotic factors such as cytochrome c into the cell (Martinou & Youle, 2011). Lastly, fission serves to eliminate damaged organelles by mitophagy, contributing to the maintenance of a healthy mitochondrial population (Kim et al, 2007).

Considering the huge variety of functions mediated by mitochondria, it is obvious that disturbances in mitochondrial homeostasis have severe consequences at the cellular level. As neurons generally have the highest energy consumption rate of all cells, defects in the intricate system of fusion and fission particularly affect neuronal function. Thus, dysfunctions in mitochondrial dynamics are predominantly associated with neurodegenerative diseases such as Parkinson's disease, Alzheimer's disease and Huntington's disease (Itoh et al, 2013).

In FRDA, several mitochondrial pathways have been studied in detail so far, including bioenergetics, redox status and iron homeostasis. However, information about mitochondrial dynamics and quality control is scarce (Gonzalez-Cabo & Palau, 2013). Increased

mitochondrial fragmentation has been observed in yeast and *C.elegans* (Lefevre et al, 2012; Schiavi et al, 2015). In contrast, frataxin knockdown triggered the formation of enlarged mitochondria in mammals (Puccio et al, 2001; Bolinches-Amoros et al, 2014; Obis et al, 2014). Furthermore, accumulation of normal mitochondria and the occurrence of mitochondria with disorganized cristae have been reported in cultured human cells (Hick et al, 2013). This suggests that the mitochondrial response might depend on the physiology and the adaptation capacity of the cell type.

1.4.3. Regulators of mitochondrial dynamics

1.4.3.1. The master regulators of fusion and fission

Extensive research over the years has led to a profound knowledge about the regulators of mitochondrial dynamics. The core mediators of fusion and fission are three membrane-remodelling enzymes, which belong to the dynamin family of large GTPases: Mfn (mitofusin; named Marf in *Drosophila*) and Opa1 (optic atrophy 1) are responsible for fusion, while Drp1 (dynamin-related protein 1) regulates fission (Figure 5).

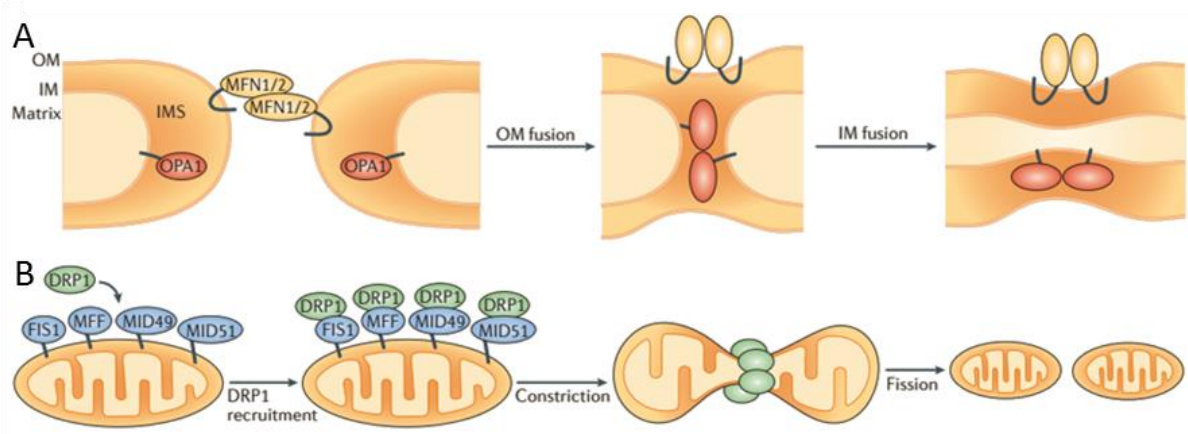

Figure 5: The key regulators of mitochondrial fusion and fission
(A) Mfn1/2 and Opa1 mediate fusion of outer and inner mitochondrial membrane, respectively. (B) For fission, cytosolic Drp1 is recruited to the outer mitochondrial membrane via molecular adaptor proteins (adapted from Mishra & Chan, 2014).

Mfn is required for fusion of the outer mitochondrial membrane (OM) and consists of two transmembrane domains, a short loop in the intermembrane space and the major part extending into the cytosol. In mammals, two functionally interchangeable isoforms of Mfn exist (Koshiba et al, 2004). In the first step, Mfn proteins of opposing mitochondria come in contact with each other and form a tether between them. Then, fusion of the OM occurs in a GTP hydrolysis-dependent manner. After the completion of OM fusion, Opa1 is required for inner mitochondrial membrane (IM) fusion and operates in a similar way: tethering with subsequent

fusion through GTP hydrolysis (Lee & Yoon, 2016). Opa1 itself is anchored within the IM, with the major part expanding into the intermembrane space (Meeusen et al, 2006).

Drp1 is the master regulator of mitochondrial fission. Drp1 is primarily found in the cytosol and is only recruited onto the OM during the fission process (Legesse-Miller et al, 2003). Assembly requires interaction with partner proteins located in the OM and causes the constriction of mitochondria and eventual division into two separate organelles. Multiple receptors are able to recruit Drp1 to the site of mitochondrial fission. Four of these interaction partners have been characterized so far in mammals: Fis1, Mff, MiD49 and MiD51 (Mishra & Chan, 2014).

1.4.3.2. *Drosophila* as a model organism for mitochondrial dynamics

The three core proteins of mitochondrial fusion/fission are well conserved among different species and the fruit fly has been a valuable asset in identifying the proteins involved. The first known mediator of mitochondrial fusion, Fzo (fuzzy onions), was discovered in *Drosophila* and established the field of mitochondrial dynamics (Hales & Fuller, 1997). It is only expressed in testis of male flies, reflecting a highly specialized function. The protein Marf (Mitochondrial assembly regulatory factor) fulfils a more general role as the homologue of the mammalian fusion protein Mfn. In contrast to mammals, there is only one variant of Marf present in the fly (Deng et al, 2008). Opa1 and Drp1 have orthologues in *Drosophila* that perform the same roles as their mammalian counterparts.

Compared to the three main regulators, the Drp1 receptors on the OM membrane seem less conserved. While Fis1 is the only receptor in yeast, it is less important in both mammals and flies (Westermann, 2010a). In mammals, Mff (Mitochondrial fission factor) seems to be the primary receptor, as loss of Mff causes the greatest decrease in fission (Loson et al, 2013). Mff is also present in *Drosophila* and is able to mediate fission (Gandre-Babbe & van der Bliek, 2008), but no further analysis has been done in the fly.

Apart from these main players, two further proteins have been shown to influence mitochondrial dynamics in *Drosophila*: Pink1 and Parkin, key factors involved in the pathogenesis of Parkinson's disease. While their main role lies in acting as checkpoints of mitochondrial integrity and in targeting mitochondria for degradation when necessary (see chapter 1.5.2), it has been suggested that they are also able to regulate mitochondrial morphology (Clark et al, 2006). Several reports have demonstrated that Pink1 and parkin interact genetically with the fusion/fission machinery to promote mitochondrial fission and/or inhibit fusion. Overexpression of Drp1 or knockdown of Marf is able to ameliorate the muscle

degeneration and mitochondrial abnormalities found by Pink1 and Parkin mutants (Deng et al, 2008). In addition, Pink1 overexpression promotes mitochondrial fission, whereas inhibition leads to excessive fusion (Yang et al, 2008). Similarly, loss of Pink1 results in increased mitochondrial fusion in *C.elegans* (Luz et al, 2015). However, in human cell culture Pink1 and Parkin knockdown appeared to have the opposite effect, promoting fusion instead of fission (Lutz et al, 2009).

Altogether, these results suggest that Pink1 and Parkin are likely involved, but not core components of the fusion/fission machinery.

1.5. Autophagy in neurodegenerative diseases

Autophagy in general refers to a group of intracellular degradation pathways that mediate the breakdown of intracellular material such as proteins, lipids and even whole organelles including mitochondria in the lysosome. Several subtypes of autophagy have been described so far, but most research has been dedicated to macroautophagy, as it is the most important pathway with the highest capacity for degradation. It is also the only pathway capable of organelle turnover (Mulakkal et al, 2014).

Neurons are particularly vulnerable to defects in this system because of their size and lack of cell division. Without functional autophagy, neurons accumulate protein aggregates and ultimately degenerate, as toxic waste cannot be diluted through self-replication. Therefore, it is not surprising that mutations in autophagy-related genes are closely linked to neurodegenerative diseases (Nixon, 2013).

1.5.1. The macroautophagy pathway

Macroautophagy, hereafter simply referred to as autophagy, includes several steps (Figure 6). The master regulator of autophagy is the serine/threonine kinase Tor (target of rapamycin) (Noda & Ohsumi, 1998). Tor activity is highly dependent on the presence of nutrients and stimulates protein synthesis. Under starvation conditions, Tor is inhibited, which in turns shuts down translation and induces autophagy (Scott et al, 2004; Figure 6A).

After induction, Atg1 (autophagy related 1) is activated via phosphorylation, recruits the Atg1 protein kinase complex and initiates the formation of the isolation membrane or phagophore. In turn, this triggers the translocation of a multi-protein complex from the cytoskeleton to the phagophore assembly site and induces vesicle elongation, forming a closed vesicle, the autophagosome (Nixon, 2013; Figure 6C).

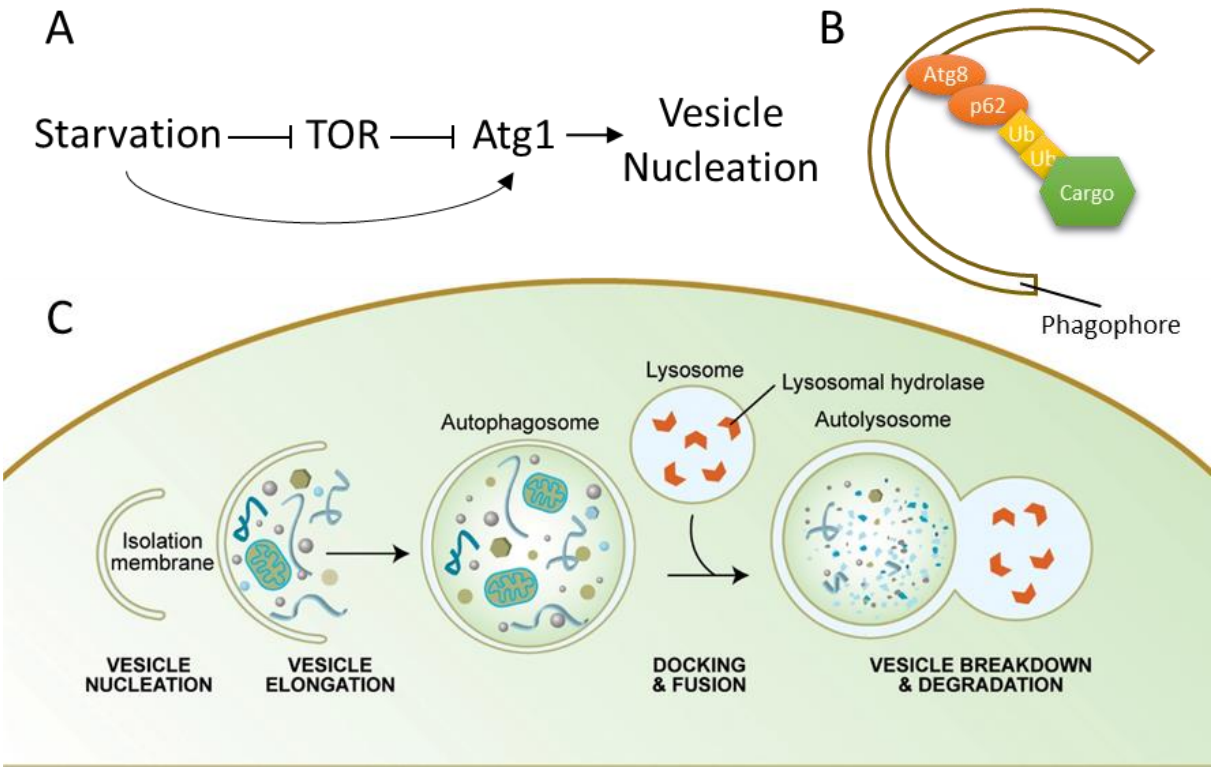

Figure 6: Schematic overview over the main steps of autophagy

(A) Under starvation conditions, the autophagy master regulator Tor is inhibited. In turn, this activates Atg1 and induces vesicle nucleation. (B) Cargo selected for degradation is polyubiquitinated and becomes linked to the phagophore via p62 and Atg8. (C) After autophagy induction, the isolation membrane or phagophore forms (vesicle nucleation). The phagophore is then expanded through the interaction of the autophagy core machinery proteins at the phagophore assembly site, forming the autophagosome (vesicle elongation). It can engulf targeted cargo, including proteins or even whole organelles, specifically. The autophagosome then fuses with a lysosome to form the so called autophagolysosome (docking & fusion). Finally, the contents of the autophagolysosome are degraded by the lysosomal hydrolases and can be recycled (vesicle breakdown & degradation). Adapted from Melendez & Levine, 2009.

While autophagy originally emerged as a non-selective process, it can also target proteins or organelles specifically. Atg8 is a protein anchored to the inside of the phagophore during vesicle elongation and is able to bind selected cargo via distinct receptor proteins that serve as adapters between Atg8 and the substrate. One of these receptors is p62, which recognizes ubiquitinated proteins that have been targeted for degradation and links them to Atg8, thus connecting them to the phagophore (Johansen & Lamark, 2011; Figure 6B).

After autophagosome formation is complete, it fuses with intracellular lysosomes to so-called autolysosomes. Through Vacuolar-type H^+-ATPase (vATPase) activity, a multimeric proton pump in the lysosomal membrane, the interior of the autolysosome becomes acidic, activating hydrolases. The contents of the autolysosome are then digested and released into the cytosol for recycling (Nixon, 2013).

1.5.2. Mitophagy

Autophagy is also responsible for selective degradation of defective mitochondria, a process dubbed mitophagy. While recent advancements have uncovered additional pathways for targeting mitochondria for degradation, the best understood pathway is the Pink1/Parkin-mediated mitophagy, originally discovered in *Drosophila* (McWilliams & Muqit, 2017). A schematic overview can be seen in Figure 7.

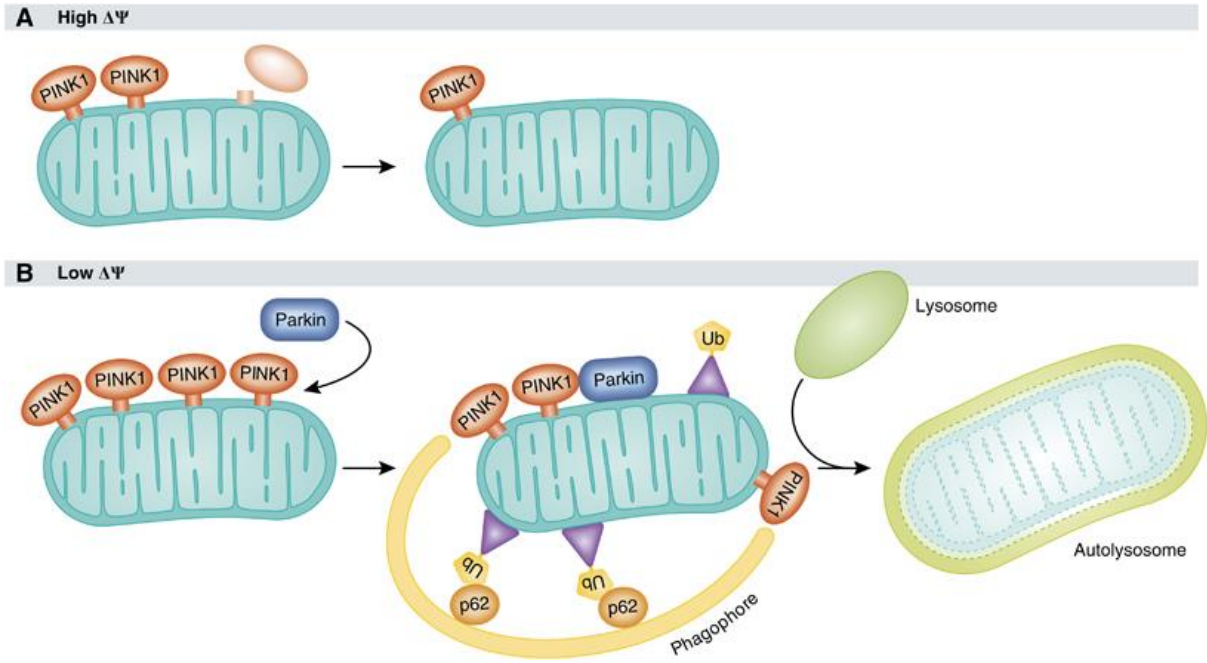

Figure 7: Mechanism of Pink1/Parkin induced mitophagy

(A) In healthy mitochondria, Pink1 imported to the mitochondria is rapidly degraded, resulting in low levels of Pink1 on the outer mitochondrial membrane. (B) Following loss of membrane potential, Pink1 is stabilized on the outer membrane and recruits Parkin to ubiquitinate mitochondrial membrane proteins. Ubiquitinated proteins are recognized by the autophagy receptor protein p62 and guided towards the phagophore, resulting in engulfment of the mitochondrion. The phagophore then matures into an autophagosome and fuses with lysosomes to form the autolysosome (adapted from Exner et al, 2012).

Under normal conditions, Pink1 is constantly imported onto the outer mitochondrial membrane and rapidly degraded (Jin et al, 2010). When import is disrupted because of mitochondrial depolarization, Pink1 is stabilized and accumulates on the outer membrane. Pink1 then recruits the E3 ubiquitin ligase Parkin and activates it through its kinase activity (Lazarou et al, 2012).

In turn, Parkin ubiquitinates several target proteins located in the outer membrane, among them Marf (Ziviani et al, 2010). Ubiquitinated proteins are then recognized by autophagy receptors such as p62 to guide them towards the phagophore through binding to Atg8 (Pickrell & Youle, 2015). Subsequently, the phagophore closes around the organelle to form an autophagosome and the process continues as described in chapter 1.5.1.

More recently, Pink1 has emerged as the key regulator of mitophagy. According to the updated model, phosphorylation of ubiquitinated proteins on the outer mitochondrial membrane by Pink1 initiates mitophagy, while additional ubiquitination via Parkin amplifies the signal (Lazarou et al, 2015).

1.5.3. Autophagy defects are closely tied to neurodegeneration

Defects in autophagy have been recognized to be of major importance in the pathology of most neurodegenerative diseases. Disturbances in every step of the pathway have been associated with them, from autophagy induction over substrate recognition to lysosomal digestion (Kiriyama & Nochi, 2015).

In Huntington's disease, Tor is sequestered into huntingtin aggregates, reducing its activity (Ravikumar et al, 2004). Mutations in the autophagy receptor p62 have been implicated in amyotrophic lateral sclerosis (Fecto et al, 2011). Defects in vATPase targeting to lysosomes results in impaired acidification in a mouse model of Alzheimer's disease (Lee et al, 2010). A hallmark of Parkinson's disease is the accumulation of damaged mitochondria. In some forms, mutations in the mitochondrial quality control genes *Pink1* and *Parkin* prevent damaged mitochondria from degradation, ultimately resulting in neuronal cell loss (Nguyen et al, 2016).

As autophagy appears to be a central component of virtually every neurodegenerative disease, it is conceivable that autophagy, and particularly mitophagy, might be affected in FRDA as well. Information about mitophagy function in Friedreich's ataxia, however, is limited. In a conditional mouse knockout model, Atg8 and p62 expression was increased and this correlated with increased expression of a mitophagy marker (Huang et al, 2013). Further studies could show that frataxin knockdown results in increased basal autophagy levels in *C.elegans* and human cell culture (Schiavi et al, 2013; Bolinches-Amoros et al, 2014). In case of the worm, this corresponded to enhanced mitophagy (Schiavi et al, 2015).

Apart from that, no detailed analysis has been done *in vivo* to examine mitophagy in FRDA.

1.6. Endoplasmic reticulum stress in the pathogenesis of neurodegenerative diseases

1.6.1. The unfolded protein response

The endoplasmic reticulum (ER) is an important organelle within the cell responsible for synthesis and export of proteins as well as Ca^{2+} homeostasis. Within the ER lumen, newly formed secretory and membrane proteins are correctly folded and transported from the rough ER to the Golgi apparatus. Disruptions in these processes lead to the accumulation of unfolded

proteins within the ER and trigger the unfolded protein response (UPR) (Wu & Kaufman, 2006). An overview can be seen in Figure 8.

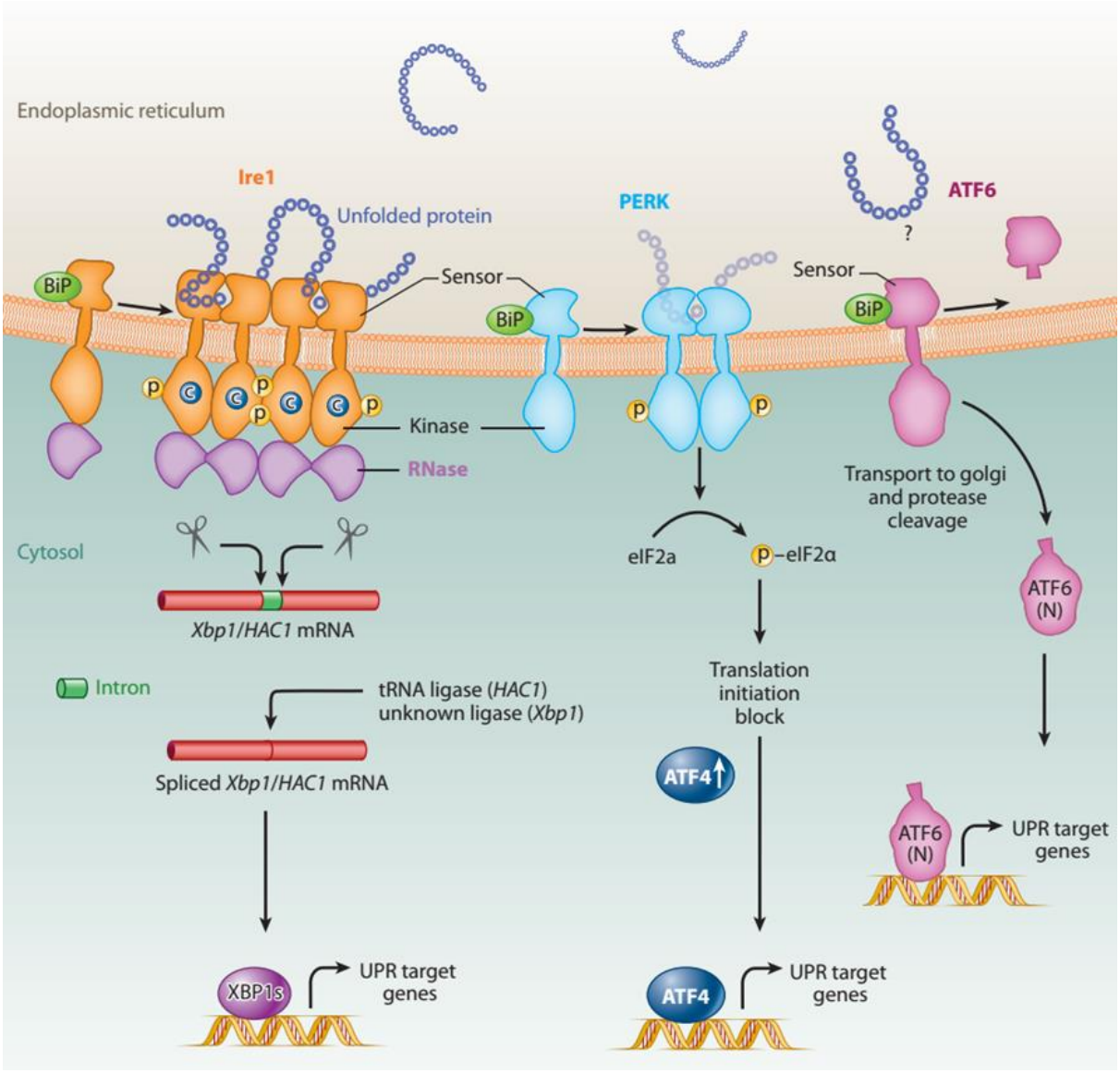

Figure 8: Overview over the unfolded protein response

The unfolded protein response (UPR) can be divided into three branches. All branches consist of a sensor (Ire1, PERK and ATF6) that recognizes unfolded proteins within the ER and triggers downstream pathways to reestablish correct protein folding within the ER. In the Ire1 branch, Xbp1 is spliced and translated. PERK phosphorylates eIF2α, who in turn activates ATF4. In the ATF6 branch, its cytosolic region is cleaved and liberated into the cytosol. Xbp1, ATF4 and ATF6 then function as transcription activators in the nucleus for target genes such as the ER chaperone BiP (adapted from Korennykh & Walter, 2012).

The UPR can be divided into three branches which work in a similar fashion. They consist of two central components: A stress sensor located in the ER membrane and a downstream transcription factor that activates target genes responsible for restoring ER homeostasis such as the ER chaperone BiP. The most conserved of the three is the Ire1 branch. Upon ER stress, Ire1 oligomerizes and is autophosphorylated. This triggers its RNAse activity and catalyses the unconventional splicing of Xbp1. Only spliced Xbp1 is translated into a functional protein,

transported into the nucleus and functions as a transcription activator. In the second branch, PERK dimerizes and phosphorylates eIF2α, ablating the translation initiation block for the transcription factor ATF4. In the last branch, the stress sensor ATF6 is cleaved and its cytosolic part can translocate into the nucleus to activate gene transcription (Xiang et al, 2017).

Downstream effects of the UPR include upregulation of genes involved in the ER-associated protein degradation, autophagy and quality control. Under conditions of irreversible or prolonged ER stress, the UPR is also able to mediate apoptosis (Hetz & Mollereau, 2014).

1.6.2. ER stress in neurodegeneration

Recently, ER stress and the unfolded protein response have come to the forefront as a common pathological symptom of neurodegenerative diseases, similar to autophagy. Accumulation of dysfunctional proteins are associated with Parkinson's disease and Alzheimer's disease, among others (Hetz & Mollereau, 2014).

In Parkinson's disease, Lewy bodies are formed within the brain consisting of mutant α-synuclein. Elevated levels of PERK and phosphorylated eIF2α have been found in post-mortem brain tissue of patients (Hoozemans et al, 2007). In several models of Parkinson's disease, ablation of Xbp1 resulted in loss of dopaminergic neurons, suggesting a neuroprotective effect of the Ire1 branch (Xiang et al, 2017).

Accumulation of amyloid-β plaques and neurofibrillary tangles are a hallmark of Alzheimer's disease. Similar to Parkinson's disease, elevated levels of PERK and phosphorylated eIF2α are also present in this disorder and are thought to mediate neuronal cell loss by triggering apoptosis (Rozpedek et al, 2015).

Originally, it was thought that UPR activation is a direct consequence of protein misfolding disorders and contributes to neuronal damage. However, this view has been challenged recently, as UPR signalling has been shown to both enhance and reduce neurodegeneration, depending on the branch that was activated (Hetz & Mollereau, 2014). Moreover, activation of the UPR has been implicated as a general, indirect response to external stressors, preceding the actual pathology. This is in agreement with the fact that most proteins related to neurodegeneration are located in the cytoplasm and are not connected to the ER in any stage of their life cycle. This suggests that ER stress might be part of the aetiology of most neurodegenerative diseases (Scheper & Hoozemans, 2015).

1.6.3. Mitochondria-ER contacts

Interestingly, the ER and mitochondria form a dynamic interconnected network within the cell. In particular, it is estimated that about 5 – 20% of the mitochondrial surface is in close proximity to the ER, forming the so called mitochondria-associated ER membranes (MAMs). These contacts enable communication between mitochondria and the ER to regulate several essential cellular processes: Ca^{2+} and phospholipid exchange, intracellular trafficking, autophagy and mitochondrial biogenesis (Rowland & Voeltz, 2012).

Naturally, MAMs are disrupted in multiple neurodegenerative diseases such as Alzheimer's disease and Parkinson's disease (Zampese et al, 2011; Cali et al, 2013).

Despite their importance, the mechanism of tethering between mitochondria and the ER remains poorly understood. In yeast, the ER-mitochondria encounter structure has been described as the tether between ER and mitochondria (Kornmann et al, 2009), but this structure appears to be yeast specific. Several studies were able to identify proteins on the ER and the outer mitochondrial membrane that are able to interact with another, suggesting possible tethering complexes (Figure 9).

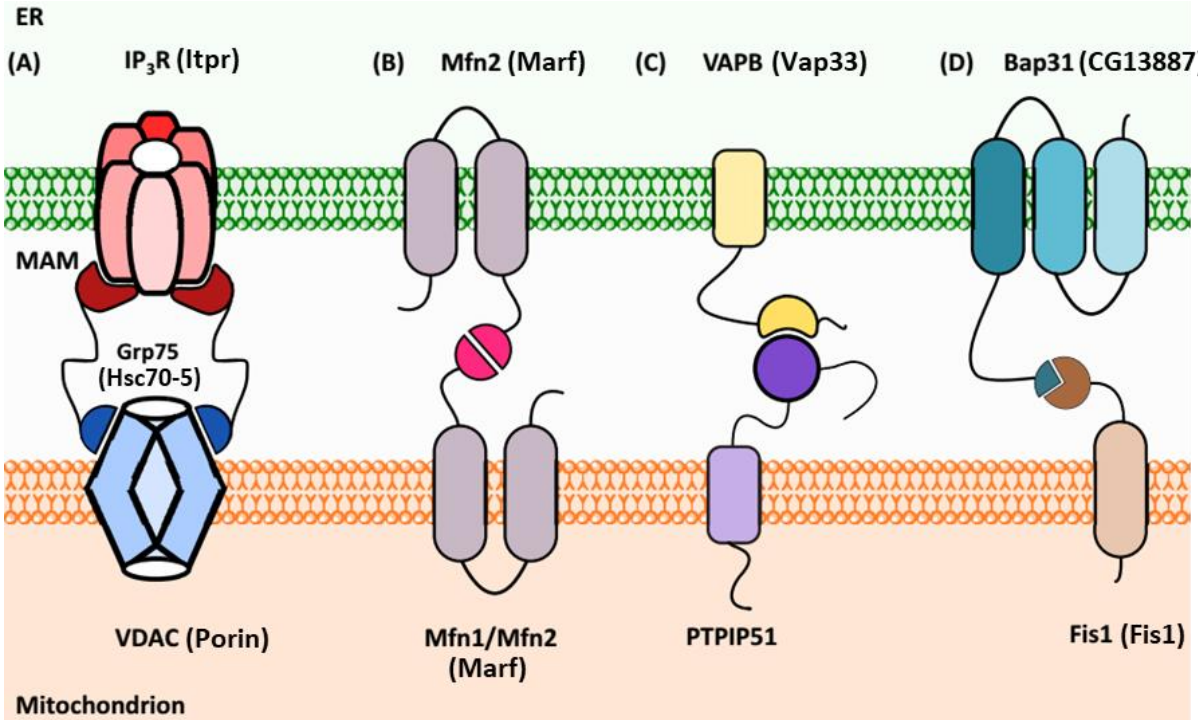

Figure 9: Overview over proposed ER-mitochondria tethering complexes

ER-located proteins are shown at the top, mitochondrial proteins shown at the bottom. The name of known *Drosophila* homologues is written in parentheses. PTPIP51 is vertebrate specific (adapted from Paillusson et al, 2016).

These four predicted tethering complexes are associated with a specific role they are proposed to mediate. IP_3R and VDAC (Itpr and Porin in *Drosophila*) in conjunction with the

coupling protein Grp75 facilitate Ca^{2+} exchange. Interestingly, the fusion protein mitofusin has also been predicted to play a role in tethering mitochondria to the ER, possibly in Ca^{2+} transfer. The role of VAPB and PTPIP51 is to promote lipid transport, while Bap31 and Fis1 have been connected to apoptosis signaling (Phillips & Voeltz, 2016). No PTPIP51 homologues are present in *Drosophila*, *C.elegans* or yeast, thus the VAPB-PTPIP51 complex appears to be vertebrate specific. By contrast, orthologues of the other proteins exist in *Drosophila* as well (Paillusson et al, 2016). CG13887, the *Drosophila* orthologue of Bap31, will be called Bap31 from now on. Additionally, Miro, a component of the mitochondrial transport machinery, interacts with both the Itpr-Porin and Marf complexes to facilitate Ca^{2+} transfer in the fruit fly (Lee et al, 2016). However, ER-mitochondrial contacts have not been studied in detail in *Drosophila* so far.

Recently, MAM disruptions have been directly linked to the UPR. Loss of mitofusin promotes ER stress and modulates the UPR via inhibition of PERK. In turn, PERK might also be able to regulate mitochondrial morphology through its interaction with Mfn (Ngoh et al, 2012; Munoz et al, 2013). Furthermore, several ER chaperones including BiP can be found within MAMs (Hayashi et al, 2009).

Thus, it is possible that crosstalk between the ER and mitochondria facilitates not only ER stress and activates the UPR, but has a direct impact on mitochondrial homeostasis as well.

1.7. The *Drosophila* model of Friedreich's ataxia

After the protein responsible for Friedreich's ataxia was discovered in humans in 1997, the search for frataxin homologues (fh) in other species began quickly. Frataxin was found to exist in virtually every organism (see chapter 1.2.1) and the putative *Drosophila* homologue, located on the X chromosome, was first described shortly thereafter (Canizares et al, 2000). The protein shares the same secondary structural elements as its human counterpart and also exhibits strong iron binding capacity. Finally, it was shown to be capable of mediating the formation of ISCs *in vitro* (Kondapalli et al, 2008). Furthermore, overexpression of the human protein is able to rescue frataxin depletion in flies, suggesting a functional equivalence (Navarro et al, 2011; Tricoire et al, 2014; Chen et al, 2016).

1.7.1. Two RNAi models for FRDA

After its discovery, the first working model of FRDA in *Drosophila* was established in 2005 by Anderson et al. Because, like in mammals, complete knockout of frataxin is embryonic lethal, this model mimics the pathology of the disease by reducing frataxin levels via RNAi.

The UAS-fhRNAi line they created reduces frataxin to near undetectable levels and leads to a developmental arrest in the larval stage when ubiquitously expressed. Frataxin depleted flies show typical hallmarks of FRDA: reduced life span, diminished activities of ISC containing enzymes, loss of intracellular iron homeostasis and increased susceptibility to oxidative stress (Anderson et al, 2005; Anderson et al, 2008).

A later study could show that frataxin depletion in motor neurons results in loss of mitochondrial membrane potential, reduced ATP production and defects in the axonal transport of mitochondria (Shidara & Hollenbeck, 2010). Interestingly, the importance of lipid metabolism in FRDA was established in this model. Navarro et al could show that frataxin knockdown results in increased fatty acid content and enhanced lipid peroxidation. This study also highlights the importance of glial cells in the pathology of the disease. Frataxin depleted glia accumulate lipid droplets in the brain and display reduced locomotor activity (Navarro et al, 2010). Further research has emphasized the role of mitochondrial iron overload. Frataxin depleted flies are hypersensitive to iron, which can be rescued by downregulating mitoferrin, a protein responsible for iron transport into mitochondria (Navarro et al, 2015). In a cardiac model of FRDA, frataxin depletion recapitulates the impairments found in the hearts of patients (Tricoire et al, 2014).

Overall, this model has been used to successfully mimic loss of frataxin phenotypes and serves as an excellent tool to investigate downstream effects of frataxin depletion in a tissue-specific manner. This line is used as fhRNAi1 in this thesis.

In 2007, Llorens et al developed a second RNAi model that leads to a more moderate frataxin knockdown (to about 30%). In this fhRNAi line, flies are able to develop normally under ubiquitous knockdown, permitting a systemic depletion through ubiquitous drivers that more closely resembles the human condition. This model also recapitulates hallmarks of FRDA: Shortened life span, reduced locomotor ability, involvement of glial cells and increased susceptibility to oxidative stress and iron (Llorens et al, 2007; Navarro et al, 2010; Navarro et al, 2015). In addition, this model suggests that other metals besides iron may be involved in the pathology of FRDA. Zinc, copper, manganese and aluminium levels were increased in frataxin knockdown flies and locomotor performance could be improved through activation of metal detoxification pathways (Soriano et al, 2016). Due to the lower knockdown, phenotypes generally appear later and are less severe. This line has therefore been used to study the efficacy of potential therapeutic approaches in the fly. Two studies could show a beneficial effect of certain drugs targeting affected pathways. The iron chelator deferiprone, the antioxidant

idebenone and the autophagy activator rapamycin all improved life span and motor ability of the flies (Soriano et al, 2013; Calap-Quintana et al, 2015).

This line is used as fhRNAi2 in this thesis.

1.7.2. A *Drosophila* fh mutant

Apart from the two RNAi knockdown models, a third model has recently been developed by Chen et al. They identified a missense mutation of fh via a forward genetic EMS (Ethyl methane sulfonate) screen which induces a severe loss-of-function. The mutation is located in the ISC assembly complex binding domain and results in lethality in the L3/pupal stage. In mosaic clones of adult photoreceptor neurons, both iron and lipid accumulation could be detected, similar to the phenotypes found in the fhRNAi1 line. This in turn activated the Pdk1/Mef2 pathway, a known downstream effect of lipid accumulation in yeast, contributing to photoreceptor degeneration (Chen et al, 2016). However, they questioned the role of oxidative stress, since ROS levels were not increased and treatment of flies with the antioxidant AD4 did not suppress neurodegeneration in their model.

1.8. Aims of the thesis

The main goal of this thesis is to further analyse the downstream effects of frataxin depletion in a multicellular organism like *Drosophila melanogaster*. To reach this goal, I first wanted to establish the mitochondrially enriched indirect flight muscles as a model tissue for the study of Friedreich's ataxia in the fruit fly to complement the previously described glial system.

Even though frataxin is a mitochondrial protein and Friedreich's ataxia is closely linked to mitochondrial dysfunction, information about mitochondrial dynamics and quality control is lacking in most of the existing models. To elucidate this matter, I wanted to examine the effects of frataxin deficiency on several parameters playing a key role in mitochondrial homeostasis, including morphology, dynamics and degradation.

Next, I wanted to study if genetic manipulation of mitochondrial homeostasis would be able to ameliorate frataxin deficiency. After identifying a positive interaction, the subsequent goal was to unravel the molecular and cellular mechanism underlying such an interaction.

Finally, I wanted to test if pharmacological treatment targeting identified pathways would be able to alleviate frataxin phenotypes.

2. Material and Methods

2.1. Material

2.1.1. Fly strains

Fly stocks were kept in glass vials containing Drosophila standard medium (cornmeal, agar, soy meal, molasses, malt flour, yeast and nipagine as a fungicide). The vials were stored in a humid incubator at a temperature of 25°C, a relative humidity of 65 % with a 12 hour light/dark cycle.

Driver Stocks, mutants and balancers			
Genotype	**Chrom.**	**Details**	**Origin**
w^{1118}	X	white mutation	Bloomington Stock Collection #3605
$Atg8a^{KG07569}$/FM7c	X	Atg8a mutant	Bloomington Stock Collection #14639
actin-Gal4/TM6B	III	ubiquitous driver	Bloomington Stock Collection #3954
Repo-Gal4/TM6B	III	glia cell driver	Bloomington Stock Collection #7415
Mef2-Gal4	III	muscle driver	Bloomington Stock Collection #27390
yw; *vas*-dΦ-zh2A; *zh*-86Fb;	II;III	PhiC31 integration line for germline transformation	Michael Krahn
w; D3/TM3	X; III	Double balancer for the third chromosome	chair stock
Responder Stocks			
Genotype	**Chrom.**	**Details**	**Origin**
UAS-cherryRNAi	II	knockdown of cherry	Bloomington Stock Collection #35787
UAS-fhRNAi1	II	strong knockdown of frataxin	John P. Phillips
UAS-fhRNAi1	III	strong knockdown of frataxin	John P. Phillips
UAS-fhRNAi2	II	moderate knockdown of frataxin	Maria D. Moltó
UAS-nGFP	II	overexpression of nuclear GFP	Bloomington Stock Collection #64502
UAS-mitoGFP/CyO	III	overexpression of mitoGFP	Bloomington Stock Collection #8433
UAS-mitoGFP	III	overexpression of mitoGFP	Bloomington Stock Collection #8442
UAS-GFP	II	overexpression of cytosolic GFP	Andrea Brand

Genotype	Chrom.	Details	Origin
UAS-mitoroGFP-Grx1/CyO	II	overexpression of mitoGrx1-roGFP	Albrecht et al, 2011
UAS-fh	II	overexpression of frataxin	Llorens et al, 2007
MitoCatalase	III	ubiquitous expression of mitochondrial catalase	William Orr
UAS-Spargel	II	overexpression of Spargel	Christian Frei
UAS-SpargelRNAi	II	knockdown of Spargel	Bloomington Stock Collection #33914
UAS-Marf	II	overexpression of Marf	Alex Whitworth
UAS-MarfRNAi	II	knockdown of Marf	Bloomington Stock Collection #31157
UAS-Opa1	III	overexpression of Opa1	Alex Whitworth
UAS-Opa1RNAi	III	knockdown of Opa1	Ming Guo
UAS-drp1	II	overexpression of drp1	Ming Guo
UAS-drp1RNAi	III	knockdown of drp1	Bloomington Stock Collection #27628
UAS-Pink	II	overexpression of Pink	Alex Whitworth
UAS-PinkRNAi	III	knockdown of Pink	Bloomington Stock Collection #31282
UAS-Parkin	II	overexpression of Parkin	Alex Whitworth
UAS-ParkinRNAi	III	knockdown of Parkin	Bloomington Stock Collection #31255
UAS-GFP-Atg8a	III	overexpression of GFP-Atg8	Thomas P. Neufeld
UAS-Atg8a	III	overexpression of Atg8a	Jose Botella
UAS-LAMP1-GFP/CyO	II	overexpression of LAMP1-GFP	Fabio Demontis
UAS-p62	II	overexpression of p62	L. Miguel Martins
UAS-Xbp1-GFP/CyO	II	overexpression of Xbp1-GFP	Pedro Domingos
UAS-ER-GFP	II	overexpression of ER-GFP	Bloomington Stock Collection #9898
UAS-mtRosella/TM3	III	overexpression of mtRosella	chair stock
UAS-PERKRNAi	III	knockdown of PERK	Bloomington Stock Collection #42499
UAS-Sar1RNAi	III	knockdown of Sar1	Bloomington Stock Collection #32364
UAS-Bap31RNAi	III	knockdown of Bap31	Bloomington Stock Collection #32917
UAS-ItprA	III	overexpression of Itpr	Bloomington Stock Collection #30743
UAS-ItprRNAi	III	knockdown of Itpr	Bloomington Stock Collection #51795

Genotype	Chrom.	Details	Origin
UAS-PorinRNAi	III	knockdown of Porin	Bloomington Stock Collection #29572
UAS-Fis1RNAi	III	knockdown of Fis1	Bloomington Stock Collection #63027
UAS-fhRNAi1/CyO; UAS-cherryRNAi/TM3	II;III	co-knockdown of fhRNAi1 and cherry	chair stock
UAS-mitoGFP/CyO; UAS-fhRNAi1	II;III	knockdown of frataxin and overexpression of mitoGFP	chair stock
UAS-MarfRNAi/CyO; UAS-fhRNAi1	II;III	co-knockdown of Marf and frataxin	chair stock
Combined Driver and Responder Stocks			
Genotype	**Chrom.**	**Details**	**Origin**
UAS-mitoGFP/CyO; *Repo*-Gal4/TM3	II;III	Glial driver with overexpression of mitochondrial GFP	chair stock
UAS-nGFP/CyO; *Repo*-Gal4/TM3	II;III	Glial driver with overexpression of nuclear GFP	chair stock
UAS-fhRNAi1; *Repo*-Gal4/TM6B-*tub*-Gal80	II;III	Glial driver with knockdown of frataxin	chair stock
UAS-ER-GFP/CyO; *Repo*-Gal4/TM6B-*tub*-Gal80	II;III	Glial driver with overexpression of ER-GFP	chair stock
UAS-Xbp1-GFP/CyO; *Repo*-Gal4/TM6B	II;III	Glial driver with overexpression of Xbp1-GFP	chair stock
UAS-mitoGFP/CyO; *Mef2*-Gal4/TM3	II;III	Muscle driver with overexpression of mitoGFP	chair stock
UAS-fhRNAi1; *Mef2*-Gal4/TM6B-*tub*-Gal80	II;III	Muscle driver with knockdown of frataxin	chair stock
UAS-ER-GFP/CyO; *Mef2*-Gal4/TM3	II;III	Muscle driver with overexpression ER-GFP	chair stock
UAS-Xbp1-GFP/CyO; Mef2-Gal4/TM6B-*tub*-Gal80	II;III	Muscle driver with overexpression of Xbp1-GFP	chair stock

Table 1: List of fly stocks

2.1.2. Buffers and solutions

Name	Components	Task
Blocking Buffer	OBB:TBS = 1:1	membrane blocking for Western Blot
DEPC-H_2O	1% DEPC in ddH_2O	RNA Extraction

Name	Components	Task
Laemmli buffer	0.06 M Tris/HCl pH 6,8 10 % glycerol 2 % SDS 0.002 % bromophenol blue	SDS-PAGE
Electrophoresis buffer for SDS-PAGE	0.025 M Tris 0.2 M glycine 0.1 % SDS	SDS-PAGE
Fixing solution	4 % paraformaldehyde 0.5 % Triton X-100	Fixation of flies for whole mounts
PBS	137 mM NaCl 2.7 mM KCl 4.3 mM Na_2HPO_4 1.47 mM KH_2PO_4 adjust pH to 7.2	Dissection of brains and muscles
PBST	PBS with 0.1 or 0.5 % Triton X-100	Histology washes (0.1 %) Histology AB staining (0.5 %)
Relaxing solution	20 mM KH_2PO_4 5 mM $MgCl_2$ 5 mM EGTA 5 mM ATP	TMRE staining
RIPA buffer	50 mM Tris-HCl, pH 8.0 150 mM NaCl 1% Igepal CA-630 (NP-40) 0.5% sodium deoxychelate 0.1% SDS	Protein extraction
Semi-dry blotting buffer	50 mM Tris 40 mM glycine 20 % methanol 0.000375 % SDS	Western Blot blotting
TBS	0.01 M Tris 0.15 M NaCl adjust pH to 7.5	Western Blot
TBST	TBS with 0.05 % Tween-20	Western Blot washes
ATP buffer	100 mM Tris 4 mM EDTA, pH 7.75	ATP assay
Homogenization buffer	0.2 mM NaCitrate 5 0mM Tris/HCl, pH 7.4	Aconitase activity
Carnoy	99 % Ethanol : chloroform : acetic acid = 6 : 3 : 1	Fixation reagent for paraffin sections

Table 2: List of Buffers and Solutions

2.1.3. Oligonucleotides

Description	Sequence 5' → 3'	Annealing temperature	Application
RP49	Fw: CCAAGGACTTCATCCGCCACC	60° C	real-time PCR
	Rv: GCGGGTGCGCTTGTTCGATCC		
Opa1	Fw: TGCACAGTCAGGTTCTCAAAA		
	Rv: TATGAATTCCTGCGTGCAACG		
drp1	Fw: GGACAAGAATCTGGATGAGGTC		
	Rv: CGCTATGACCTCCAGTTGC		
Marf	Fw: ACCTCACCTCGGCCAACT		
	Rv: GTGGTGGCGGTATCAACC		
Frataxin	Fw: GTCACAGTCCGTGGACTTCC		
	Rv: CAAAATCGAACGTTTCAACCG		
Pink	Fw: TCGACGATTTCGCCTTGTA		
	Rv: GTGGTGGTTGTGGTGCAG		
Parkin	Fw: GCCTGCACGGATGTGAGT		
	Rv: AAACGGGAACGGCAATAAT		
Spargel	Fw: TCTGCCCTATGGAAGCATTAAAC		
	Rv: CATACATGCTTATTTGCGAGTCTCT		
Tfam	Fw: CACCTCGACGGTGGTAATCT		
	Rv: AAGACCCTGGAGGAGCAGTT		
p62	Fw: CGTAAGGACCTTCTGGATCG		
	Rv: GTGCATATTGCTCTCGCACT		
BiP	Fw: TGTCACCGATCTGGTTCTTCAGGC		
	Rv: GTCCCATGACCAAGGACAACCATC		
Xbp1	Fw: CATCAACGAGTCACTGCTGGCCAA		
	Rv: CGCTGACGACTGTGTGTCC		

Table 3: List of Oligonucleotides

2.1.4. Antibodies

Description	Origin	Dilution	Application
mouse anti-Repo	8012 DSHB	1:100	Whole mount
rat anti-BiP	Babraham BT-GB-143P	1:200	Whole mount
rabbit anti-p62	Sébastien Gaumer (Nezis et al, 2008)	1:500	Whole mount
goat anti-GFP	Rockland	1:100	Whole mount
goat anti-rabbit Cy3	Jackson 111-165-045	1:200	Whole mount
goat anti-mouse AF 488	Invitrogen A11029	1:200	Whole mount
goat anti-mouse Cy3	Jackson Dianova 115-165-146	1:200	Whole mount
goat anti-rat AF 555	Mol. Probes A-21434	1:200	Whole mount
donkey anti-goat AF 488	Invitrogen A-11055	1:200	Whole mount
donkey anti-mouse AF 555	Invitrogen A-31570	1:200	Whole mount
donkey anti-rabbit AF 594	Invitrogen A-21207	1:200	Whole mount
TRITC-conjugated Phalloidin	Sigma-Aldrich	1:500	Whole mount
DAPI	Sigma-Aldrich	1:500	Whole mount
rabbit anti-actin	Sigma Aldrich A2066	1:2500	Western Blot
mouse anti-Tubulin	Sigma Aldrich T9026	1:15000	Western Blot
rabbit anti-GFP	Invitrogen A-6455	1:2500	Western Blot
rabbit anti-p62	Gabor Juhasz (Pircs et al, 2012)	1:3000	Western Blot
rabbit anti-EIF2S1 (P-eIF2α)	abcam ab32157	1:2000	Western Blot
goat anti-mouse 680 nm LT	Li-Cor 926-68020	1:15000	Western Blot
goat anti-rabbit 800 nm CW	Li-Cor 926-32211	1:15000	Western Blot

Table 4: List of Antibodies

2.1.5. Chemicals and consumable materials

Chemicals and consumable materials were purchased from the following suppliers: BioRad, Biozym, Braun, Fluca, Intenso, Balur, Kimberley-Clark, Marienfeld, Menzel, Merck, Pall, Pharmacia, PeqLab, Polysciences, Qiagen, Roche, Roth, Sarstedt, Schleicher & Schuell, Serva, Sigma, TPP and Verbatim.

Deionized, purified water was taken from the ELGA PURELAB *classic* water filtration system.

2.1.6. Kits

Kit	Provider	Application
ATP Bioluminescence Assay Kit CLS II	Roche Diagnostics GmbH	ATP measurement
PeqGOLD TriFast	PeqLab	RNA Extraction
QuantiTect Reverse Transcription Kit	Qiagen GmbH	Reverse transcription of mRNA
qPCR Green ROX L Mix	highQu GmbH	Real-time qPCR
BIOXYTECH Aconitase-340	OxisResearch	Aconitase activity assay
Coomassie Plus Protein Assay	Thermo Scientific	Bradford assay

Table 5: List of Kits

2.1.7. Equipment

Machine	Provider	Application
Centrifuge 5415D	Eppendorf	Microcentrifuge
digital pH/millivolt meter 611	Orion Research	pH meter
Axiophot	Zeiss	Fluorescence microscope
Leica M2 Fl III	Leica	Stereo fluorescence microscope
TCS SP8	Leica	Confocal microscope
Odyssey Infrared Imaging System	Li-Cor	Western Blot detection
CFX 96 Connect	Bio-Rad	Light cycler for qPCR
Stemi 2000 Stereomicroscope	Zeiss	Fly collection and preparation
Tecan infinite F500 plate reader	TECAN	ATP measurement
NanoDrop Spectrophotometer	PeqLab	Determination of RNA/DNA concentration
Ultrospec 3000 photometer	Pharmacia Biotech	Bradford and aconitase activity assays

Table 6: List of Equipment

2.1.8. Software

Program	Version	Provider	Application
CFX Manager	3.1	Bio-Rad	Operating software of CFX 96 Connect light cycler
GraphPad Prism	5.03	GraphPad Software	Graph design and statistical analysis
LAS X	3.01	Leica	Operating software of the Leica SP8 confocal microscope
Odyssey Software	1.2.15	Li-Cor	Operating software of Odyssey Imager
Image Studio Lite	5.2	Li-Cor	Western Blot Quantification
Tecan i-control	1.5.14.0	TECAN	Operating software of TECAN infinite F500
Fiji	2.0.0	Schindelin et al, 2012	Image processing and analysis
Office	2013	Microsoft	Figure design and writing of the thesis
Citavi	5.5.0.1	Swiss Academic Software GmbH	Citation Manager

Table 7: List of Software

2.2. Methods

2.2.1. Analysis of mRNA Expression

2.2.1.1. RNA extraction

15 flies, thoraces or 30 heads of the desired age were homogenized in 1 ml *TriFast* and centrifuged for 10 min (12000 g, 4°C). The RNA-containing supernatant was incubated for 5 min at RT and after addition of 200 µl of chloroform shaken for 10 s. After 2 min at RT and another centrifugation step (15 min, 12000 g, 4°C), the upper aqueous phase was transferred to a new tube and the RNA was precipitated with 0.5 ml isopropanol and incubated for 10 min at RT. After centrifugation (10 min, 12000 g, 4°C) the pellet was washed with 75% ethanol (in DEPC-H_2O), then solved in 50 µl DEPC-H_2O and incubated at 55°C for 10 min. Isolated RNA was quantified by measuring the absorbance at 260 nm with a *NanoDrop* spectrophotometer and frozen at -80°C.

2.2.1.2. gDNA wipe-out and reverse transcription

Reverse transcription of 500 ng isolated RNA was carried out with the *Quantitect Reverse Transcription Kit* according to manufacturer's instructions. The resulting cDNA was stored at -80°C.

2.2.1.3. Quantitative Real-time PCR

The cDNA was used for qPCR with *ORA qPCR Green ROX L Mix* on a CFX *connect* Real-Time PCR Detection System. The house-keeping gene RP49 was used as an internal control.

One reaction was composed of:

Template cDNA	0.5 µl
SYBR Green	5 µl
10 µM Primer fw	0.5 µl
10 µM Primer rv	0.5 µl
H_2O	ad 10 µl

The following PCR program was used for amplification:

Step/Repeats		Temperature	Duration
Pre-denaturation and activation of polymerase		95°C	2 min
Denaturation	40x	95°C	10 s
Annealing		60°C	10 s
Elongation		65°C	30 s

Table 8: qPCR program

The results were analysed using the comparative C_T method. The C_T value – standing for cycle threshold – represents the number of cycles at which the fluorescence exceeds a specific threshold value. The ΔC_T value represents the difference between the C_T of the target gene and the C_T of the housekeeping gene. The difference between the ΔC_T values of the genotypes compared is the $\Delta\Delta C_T$ value which is used for the calculation of the final ratio:

ΔC_T (control) = C_T (gene of interest) – C_T (housekeeping gene)

ΔC_T (sample) = C_T (gene of interest) – C_T (housekeeping gene)

$\Delta\Delta C_T = \Delta C_T$ (sample) – ΔC_T (control)

$2^{-\Delta\Delta CT}$ = final ratio

The mean ΔC_T value of all control reactions for a given gene was used as a reference and the other values were referred to this one to obtain the final fold change.

2.2.2. Analysis of protein expression

2.2.2.1. Protein extraction

For protein isolation, 10 flies, 15 thoraces or 30 heads were homogenized on ice in 100 µl Radioimmunoprecipitation assay (RIPA) extraction buffer containing 1x protease inhibitor (*cOmplete Mini*, Roche). After two centrifugation steps (6 min, 10000 rpm, 4°C) the supernatant was collected and frozen at -80°C.

2.2.2.2. SDS-PAGE

For Polyacrylamide gel electrophoresis (PAGE), 15 µl protein lysate was mixed with 5 µl 4x Laemmli buffer, boiled at 95°C for 5 min and loaded onto the gel.

Proteins were separated on 5% stacking and 10% separating gels containing the following ingredients:

5 % Stacking gel	10 % Separating gel
2.96 ml ddH_2O	3.88 ml ddH_2O
0.5 ml 40% Acrylamide-Bisacrylamide	2 ml 40% Acrylamide-Bisacrylamide
0.5 ml 1 M Tris-HCl pH 6.8	2 ml 1.5 M Tris-HCl pH 8.8
40 µl 10% SDS	80 µl 10% SDS
40 µl 10% APS	50 µl 10% APS
4 µl TEMED	5 µl TEMED

Table 9: Components of a SDS gel

Gel runs were performed at 110 V for 2 h.

2.2.2.3. Semi-dry Western Blot

After gel electrophoresis, separated proteins were transferred to a nitrocellulose membrane through semi-dry blotting. The setup of the blot is shown in Figure 10. Negatively charged SDS-protein complexes were transferred to the membrane by applying 400 mA current for one hour.

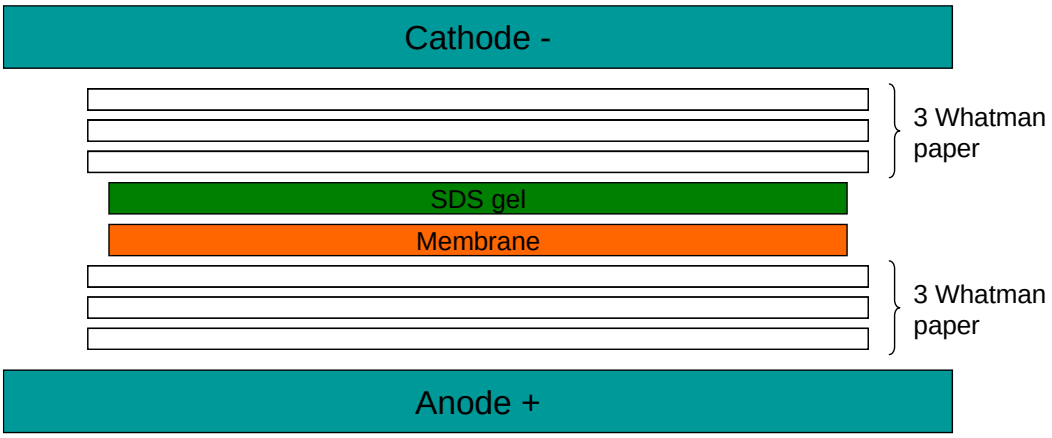

Figure 10: Semi-dry blotting setup

The anode is at the bottom, followed by 3 whatman papers, the membrane, the gel and 3 more whatman papers. At the top is the cathode.

2.2.2.4. Antibody staining

After blotting, the membrane was agitated in 1x TBS (tris buffered saline) for 5 min to wash off residual methanol. The membrane was blocked in OBB:TBS 1:1 for 2 h afterwards to prevent unspecific binding of the primary antibody to the membrane. Incubation with the primary antibody was performed overnight at 4°C and gentle shaking. After three 10 min washing steps with 1x TBST (TBS with *Tween 20*) to remove excess primary antibody, the membrane was incubated with the appropriate secondary antibody for 2 h. Finally, the membrane was washed three times with 1x TBST for 10 min and stored in 1x TBS. Western blots were scanned with the *Odyssey Infrared Imaging System*. Protein levels were determined by comparing the ratio of the signal intensity from the protein of interest with a housekeeper protein using *Image Studio Lite*.

2.2.3. Determination of protein concentration for biochemical assays

To determine the concentration of protein content in samples, a Bradford assay was performed using the *Coomassie Plus Protein Assay*.

Prior to the assay, the Bradford reagent was allowed to warm up to RT. 20 µl of sample were added to 1 ml of reagent and incubated at RT for 5 min. After that the absorbance at 595 nm was measured with an Ultrospec 3000 Photometer and subtracted from the blank value (20 µl of respective buffer added to 1 ml Bradford reagent). The absorbance was then plotted against a bovine serum albumin (BSA) standard curve derived from the measurement of a series of BSA stock dilutions of a known concentration.

2.2.4. Analysis of ATP concentration

2.2.4.1. Sample preparation

5 thoraces of anesthetized flies were separated from the rest of the body and transferred to microcentrifuge cups. After homogenization in 200 µl boiling ATP buffer, the cups were heated at 95°C for 2 min and centrifuged (3500 rpm, 1 min). The supernatant was transferred to a new cup and diluted 1:3.

2.2.4.2. Luciferase assay

ATP levels were measured with the *ATP Bioluminescence Assay Kit CLS II*.

In one well of a 96-well plate (*Greiner Flat Bottom Black Polystyrol*), 50 µl of the diluted sample were mixed with 50 µl luciferase. The plate was then placed in the *TECAN Infinite F500 micro plate reader* and the luminescence was measured using the following parameters:

Integration time: 10000 ms
Settle time: 1000 ms
Attenuation: Automatic

The concentration of ATP in µM was determined by plotting the luminescence values against an ATP standard curve derived from the measurement of a series of dilutions of ATP stock solutions of known concentrations. Finally, dividing the ATP concentration by the protein amount obtained from the Bradford assay yielded the normalized ATP concentration.

2.2.5. Measurement of aconitase activity

Total aconitase activity was determined from whole individuals using the BIOXYTECH Aconitase-340 Spectrophotometric Assay kit. 10 whole flies or 15 thoraces were placed in a tube containing 500 µl of ice-cold homogenization buffer and squished. The resulting suspension was centrifuged twice at 800 g for 10 min at 4ºC discarding the pellet every time. The supernatant was then disrupted by sonication for 30 s with 1 s interval between each pulse.

For the assay, 100 µl of the extraction was pipetted into cuvettes and complemented by adding 100 µl assay buffer, 200 µl substrate, 200 µl enzyme and 200 µl NADP, all part of the Aconitase Assay kit. The absorbance at 340 nm was then measured over 25 min at 37°C in the *Ultrospec 3000* Photometer and the aconitase activity was calculated according to manufacturer's instructions. Finally, the aconitase activity was normalized to the protein amount of each sample using the Bradford assay.

2.2.6. Germline transformation of mtRosella clones

2.2.6.1. Microinjection

The mtRosella vector was kindly provided by Prof Dr. Benedikt Westermann (Böckler & Westermann, 2014) and cloned into the Gateway® entry vector pENTR/D-TOPO® by the lab technical assistant Gudrun Karch. The transgene was then integrated into the third chromosome of the *Drosophila* genome using the PhiC31 integrating cassette as follows:

50 ng/µl of plasmid DNA was injected into 30 – 60 min old embryos at 18°C. The embryo's chorion was removed via double-adhesive tape and the embryos were strung together on apple juice agar. Afterwards, they were dried for 10 min on silica gel and overlaid with voltalef oil. Then, the plasmid DNA was injected near the pole cells through a broken glass needle with a pressure of one bar. The injected embryos were placed on apple juice agar plates and kept at 18°C until hatching. Hatched larvae were transferred to food vials and kept at 25°C until eclosion.

2.2.6.2. Selection of transformants and creation of stable lines

Adult males were crossed to virgins of the genotype w; D3/TM3. Offspring of the genotype w; UAS-mtRosella/TM3 were then crossed among each other to generate the stable line UAS-mtRosella/TM3.

Three independent lines were obtained for the construct.

2.2.7. Whole mount preparation and image acquisition

2.2.7.1. Brain and muscle dissection

Adult flies of the appropriate age were fixed in PBS (phosphate buffered saline) with 4% paraformaldehyde and 0.5% Triton X-100 for 2 h. Brains or thoraces were then dissected in 0.1% PBST under the binocular and either mounted directly or stained with antibody.

For antibody staining, all steps were conducted in the dark. Brains/muscles were washed twice for 10 min each with 0.1% PBST and then blocked in 0.5% PBST containing 10% normal goat serum (NGS) to prevent non-specific antibody binding. The brains/muscles were incubated with primary antibody in 0.5% PBST with 10% NGS overnight at 4°C. On the next day, they were washed 5 times for 10 min with 0.1% PBST and incubated with the secondary antibody overnight at 4°C. After washing again 5 times for 10 min, the brains/muscles were mounted in VectaShield on microscope slides, sealed with nail polish and kept at 4°C in the dark until further use.

For TMRE staining, muscles were dissected without fixation and the hemithoraces incubated with 1 µm TMRE in Relaxing solution for 15 min. After washing twice with Relaxing solution for 5 min, they were mounted in VectaShield and immediately imaged. Unfortunately, this dye could only be used in muscles, since unfixed tissue is needed for the staining and brains did not maintain their integrity during the staining protocol.

2.2.7.2. Confocal microscopy

All samples were scanned with a Leica TCS SP8 confocal microscope and image acquisition settings were kept constant for every condition. Samples were excited with a UV diode at 405 nm, an argon laser at 488 nm (10% tube current), a DPSS laser at 561 nm and a helium-neon laser at 594 nm. Emitted signals were detected with a HC PL APO 40x/1.30 Oil CS2 objective (brains) or HC PL APO 63x/1.30 Glyc CORR CS2 objective (muscles) at 410-470nm (DAPI), 490-540nm (GFP, AF488), >565nm (AF555, Cy3), > 595nm (AF594), >640nm (AF633). Images were generated at a resolution of 1024 x 1024 pixels. Brains and muscles were scanned in z-stacks (1 µm and 0.33 µm, respectively) with 30-35 images per brain/muscle.

For ratiometric analysis of mitoroGFP-Grx1, acquisition parameters were chosen so that the 405 nm/488 nm ratio of controls was approximately 1.0.

2.2.7.3. Image handling and editing

All confocal images were further processed with the image processing software Fiji 2.0.0 (Schindelin et al, 2012). In detail, background was subtracted in ImageJ via the ‘Rolling Ball’ method (Radius = 50 pixels). Maximum projections of three (muscle images) to thirty (brain images) slices were made and the resulting image was again subjected to background subtraction. Finally, contrast of each image was adjusted to improve quality of signal.

2.2.8. Image quantification

2.2.8.1. Number of giant glial cells

For the counting of giant glial cells of the inner optic chiasm, brains were co-labelled with nuclear GFP and anti-Repo. Brain projections were generated as described above and the amount of cells forming the inner crescent in the optic lobe (see Figure 11A) were counted manually. Only cells displaying both signals were considered.

2.2.8.2. Ratio of mitochondrial to cytosolic TMRE

For quantification of the ratio of mitochondrial to cytosolic TMRE signal, five flies per genotype were analysed. For each fly, three independent squares (1600 µm^2 each) of single slices were used for the analysis and the results averaged. Mitochondrial and cytosolic (total – mitochondrial) TMRE signals were quantified and a ratio of both signals was calculated to determine the percentage of mitochondrial signal in both genotypes. In all cases, background was subtracted (Rolling Ball; 25 pixel size), images were filtered to improve segmentation (Median with Radius = 1) and automatic thresholding (Li method) was used to avoid excessive manipulation.

2.2.8.3. Number of p62-positive vesicles

For the quantification of p62-positive vesicles, five thoraces per genotype and condition were analysed. For each thorax, five independent areas of 1600 µm^2 were selected and a z-projection of 30 single images was generated (diameter: 10 µm). In each random square of 1600 µm^2, the threshold was set using the default method in ImageJ. The particles were then analysed with the following options to receive the number of p62 vesicles present in a square: Size 30-Infinity, Circularity 0.40-1.00, Include holes. The results of each thorax were averaged.

For co-localization with GFP-Atg8a or LAMP1-GFP, each p62 vesicle was manually identified for co-localization with the respective marker.

For co-localization with TMRE, each p62 vesicle was manually identified for co-localization with both pHluorin and dsRed.

2.2.8.4. GSSG/GSH ratio

For ratiometric quantification of mitoroGFP-Grx1, each slice of a z-stack was processed as follows: After background subtraction in each channel, a ratio image was generated by dividing the 405 nm channel (GSSG) by the 488 nm channel (GSH) pixel by pixel. For image segmentation, the 488 nm channel was filtered (Median; radius = 1), thresholded with the Li method in Fiji and the resulting selection transferred to the 405/488 ratio channel to distinguish the mitochondrial region. Pixel intensity was then measured for the selection and averaged over all slices. For visual representation, all pixels outside the selection were set to NaN (not a number) and the image displayed in false colors using the lookup table “Fire”.

2.2.9. Paraffin sections of fly brains

Paraffin sections were performed from 35-day-old adult flies. Flies were strung on a collar, fixed for 4 h in carnoy, dehydrated in ethanol three times for 30 min and left overnight in

methylbenzoate. The next day, the collars were placed in a 1:1 solution of methylbenzoate/ paraffin at 60°C for 1 h, washed 6 times for 30 min each at 60°C in paraffin and finally embedded in paraffin. Paraffin sections (7 µm) were made using a Reichert Jung microtome, transferred to slides coated with glycerine-BSA and covered in water. The slices were flattened on a heating plate at 40°C and left to dry overnight. The next day, the slides were washed twice in xylole for 30 min, mounted with DPX and analysed under a fluorescence microscope.

For quantification of brain vacuolization, the size of the combined medulla and lamina region (Figure 24A) and whole vacuole size were measured in Fiji. The affected area was then referred to as percentage of total brain area.

2.2.10. Semi-thin epon plastic sections of fly brains

For examination of lipid accumulation with light microscopy, semithin epon plastic sections from 35-day-old adult fly brains were prepared as follows: Heads were fixed in 5% Glutaraldehyd overnight and then dehydrated seven times for 10 min each in ethanol and three times for 10 min in propylenoxide. Afterwards, they were kept in a 1:1 solution of propylenoxide and Epon overnight and then in Epon for five hours. Finally, they were embedded in Epon by keeping them at 60°C overnight. Epon sections (1 µm) were made using a microtome, transferred to slides, dried at 50°C and mounted with DPX.

Lipids were identified by characteristically dark droplet-like structures.

2.2.11. Life span determination

To determine the life span of flies, 100 male flies were collected within 24 h after eclosion and evenly distributed to four vials without yeast. Every two to three days the flies were transferred to new vials containing fresh food. Lifespan experiments were conducted in standard cornmeal agar medium.

2.2.12. Chemical treatment and hyperoxia

For chemical treatments, Instant Drosophila Medium (Formula 4-24, Carolina Biological, North Carolina) was rehydrated with the following chemicals: 15 mM Tauroursodeoxycholic acid (TUDCA), 50 µm Rapamycin. As control treatment, Instant Drosophila Medium was reconstituted with distilled water (for TUDCA) or dimethyl sulfoxide (DMSO) diluted in distilled water (for Rapamycin). Within 24h after eclosion, flies were transferred to vials containing the corresponding food.

Hyperoxia treatment started one day post-eclosion and was performed by exposing flies in a glass container with a constant flux of 99.5% oxygen under a low positive pressure at 25°C (Botella et al, 2004).

2.2.13. Negative geotaxis assay

Locomotor assays were performed as previously described in Botella et al, 2004. 10-12 flies per genotype were assessed and each fly was recorded 3 times. The mean value of each fly was used for the subsequent analysis.

2.2.14. Statistical analysis and graphing

Results were analysed statistically and graphed using GraphPad Prism 5.03. Survival data were analysed using the Log-rank (Mantel-Cox) test. In all further experiments, data are represented as mean ± s.e.m. Significance was determined by two-tailed T-test or by One-way ANOVA with post hoc Dunnett or Tukey Multiple Comparison Test (***: $P < 0.001$; **: $P < 0.01$ and *: $P < 0.05$).

3. Results

3.1. Glia and muscles as model tissues to study mitochondrial homeostasis in FRDA

As a mitochondrial protein, loss of frataxin adversely affects mitochondrial function (Pandolfo, 2012). Therefore, it appeared interesting to analyse the complete mitochondrial network and to study how the cells try to counteract the defects. In this thesis, I decided to forgo neurons, even though FRDA is primarily a neurodegenerative disease, However, during my previous master thesis (Edenharter, 2013), I could show that concomitant dicer2 co-expression (which enhances the effect of RNAi) is necessary in neurons to elicit a mitochondrial phenotype, except under prolonged hyperoxic conditions. Unfortunately, dicer2 expression by itself already proved to influence mitochondrial morphology in neurons (see Appendix Figure 38). Therefore, I chose to focus on two other tissues described to be involved in FRDA: glia and muscles.

Glia have already been described as a prime target of frataxin depletion in patients (Morral et al, 2010), while muscles display high mitochondrial density. In addition, both tissues share the advantage that strong depletion of frataxin (fhRNAi1) is compatible with flies reaching adulthood. Frataxin knockdown in glial cells using the *Repo*-Gal4 driver line has already been shown to evoke phenotypes that resemble the human condition, such as locomotor deficits, damage to brain integrity and reduction of lifespan (Navarro et al, 2010). In addition, influencing iron metabolism in glia alone was able improve fly fitness (Navarro et al, 2015).

As there is a number of different glial cell populations, I decided to focus on one specific subgroup in this work, the giant glial cells (GGC) of the inner optic chiasm (Figure 11A). These cells are a specialized form of ensheathing glia that wrap around the axon tracts which project between neuropils (Tix et al, 1997). They possess certain characteristics which make them ideal for the task: They are large, easily distinguishable from surrounding glial populations and localized in the brain region where vacuolization was detected upon frataxin depletion (Navarro et al, 2010).

Drosophila muscles, on the other hand, emerged as a promising tissue to study mitochondrial dynamics because of their mitochondrial density. Due to their high energy demands, muscles are comprised of a sizeable amount of mitochondria and thus are highly sensitive to disturbances in mitochondrial homeostasis. Mitochondria are embedded between the myofibrils along their entire length to provide ample supply of ATP to the sarcomeres (Figure 11B). Here, I specifically focused on the indirect flight muscles (IFM), as they are easily

dissected and visualized, having been used before in the study of other neurodegenerative diseases such as Parkinson's disease (Pesah et al, 2004; Deng et al, 2008; Pogson et al, 2014).

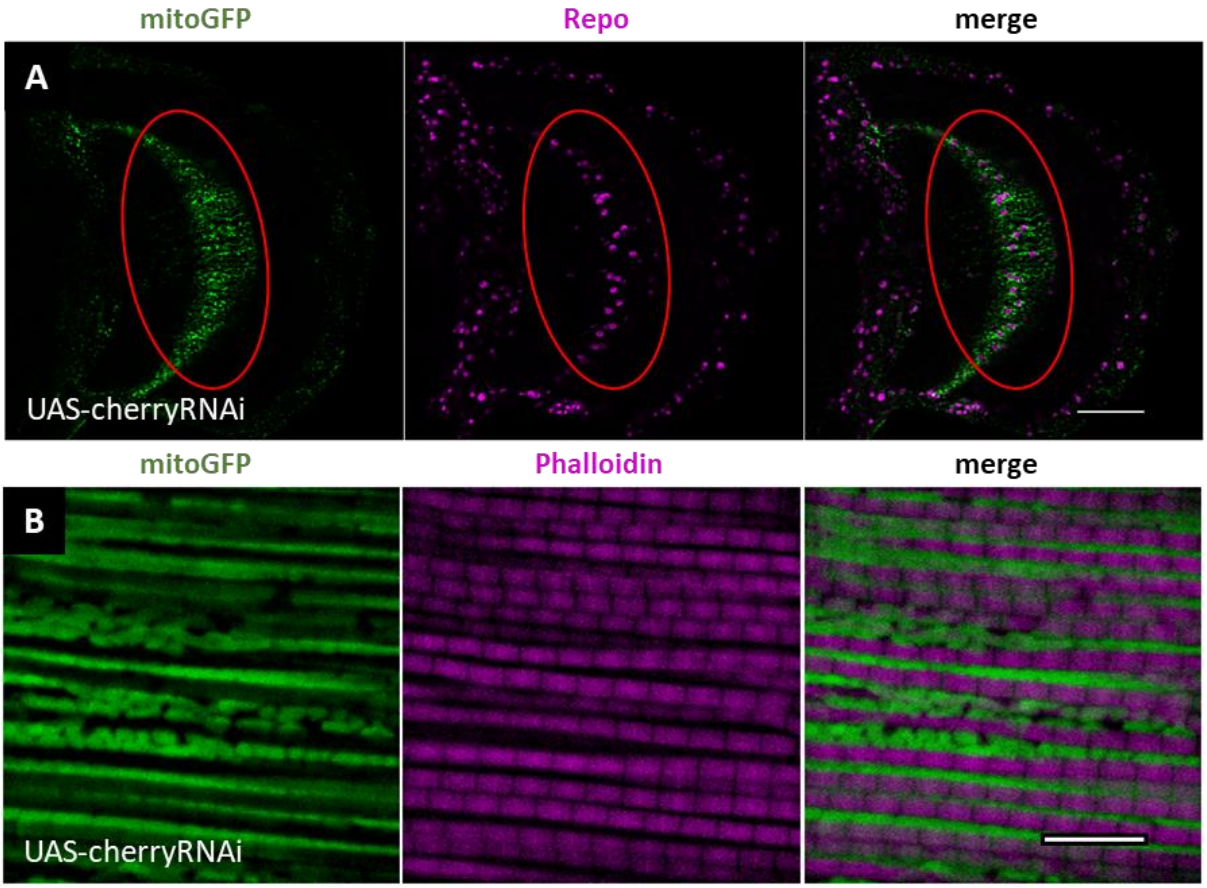

Figure 11: Overview of areas investigated in the glial and muscle systems

(A) Representative optic lobe of a control fly (*Repo*-Gal4 > UAS-mitoGFP, UAS-cherryRNAi) labeled with mitoGFP (green) and stained for Repo (magenta). Red oval denotes the GGC region of the inner optic chiasm. Scale bar represents 40 µm. (B) Representative IFM of a control fly (*Mef2*-Gal4 > UAS-mitoGFP, UAS-cherryRNAi) labeled with mitoGFP (green) and stained with Phalloidin (magenta). Mitochondria are organized in chains in between the myofibrils. Scale bar represents 10 µm.

As there has been no previous study describing the effects of targeted frataxin knockdown in the *Drosophila* muscular system, I first wanted to verify if frataxin silencing in muscles using the driver line *Mef2*-Gal4 would reproduce the alterations described in ubiquitous knockdown (Figure 12). Interestingly and in contrast to glial specific knockdown (Navarro et al, 2010), larval development and pupal eclosion rate were normal, even though fly fitness was severely affected. Frataxin depletion led to a severe reduction in both median (from 59d to 9d) and maximum (from 62d to 13d) lifespan (Figure 12A). Locomotion of flies was strongly reduced already at 3d (66 %) and completely abolished at 5d (90 %; Figure 12B). At this age, flies were basically unable to move and mostly remained at the bottom of the vial. In agreement, ATP production was reduced in all tested ages, being significantly lower at 5d (66 %) and 10d (50

%) (Figure 12C). In line with these results, aconitase activity was already reduced by 40% after 5d (Figure 12D).

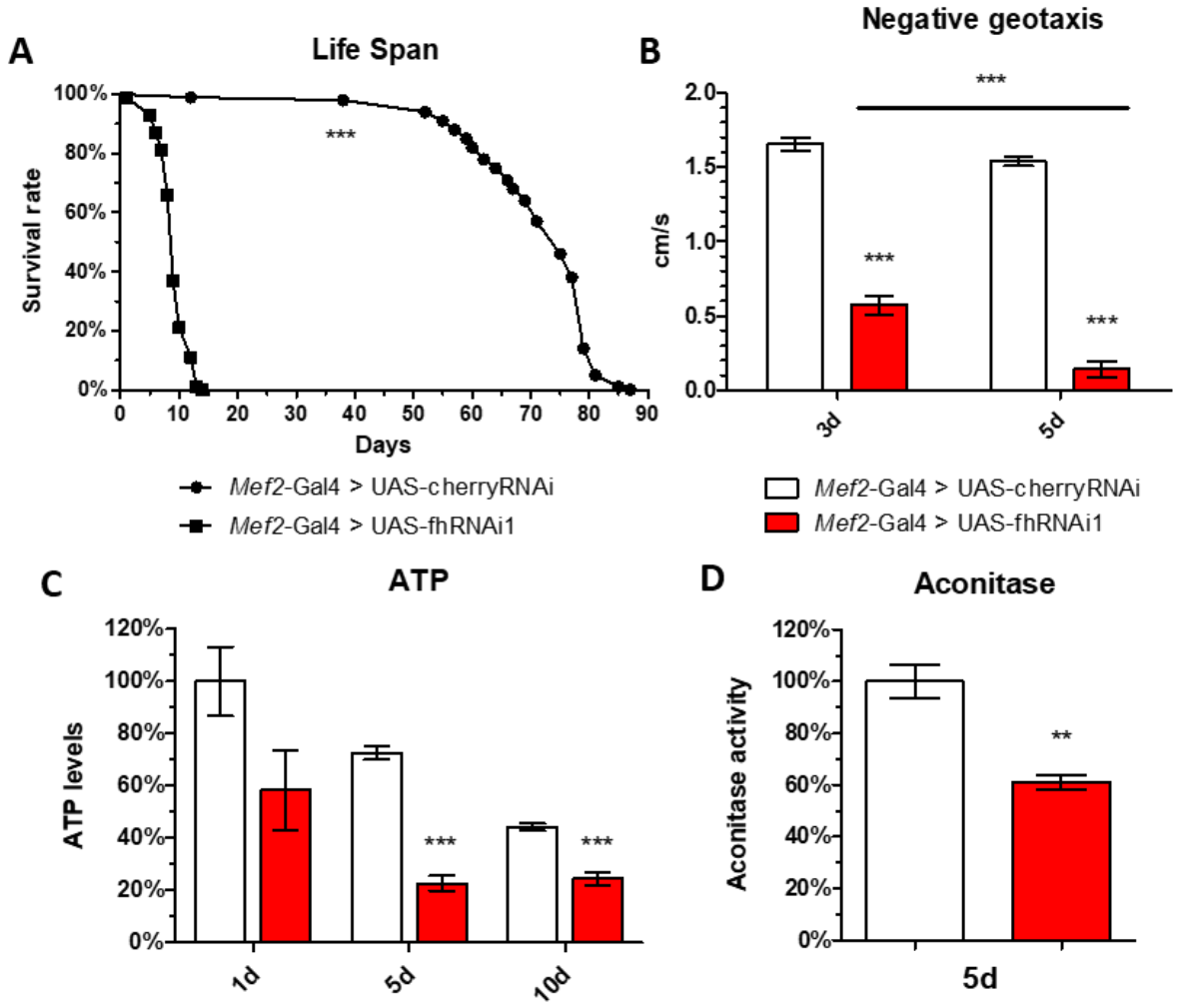

Figure 12: Frataxin depletion in muscles is deleterious

(A) Life span of frataxin depleted flies is severely lowered. n = 100. (B) Negative geotaxis of flies is diminished after 3 days and almost completely abolished after 5 days. n = 12. (C) Frataxin knockdown leads to an age-dependent reduction in available ATP. n = 5. (D) Aconitase activity is reduced after 5d. n = 3.

Taken together, loss of frataxin in muscles was enough to recapitulate known hallmarks of FRDA and therefore confirmed the feasibility of this tissue for further analysis.

3.2. Frataxin silencing affects mitochondrial integrity and dynamics

3.2.1. Mitochondrial morphology is altered

First, I wanted to determine if and how the mitochondrial network is altered when frataxin is depleted. For visualization of mitochondria, I used a mitochondrial-targeted GFP variant (mitoGFP).

In glial cells, co-staining with anti-Repo enabled me to determine the position of the nuclei. An overview over the optic lobe suggested a difference in the mitoGFP pattern after 35d in the GGCs (Figure 13A, B). A closer inspection of this region revealed that mitochondria in control flies were more evenly distributed (Figure 13A'), while they were clustered around the nuclei in frataxin depleted flies (Figure 13B').

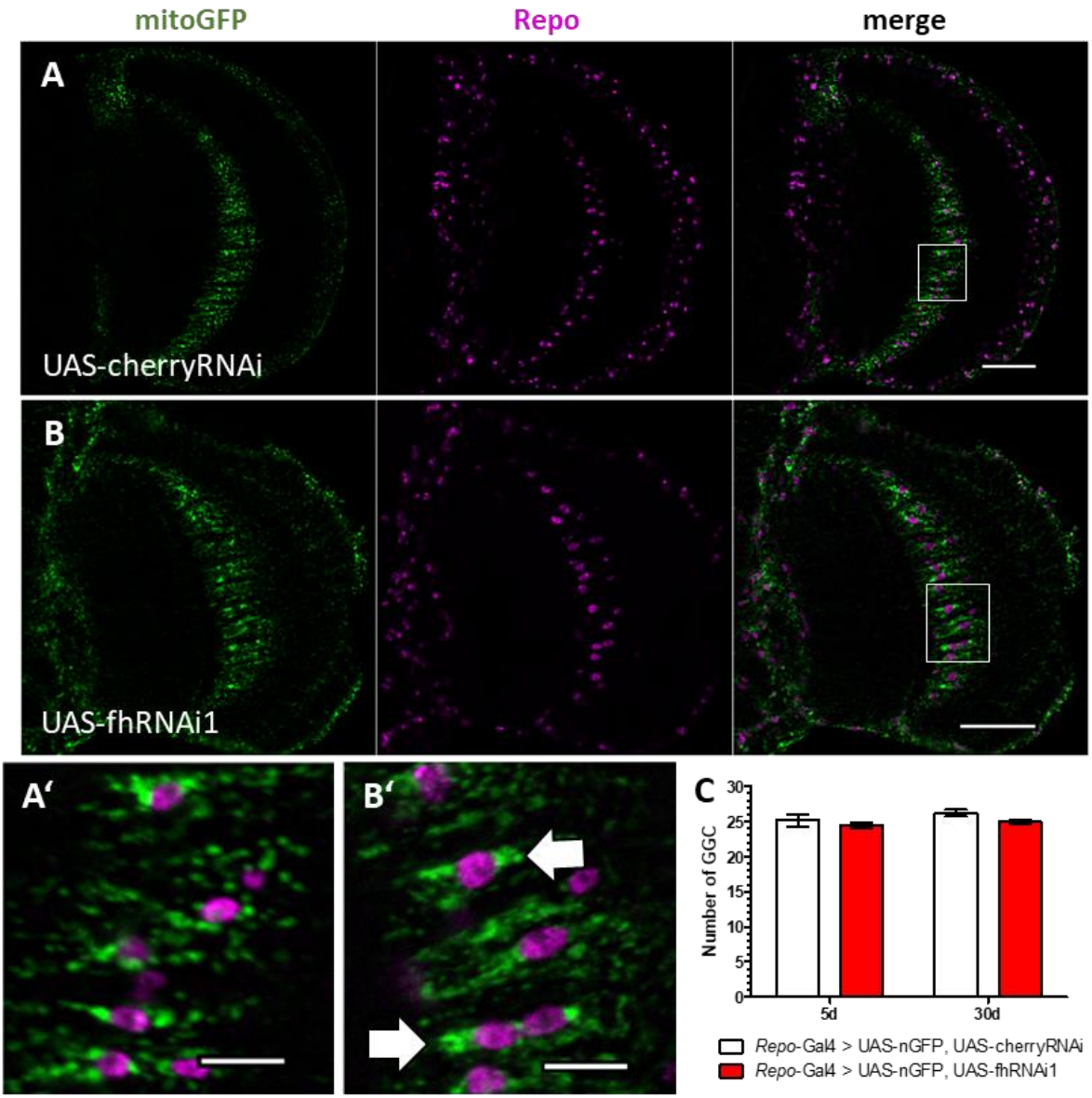

Figure 13: Mitochondrial morphology and distribution is altered in glia

(A-B) Representative optic lobes of 35d old control (A; *Repo*-Gal4 > UAS-mitoGFP, UAS-cherryRNAi) and frataxin knockdown flies (B; *Repo*-Gal4 > UAS-mitoGFP; UAS-fhRNAi1) labeled with mitoGFP (green) and stained for Repo (magenta). Scale bar represents 40 µm. (A'-B') Magnification of the GGC region of the inner optic chiasm from A and B, respectively (white squares). Control mitochondria are more evenly distributed (A'), while frataxin knockdown mitochondria accumulate around nuclei (B'), forming clusters (arrows). Scale bar represents 10 µm. (C) Quantification of the amount of GGCs in control (*Repo*-Gal4 > UAS-nGFP; UAS-cherryRNAi) and frataxin deficient flies (*Repo*-Gal4 > UAS-nGFP, UAS-fhRNAi1). The total number of GGCs per brain hemisphere is approximately 25 and is not affected in frataxin knockdown flies. n = 5.

Even though the mitochondrial network appeared disturbed, this did not induce loss of glial cells (Figure 13C). The total number of GGCs was approximately 25 in both controls and frataxin depleted flies at young and advanced ages.

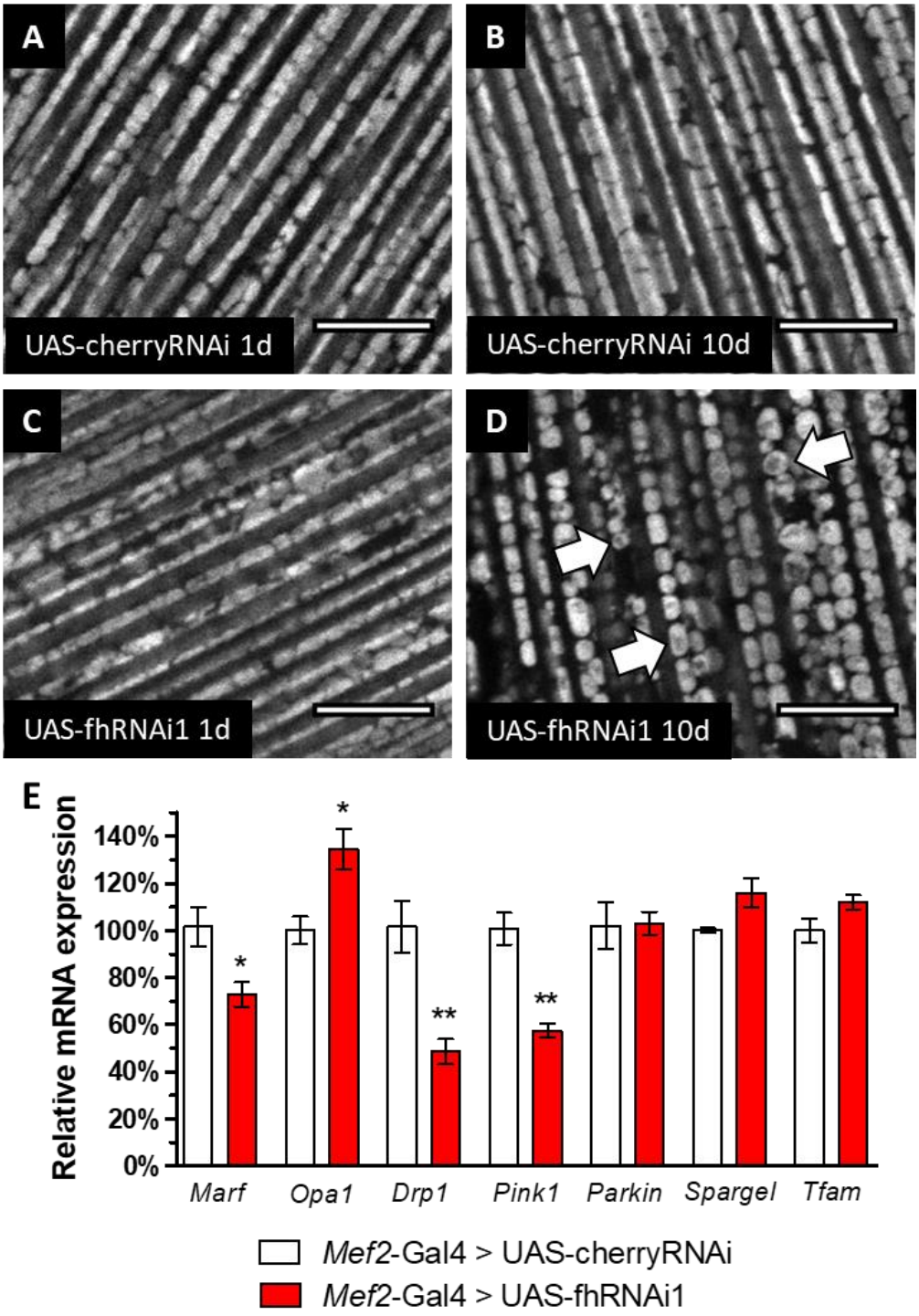

Figure 14: Mitochondrial morphology is disturbed in muscles

(A-D) Representative IFM labeled with mitoGFP. Scale bars represent 10 µm. (A-B) 1d (A) and 10d (B) old control flies (*Mef2*-Gal4 > UAS-mitoGFP, UAS-cherryRNAi). Mitochondrial morphology appears normal. (C-D) 1d (C) and 10d (D) old frataxin knockdown flies (*Mef2*-Gal4 > UAS-mitoGFP, UAS-fhRNAi1). Mitochondrial morphology is comparable to controls after 1d, but a strong fragmentation occurs after 10d. Arrows indicate 'donut'-like mitochondria. (E) Relative transcription levels of genes involved in mitochondrial dynamics, mitochondrial quality control and biogenesis. n = 4.

In muscles, mitochondria in control flies formed a continuous network with long, linear chains (Figure 14A, B). In frataxin knockdown flies, the mitochondrial network initially did not differ from controls (shortly after eclosion; Figure 14C). However, mitochondrial integrity was clearly compromised after 10d (Figure 14D). Mitochondria were smaller and rounded, with visible gaps in the chain, hinting at increased mitochondrial fragmentation.

Additionally, hollow, ring-like mitochondria could be observed (arrows), termed 'donut'-like mitochondria (Liu & Hajnoczky, 2011). This mitochondrial conformation is thought to be an adaptation of the network to stress conditions or an early stage of mitochondrial degradation by mitophagy (Bhandari et al, 2014).

Since mitochondrial morphology was severely altered, I wanted to evaluate whether changes in expression level of genes involved in mitochondrial homeostasis were responsible for the observed differences (Figure 14E). I included genes involved in mitochondrial fusion and fission (*Marf, Opa1* and *drp1*), mitochondrial quality control (*Pink, Parkin*) and mitochondrial biogenesis (*Spargel, Tfam*). Spargel and Tfam function as transcriptional coactivator and transcription factor, respectively, in mediating mitochondrial biosynthesis (Tiefenbock et al, 2010; Islam et al, 2012). *Opa1*, a fusion gene, was upregulated by one third, while *drp1*, a fission gene, was downregulated by about 50%, suggesting a tendency for increased fusion. This seems to be in contrast to the observed mitochondrial fragmentation. Remarkably, the expression level of the fusion gene *Marf* was slightly lower in FRDA flies, indicating a unique role for *Marf* in this context. *Pink1* was downregulated to 50%, while *Parkin* levels were unaffected. This was surprising considering that *Pink1* and *Parkin* are known to work together in promoting mitophagy. Lastly, both *Spargel* and *Tfam* levels were unaffected, implying an unaltered regulation of mitochondrial biogenesis. Overall, visible changes in mitochondrial morphology could not directly be correlated to adjustments in expression profiles of mitochondrial homeostasis genes.

3.2.2. Mitochondrial membrane potential is compromised

As mitochondrial structure was unquestionably impaired, I next wanted to ascertain that the visible changes were corresponding to a functional damage. Therefore I used the dye TMRE, which selectively accumulates in mitochondria that exhibit normal membrane potential.

In control flies, TMRE co-localized with mitoGFP almost perfectly, both in newly eclosed flies and 6d old flies (Figure 15A and B, respectively). This indicates healthy mitochondria with normal membrane potential. Interestingly, in 1d old frataxin depleted flies that showed a normal mitochondrial structure (Figure 14C), TMRE was already absent in certain mitochondria

(Figure 15C). This result indicates the presence of both damaged (arrow) and healthy mitochondria (arrowhead).

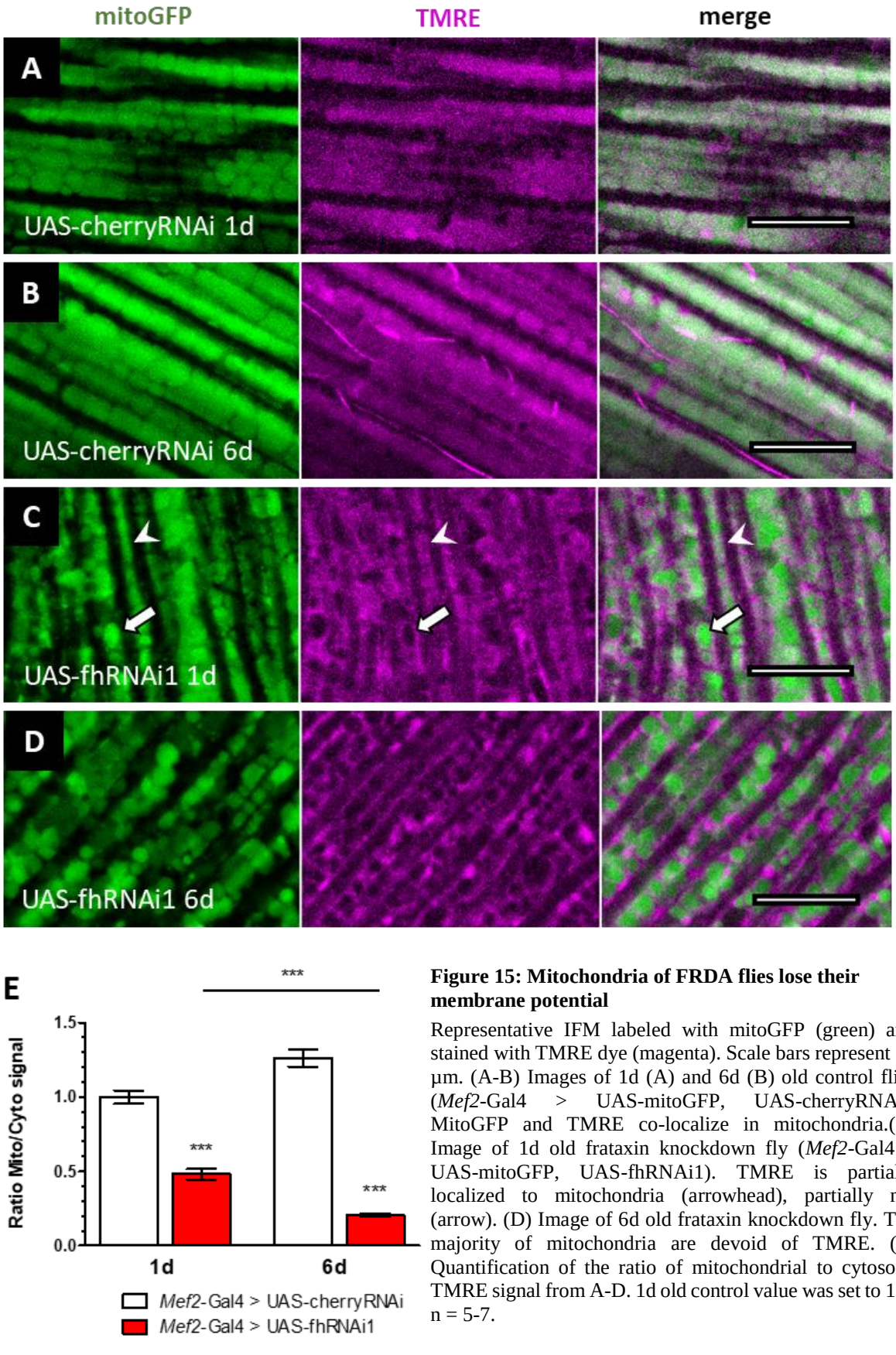

Figure 15: Mitochondria of FRDA flies lose their membrane potential

Representative IFM labeled with mitoGFP (green) and stained with TMRE dye (magenta). Scale bars represent 10 µm. (A-B) Images of 1d (A) and 6d (B) old control flies (*Mef2*-Gal4 > UAS-mitoGFP, UAS-cherryRNAi). MitoGFP and TMRE co-localize in mitochondria.(C) Image of 1d old frataxin knockdown fly (*Mef2*-Gal4 > UAS-mitoGFP, UAS-fhRNAi1). TMRE is partially localized to mitochondria (arrowhead), partially not (arrow). (D) Image of 6d old frataxin knockdown fly. The majority of mitochondria are devoid of TMRE. (E) Quantification of the ratio of mitochondrial to cytosolic TMRE signal from A-D. 1d old control value was set to 1.0. n = 5-7.

After 6d, there was almost no co-localization between TMRE and mitoGFP anymore, implying that most mitochondria show a pathological reduction of membrane potential and ultimately lost the ability to produce ATP (Figure 15D).

Quantification of the ratio of mitochondrial to cytosolic signal confirmed these results (Figure 15E). In 1d old frataxin depleted flies, the signal ratio was reduced from 1.0 to 0.5, indicating loss of membrane potential in half of the mitochondria. After 6d, the ratio was significantly decreased to 0.2, demonstrating substantial mitochondrial deficiency. These results suggest that mitochondria are predominantly still intact after eclosion, but rapidly deteriorate with age. This is in agreement with the biochemical phenotypes from Figure 12 and the mitochondrial morphology from Figure 14, which were also age-dependent.

In conclusion, frataxin knockdown leads to a disturbance in mitochondrial morphology progressing with age. This corresponds to a loss of membrane potential and subsequently function, such as ATP production.

3.2.3. Oxidative stress response is altered

Another established hallmark of Friedreich's ataxia is susceptibility to oxidative insult (Wong et al, 1999). As in humans, oxidative stress has also been found to be of importance in the *Drosophila* model. Flies lacking frataxin were highly sensitive to oxidative stress, while hydroxide scavenging improved FRDA phenotypes. Interestingly, this was also the case for glial specific frataxin depletion (Llorens et al, 2007; Anderson et al, 2008; Navarro et al, 2010).

I wanted to assess whether such sensitivity was related to a redox imbalance. An interesting tool for visualization of redox homeostasis directly *in vivo* is the development of a redox sensitive GFP, named roGFP, which changes its excitation maximum from 488 nm to 405 nm when oxidized (Hanson et al, 2004). More recently, this tool has been optimized by fusion of a glutaredoxine (Grx1) to the roGFP, which allows effective measurement of the ratio of oxidized glutathione (GSSG; 405 nm) to reduced glutathione (GSH; 488 nm) (Gutscher et al, 2008). Lastly, targeting of roGFP-Grx1 to mitochondria permits the specific measurement of the glutathione redox potential within this organelle (Albrecht et al, 2011). I used this mitoroGFP-Grx1 construct to investigate whether the redox state of the mitochondrial glutathione pool was affected. The ratio of controls was set to 1.0 (Figure 16). In glial cells of 35d old flies, the 405/488 nm ratio was decreased by 0.2 in FRDA flies, meaning that more glutathione was present in a reduced state compared to controls (Figure 16A-B). This was surprising, considering that oxidative stress, described to be present in this FRDA model, should result in an increase in the 405/488 nm ratio. In muscles, the effect was even more pronounced (Figure

16C-D). The 405/488 nm ratio was decreased to 0.58 in this tissue. Since this result conflicted with the predicted change, I tested the validity of the approach by applying DTT to the flies prior to fixation. DTT acts as a strong reductant and shifts roGFP to its most reduced state (Albrecht et al, 2011). As expected, DTT reduced the 405/488 nm ratio, to about 0.46 in muscles (Figure 16D). This confirms that loss of frataxin shifts the mitochondrial glutathione pool to a more reduced state.

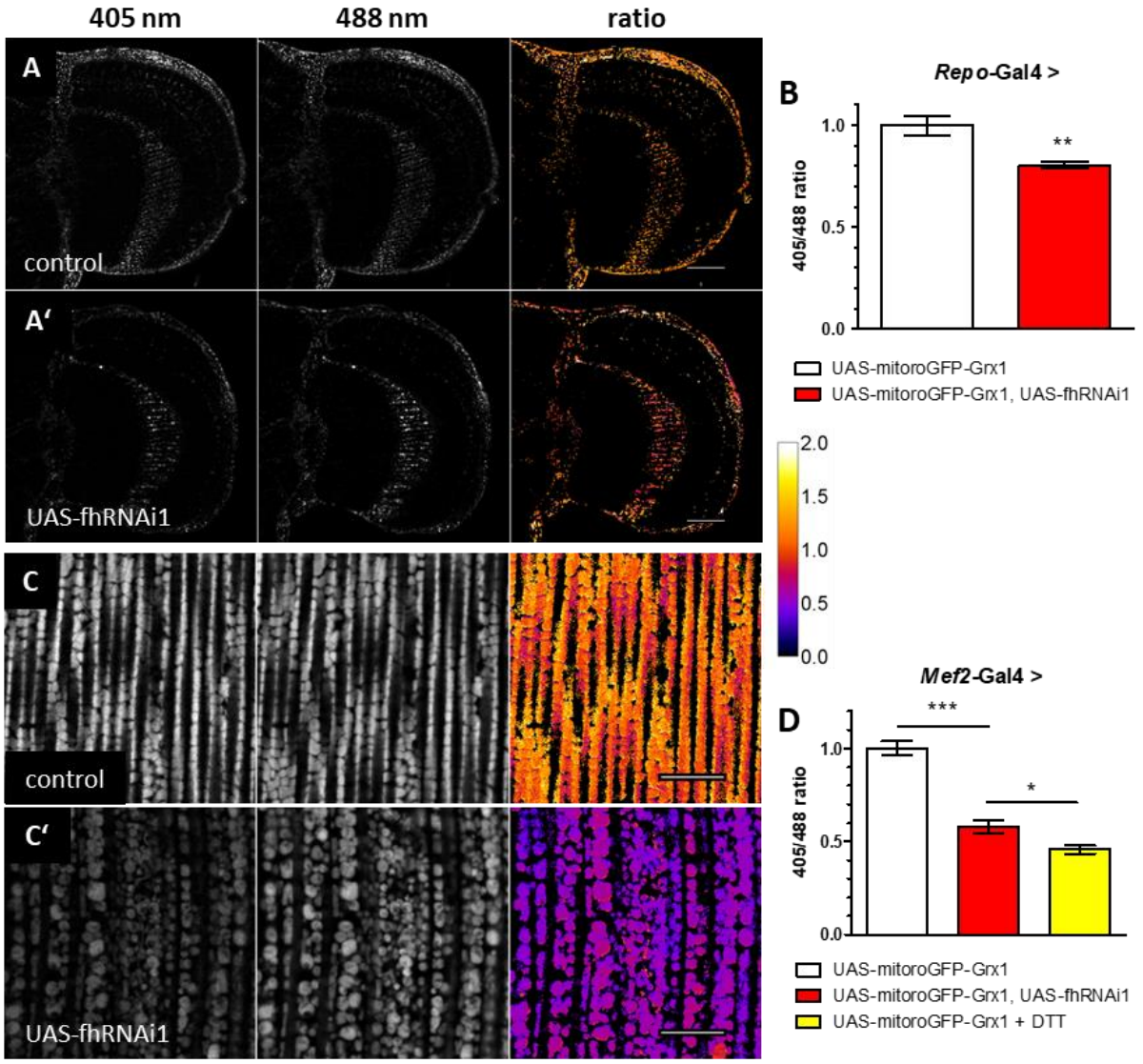

Figure 16: Glutathione is reduced upon frataxin silencing

(A-A') Representative optic lobes of 35d old control (A; *Repo*-Gal4 > UAS-mitoroGFP-Grx1) and frataxin knockdown flies (A'; *Repo*-Gal4 > UAS-mitoroGFP-Grx1; UAS-fhRNAi1). Scale bars represent 40 µm. (B) Quantification of A-A'. 405/488 nm ratio is reduced in FRDA flies. n = 5. (C-C') Representative IFM of 6d old control (C; *Mef2*-Gal4 > UAS- mitoroGFP-Grx1) and frataxin knockdown flies (C'; *Mef2*-Gal4 > UAS-mitoroGFP-Grx1; UAS-fhRNAi1). Scale bars represent 10 µm. (D) Quantification of C-C'. 405/488 nm ratio is almost halved in FRDA flies, similar to the addition of the reductant DTT. n = 5.

3.3. Mitochondrial damage activates mitophagy

Since mitochondria were clearly damaged in frataxin-depleted flies, I wanted to assess if these mitochondria were correctly targeted for degradation. Perinuclear arrangement of mitochondria as seen in glial cells has been suggested to precede mitophagy in mammalian cells (Okatsu et al, 2010). Furthermore, the increased mitochondrial fragmentation observed in frataxin-deficient muscles is consistent with mitochondria being targeted for clearance by mitophagy (Palikaras & Tavernarakis, 2014).

3.3.1. The autophagy marker p62 accumulates in frataxin-depleted flies

To test this hypothesis, I used antibodies against the autophagy marker Ref(2)P (Nezis et al, 2008; Pircs et al, 2012), the *Drosophila* orthologue of mammalian p62 (referred to as p62 from now on) and looked at brains and muscles.

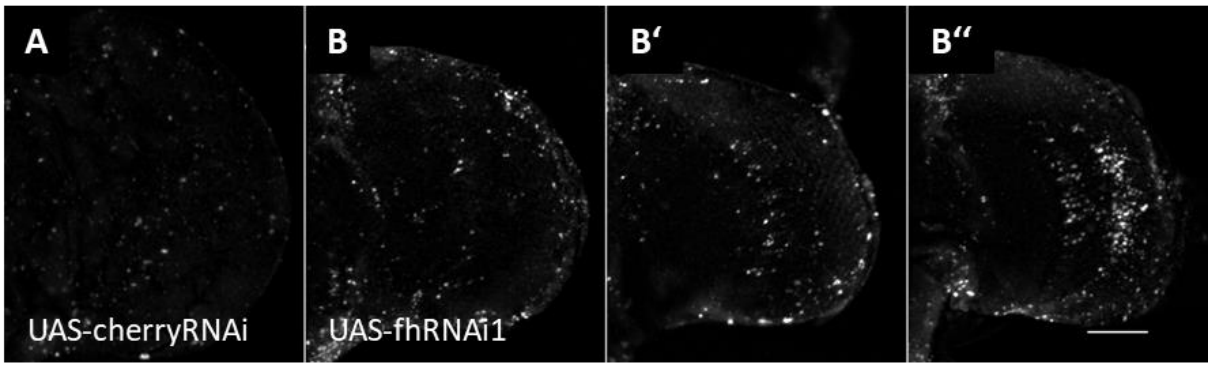

Figure 17: p62 accumulates in the optic lobe

Representative optic lobes stained for p62. Scale bar represents 40 µm. (A) 35d old control fly (*Repo*-Gal4 > UAS-cherryRNAi). (B-B'') 35d old frataxin knockdown flies (*Repo*-Gal4 > UAS-fhRNAi1). P62 accumulates in knockdown flies to a variable degree.

In brains, glial specific knockdown resulted generally in an accumulation of p62 after 35d, even though the phenotype was variable. P62 was still present in controls (Figure 17A), confirming the expected age-dependant presence of p62 in the brain described before (Nezis et al, 2008). However, the staining was clearly increased in frataxin depleted flies (Figure 17B-B''). The row from B to B'' shows a range of phenotypes from little to substantial accumulation in the region of the GGCs.

In muscles, p62 was distributed evenly without forming particular structures in controls (Figure 18A). Interestingly, p62 accumulated in vesicle-like structures in frataxin depleted flies (Figure 18B). These structures occupied the space of mitochondria and also partially co-localized with mitoGFP (insets), suggesting the formation of autophagosomes for mitochondrial degradation.

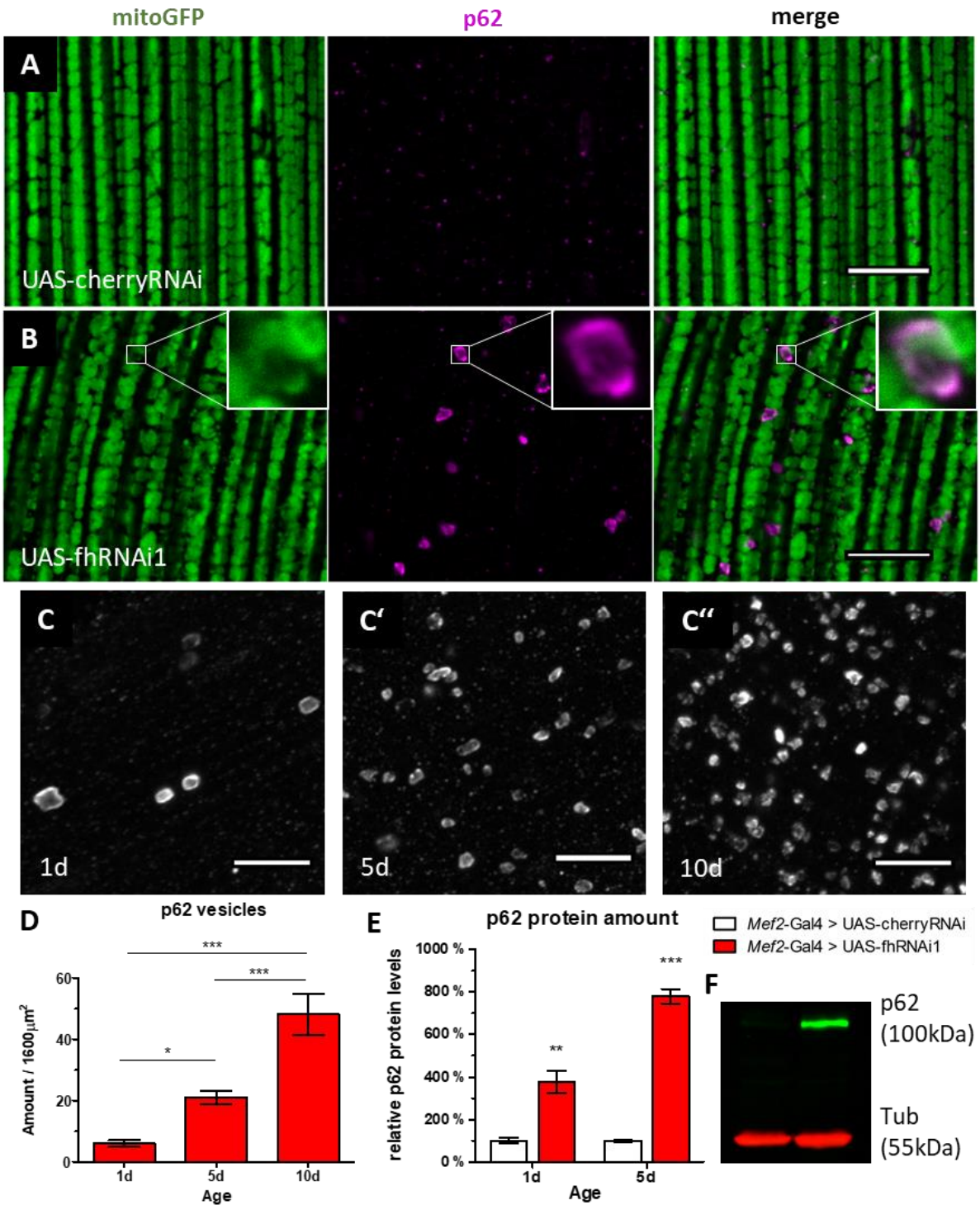

Figure 18: p62 accumulates in vesicle-like structures in muscles

Scale bars represent 10 µm. (A-B) Representative images of 5d old control (A; *Mef2*-Gal4 > UAS-mitoGFP, UAS-cherryRNAi) and frataxin knockdown flies (B; *Mef2*-Gal4 > UAS-mitoGFP, UAS-fhRNAi1) labeled with mitoGFP (green) and stained for p62 (magenta). P62 vesicles are absent in controls, but present in frataxin depleted flies and engulf mitochondria (insets). (C-C'') Representative z-projections of 1d (C), 5d (C') and 10d (C'') old frataxin deficient flies stained for p62. (D) Quantification of C. The number of p62 vesicles increases significantly with age. n = 5. (E) Quantification of p62 protein levels in FRDA flies 1d and 5d post-eclosion compared to controls. Significant accumulation of p62 upon frataxin silencing in *Drosophila* muscles. n = 3. (F) Representative p62 Western Blot of 5d old FRDA flies.

Furthermore, the amount of vesicles increased in an age-dependent manner (Figure 18C-D). In a given area (1600 µm^2), there were an average of 6 vesicles after 1d, rising to 48 after 10d, an 8-fold increase. This result was confirmed via Western Blot (Figure 18E). P62 amount was already multiplied 4-fold after 1d, rising to 8-fold after 5d, compared to controls.

Since robust accumulation of p62 is linked to autophagic blockage and inaccurate aggregate clearance (Bartlett et al, 2011), I decided to analyse the autophagy pathway in-depth to determine which step was potentially inhibited or might represent the limiting factor. Importantly, the observed phenotypes are more severe and the progression of the disease is faster in muscles than in glia. Moreover, the organelle size in this tissue allows a more accurate quantification.

Therefore, I initially concentrated on muscles for further investigation. To make sure that the detected increase in p62 amount was not simply a direct consequence of hyperactivation of p62 transcription, I compared *p62* mRNA levels of FRDA flies to controls (Figure 19A). *P62* mRNA levels were slightly upregulated by about 25%, but cannot account for the massive increase in protein amount seen in Figure 18E. In this line, overexpressing p62 in muscles did not induce formation of p62 vesicles as shown in Figure 18B (Figure 19B).

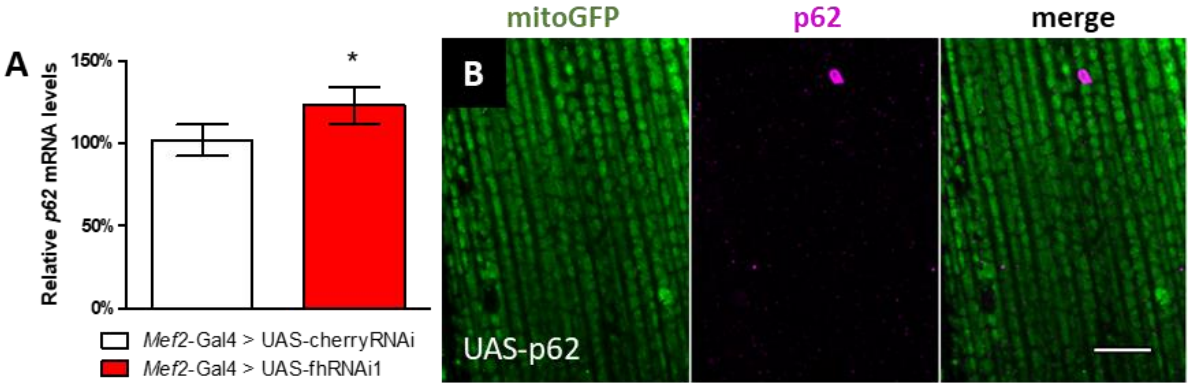

Figure 19: p62 accumulation is not a result of transcription hyperactivation
(A) P62 mRNA levels of control and frataxin-deficient flies. P62 is slightly upregulated in FRDA flies. n = 5. (B) Representative IFM with p62 overexpression (*Mef2*-Gal4 > UAS-mitoGFP, UAS-p62) labeled with mitoGFP (green) and stained for p62 (magenta). No accumulation of p62 vesicles detected. Scale bar represents 10 µm.

Taken together, these results confirm that the FRDA phenotypes are not a direct consequence of p62 upregulation.

3.3.2. Mitophagy is enhanced in FRDA flies

As mentioned above, p62 accumulation has been described as a sign of autophagy blockage (Bartlett et al, 2011). Therefore my results suggested potential defects in autosomal-lysosomal trafficking and/or degradation. Consequently, I examined the autophagic flux to determine the

step where autophagic inhibition was occurring. To reach that goal, I used the GFP-tagged autophagy markers GFP-Atg8a and LAMP1-GFP to label autophagosomes and lysosomes respectively and analysed co-localization with p62.

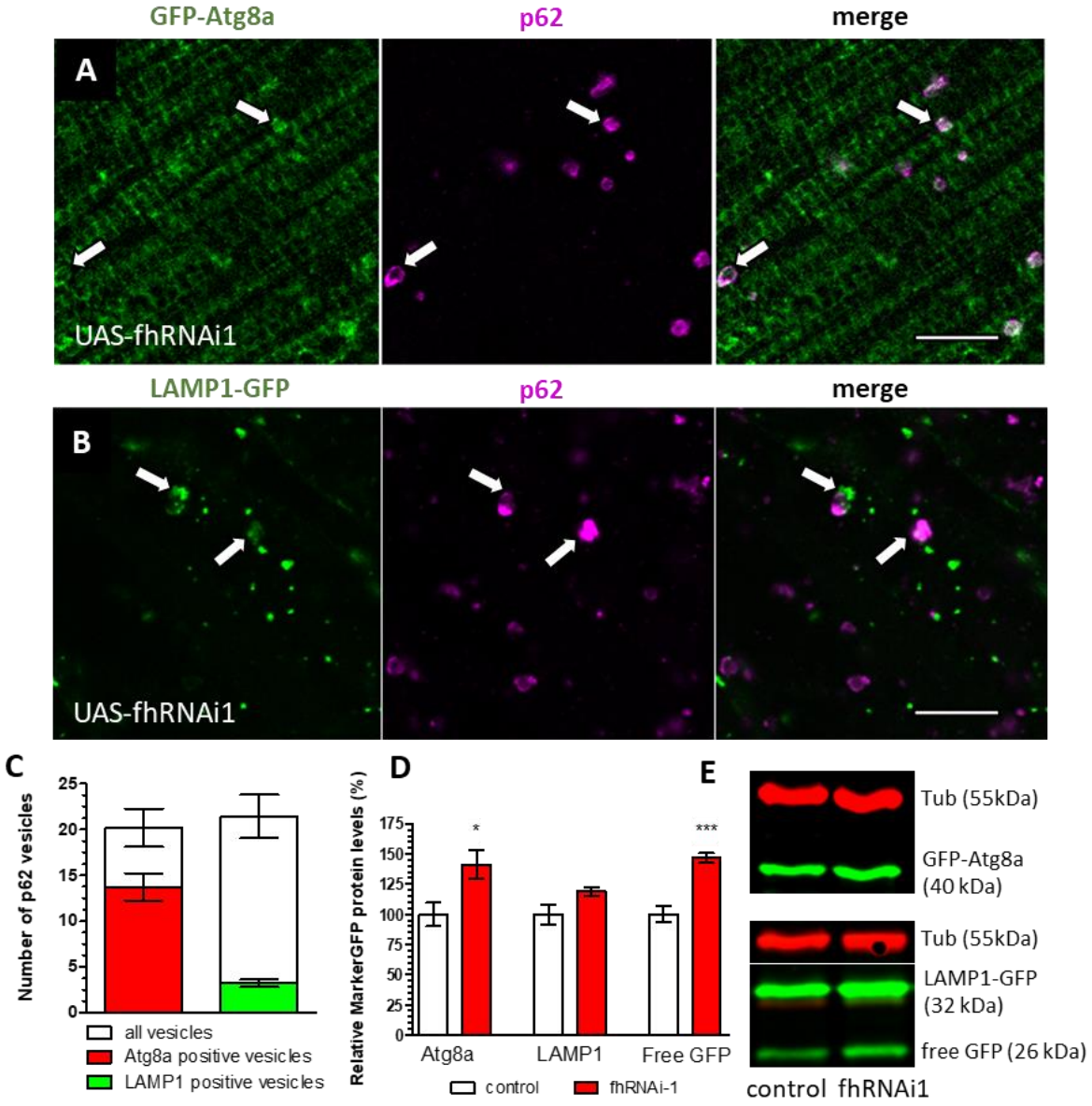

Figure 20: Analysis of mitophagic flux in *Drosophila* muscles

(A-B) Representative IFM of 5d old flies labeled with GFP-Atg8a (A,green; *Mef2*-Gal4 > UAS-GFP-Atg8a, UAS-fhRNAi1) or LAMP1-GFP (B,green; *Mef2*-Gal4 > UAS-LAMP1-GFP, UAS-fhRNAi1) and stained for p62 (magenta). Arrows denote co-localization of both signals. Scale bars represent 10 µm. (C) Quantification of co-localization from A (left bar) and B (right bar) in a 1600 µm^2 square. Number of co-localized signals are referred to total number of p62 vesicles. n = 5. (D) Quantification of Western Blots against GFP-Atg8a and LAMP1-GFP using anti-GFP antibody. Slight accumulation of GFP-Atg8a. No accumulation of LAMP1-GFP, but increase in free GFP. n = 4. (E) Representative examples of Western Blots against GFP-Atg8a (top) and LAMP1-GFP (bottom).

In frataxin knockdown flies, GFP-Atg8a was broadly distributed in the tissue (Figure 20A), with a strong co-localization to the p62 vesicles of around 70% (arrows and Figure 20C, left bar). This result suggested a proper recruitment of Atg8a to the p62 vesicles and subsequently

autophagosome formation. Regarding the second marker, LAMP1-GFP formed punctate structures that partially overlapped with p62 (Figure 20B, arrows). Remarkably, the degree of co-localization was much lower than with GFP-Atg8a, only about 20% (Figure 20C, right bar). This might indicate a problem in the fusion between autophagosomes and lysosomes. To further investigate the cellular autophagic flux, I performed Western Blots against both GFP-fusion proteins. GFP-Atg8a accumulated slightly (by about 40%), while no significant increase of LAMP1-GFP could be detected (Figure 20D and E), suggesting a working turnover of both proteins. Interestingly, I found an increased amount of free GFP in the case of LAMP1-GFP (by about 50%), a sign for enhanced turnover of the protein and consequently enhanced autophagic flux (Mauvezin et al, 2014). Overall, these results allude to a working autophagic flux. Interestingly, the speed of autophagolysosome formation appears to be the limiting factor, which might explain the apparent p62 and GFP-Atg8a accumulation.

Due to the discrepancy between the GFP-fusion marker results and the regular interpretation of p62 accumulation as a sign for autophagic impairment, I decided to use an additional approach to elucidate this contradiction. The mtRosella transgene consists of a mitochondrial-targeted dsRed fluorescent protein fused to a pH-sensitive GFP named pHluorin. Under neutral conditions, such as in autophagosomes, green and red signals overlap in mitochondria. When they are degraded in the autolysosome, they lose the green pHluorin signal due to quenching of the pH-sensitive GFP. This tool has been successfully used before to study mitophagy in yeast (Rosado et al, 2008; Böckler & Westermann, 2014), *C.elegans* (Schiavi et al, 2015) and mammalian cell culture (Sargsyan et al, 2015). However, to my knowledge, such a tool has been never applied in *Drosophila* and therefore new transgenic flies were generated in Prof. Schneuwly´s laboratory for this thesis.

In control flies, mtRosella was correctly localized to mitochondria and exhibited both signals in all organelles (Figure 21A). In FRDA flies, several mitochondria also displayed both signals (Figure 21B), denoting either healthy mitochondria or mitochondria not yet targeted for degradation. I focused on those organelles that already displayed p62 signals. Altogether, three types of p62-positive mitochondria could be observed: Mitochondria with both pHluorin and dsRed signals present (arrowhead and Figure 21C), designating the first step of mitophagy, formation of autophagosomes. Vesicles with only dsRed signal left (asterisk and D), designating the next step, fusion of the autophagosome with the lysosome and subsequent quenching of pHluorin signal. Finally, vesicles without signal left (arrows), designating the final stages of mitochondrial clearance. Quantification of the three vesicle types revealed that the majority (70%) of p62 vesicles lost both signals, around 25% displayed only dsRed signal,

while a small amount (5%) showed both signals (Figure 21E). Since blockage of mitophagy would trigger accumulation of p62 vesicles with one or both tags present, mitophagic flux is not inhibited.

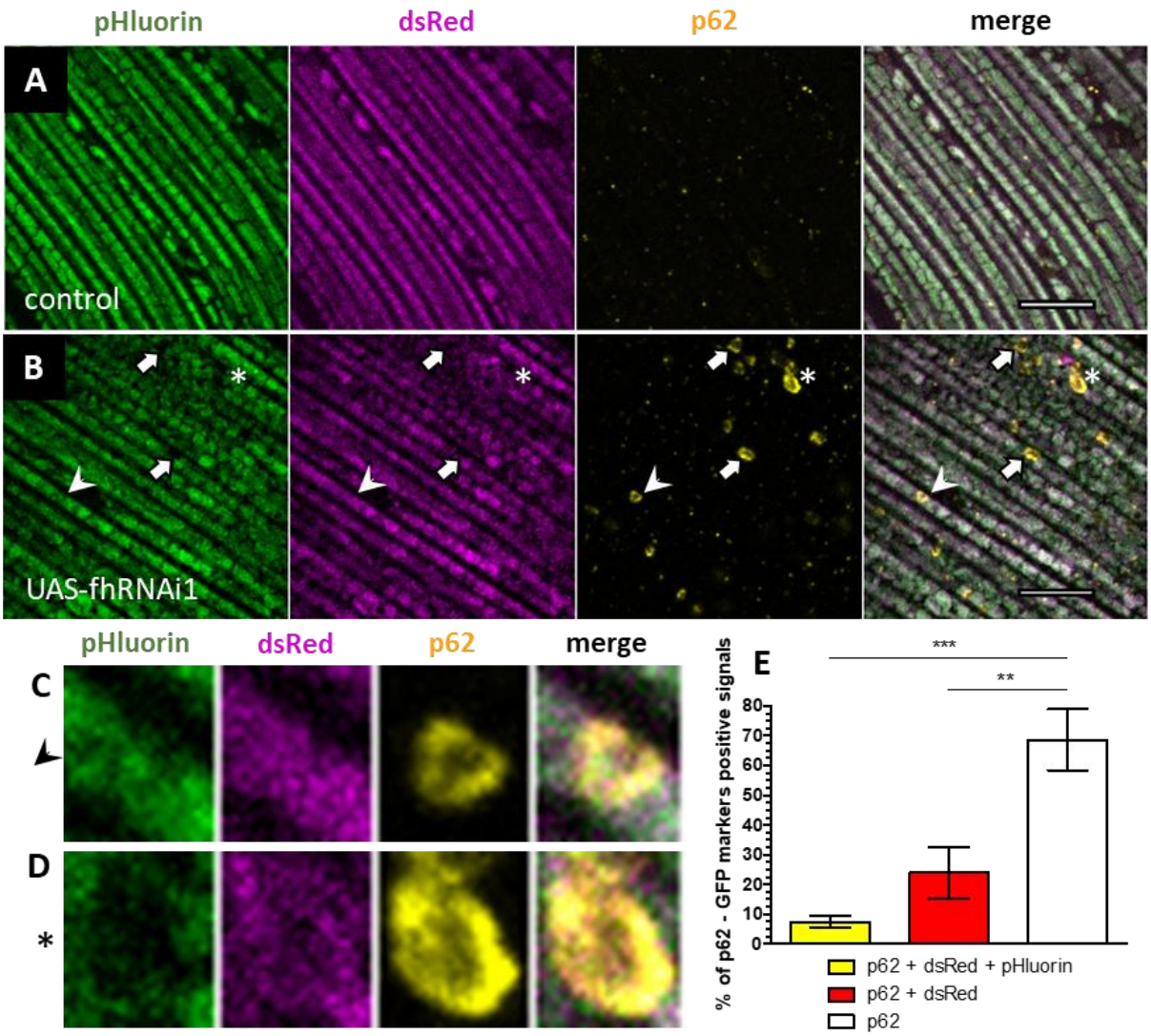

Figure 21: Application of mtRosella in *Drosophila* muscles

(A-B) Representative IFM of 5d old control (A, *Mef2*-Gal4 > UAS-mtRosella) and 5d old FRDA (B, *Mef2*-Gal4 > UAS-mtRosella, UAS-fhRNAi1) flies, labeled with pHluorin (green), dsRed (magenta) and stained for p62 (yellow). Scale bars represent 10 µm. (A) pHluorin and dsRed co-localize in all mitochondria without presence of p62 vesicles. (B). Presence of both signals in all mitochondria that have not been targeted for clearance (p62 negative). Arrows mark p62 vesicles without mtRosella signal. Arrowhead marks p62 vesicle retaining complete mtRosella signal. Asterisk marks p62 vesicle with only dsRed signal. (C) Magnification of p62 vesicle marked with arrowhead. (D) Magnification of p62 vesicle marked with asterisk. (E) Quantification of co-localization between p62, dsRed and pHluorin signal. The majority of p62 vesicles show no mtRosella signal, a small fragment displays both tags, while about one fourth only shows dsRed signal. n = 5.

Next, I wanted to confirm the results obtained in muscles also in glial cells. Therefore, I investigated the distribution of the autophagy markers GFP-Atg8a and LAMP1-GFP in glia of 35d old flies. Similar to muscles, GFP-Atg8a was distributed within the cytoplasm, both in control and frataxin depleted flies (Figure 22A and A', respectively). Remarkably, the

accumulation of p62 in the GGCs (Figure 17) was completely recovered when overexpressing GFP-Atg8a. Frataxin knockdown flies displayed a few GFP-Atg8a puncta co-localizing with p62 (inset arrow), but the phenotype was much less prominent than in muscles.

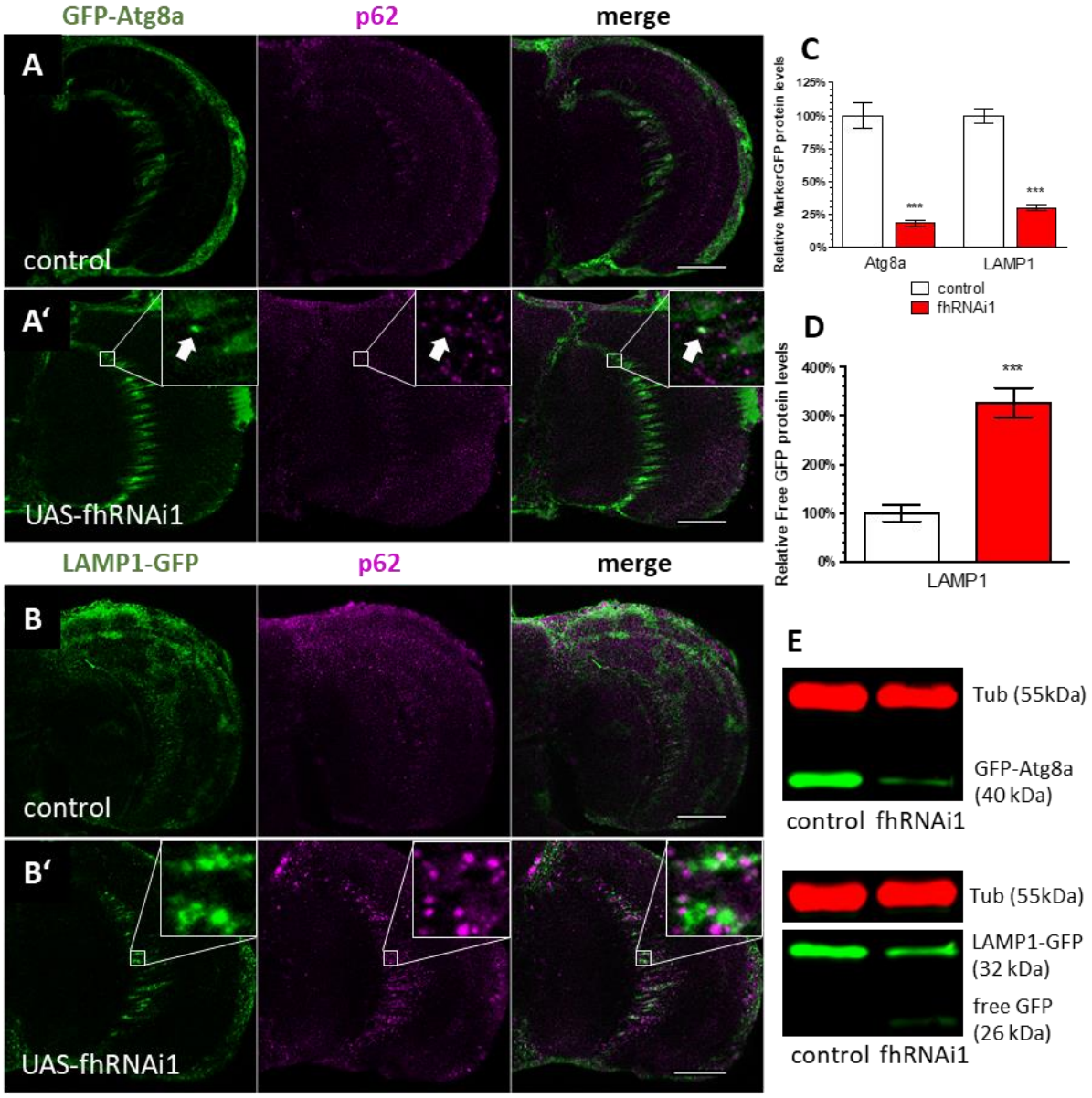

Figure 22: Mitophagic flux in glia is enhanced

(A-A') Representative optic lobes of 35d old control (A, *Repo*-Gal4 > UAS-GFP-Atg8a) and FRDA (A', *Repo*-Gal4 > UAS-GFP-Atg8a, UAS-fhRNAi1) flies labeled with GFP-Atg8a (green) and stained for p62 (magenta). No p62 accumulation found in FRDA flies. Some GFP-Atg8a puncta co-localize with p62 (inset arrow). Scale bars represent 40 µm. (B-B') Representative optic lobes of 35d old control (B, *Repo*-Gal4 > UAS-LAMP1-GFP) and FRDA (B', *Repo*-Gal4 > UAS-LAMP1-GFP, UAS-fhRNAi1) flies labeled with LAMP1-GFP (green) and stained for p62 (magenta). Increased p62 signal in GGCs. Lysosomes are in close proximity to p62 dots (inset). Scale bars represent 40 µm. (C) Quantification of Western Blots against GFP-Atg8a and LAMP1-GFP using anti-GFP antibody. The amount of both GFP-tags is significantly reduced in FRDA flies. n = 4. (D) Quantification of free GFP in LAMP1-GFP Western Blots. Levels of free GFP are markedly increased in frataxin depleted glia. n = 4. (E) Representative examples of Western Blots against GFP-Atg8 (top) and LAMP1-GFP (bottom).

LAMP1-GFP showed a diffuse pattern in control flies, but formed clear punctate structures (arrows) in FRDA flies (Figure 22B-B'). Accumulation of p62 still occurred in these flies, in

contrast to GFP-Atg8a overexpression. These results suggest an increase in mitophagic activity in glial cells of frataxin depleted flies, similar to muscles. Western Blots further confirmed this: In frataxin depleted flies, both GFP-Atg8a and LAMP1-GFP protein levels were reduced substantially (Figure 22C-E). The effect was more noticeable for GFP-Atg8a (85% reduction) than for LAMP1-GFP (70% reduction). As in muscles, free GFP levels were increased (Figure 22D-E). However, the effect itself was much stronger (around 300%), implying a robust activation of mitophagy in glial cells. Taken together, above results suggest that frataxin knockdown results in induction of mitophagy without blockage.

3.3.3. Promoting autophagy is sufficient to improve FRDA phenotypes

As indicated above, overexpressing GFP-Atg8a in glial cells seemed to have a positive effect on autophagy in glia. The p62 accumulation normally seen in FRDA flies was severely reduced in GFP-Atg8a overexpressing flies (Figure 22A'), in contrast to muscles where the amount of p62 vesicles remained constant (Figure 20C). In addition, the reduction of the corresponding GFP-tagged protein was higher when GFP-Atg8a was overexpressed instead of LAMP1-GFP (Figure 22C). Interestingly, GFP-Atg8a contains the full-length protein Atg8a (Juhasz et al, 2008), while LAMP1-GFP contains a truncated protein with only the transmembrane domain and a C-terminal cytoplasmic tail for organelle targeting (Pulipparacharuvil et al, 2005). Altogether, the data suggest that the autophagy marker GFP-Atg8a is functional and thus able to promote mitochondrial clearance in FRDA flies. In agreement with this hypothesis, genetic manipulation of endogenous Atg8a levels via overexpression was able to abolish the p62 accumulation as well (Figure 23A).

Because Atg8a overexpression was able to ameliorate p62 accumulation in glial cells, I wanted to examine if other hallmarks of FRDA would also be rescued by promoting mitophagy. Therefore I examined locomotor ability, brain vacuolization and lipid accumulation, phenotypes that have been described before (Navarro et al, 2010). Neither the wild-type Atg8a nor the GFP-tagged form were able to rescue the locomotor deficit of the flies. To assess the other two phenotypes I looked at semithin epon plastic sections of 35d old brains. Overexpressing the non-functional GFP-tagged LAMP1 displayed the typical phenotype, brain vacuolization (arrows) and formation of lipid droplets (arrowheads; Figure 23C). Interestingly, Atg8a overexpression resulted in significant reduction of brain vacuolization (arrow), but not lipid droplet accumulation (arrowheads; Figure 23D). In conclusion, these results confirm the positive effect of mitophagy stimulation on the fly model of FRDA. Enhancing mitophagy

seemed to reduce brain degeneration. However, lipid accumulation was unaffected, suggesting this phenotype does not depend on the status of mitophagy.

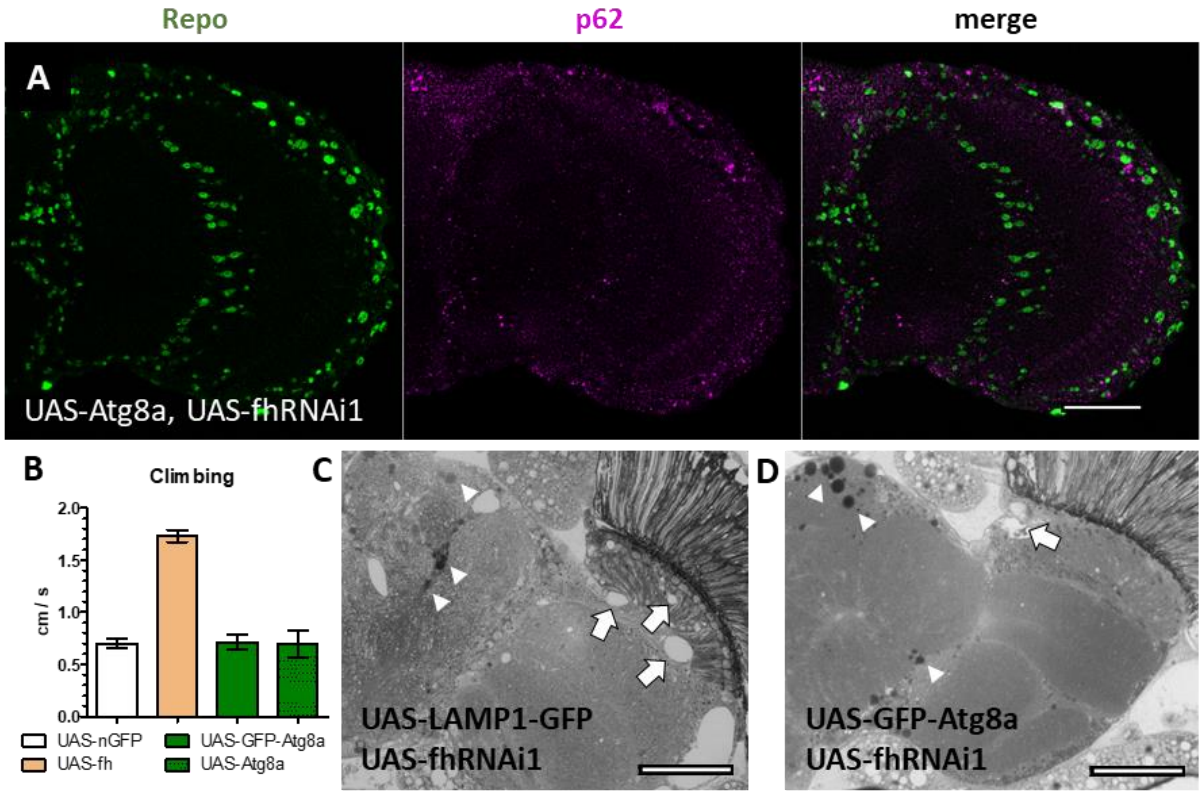

Figure 23: Overexpression of *Atg8a* in glia partially rescues FRDA phenotypes

(A) Representative optic lobe of a 35d old FRDA fly overexpressing Atg8a (*Repo*-Gal4 > UAS-Atg8a, UAS-fhRNAi1) stained for Repo (green) and p62 (magenta). Atg8a overexpression abolishes p62 accumulation. Scale bar represents 40 µm. (B) Negative geotaxis assay of 10d old FRDA flies (*Repo*-Gal4 > UAS-fhRNAi1) with co-expression of another transgene (legend). Neither GFP-Atg8a nor Atg8a overexpression are capable of rescuing the climbing defect. n = 12. (C-D) Representative semi-thin epon plastic sections of 35d old FRDA flies overexpressing LAMP1-GFP (C) or GFP-Atg8a (D). Scale bars represent 50 µm. (C) Presence of lipid droplets (arrowheads) and vacuolization of brain tissue (arrows). (D) Atg8a overexpression reduces brain vacuolization (arrow), but does not improve lipid accumulation (arrowheads).

Nevertheless, increasing autophagic flux seemed a promising way to at least partially improve the flies' condition. Therefore I tested whether pharmacological induction of autophagy might provide a similar beneficial effect. Rapamycin is a prominent inducer of autophagy and has been successfully used in another *Drosophila* model of FRDA before (Calap-Quintana et al, 2015).

First, I assessed whether Rapamycin would have a positive effect on the locomotor deficit. Similar to Atg8a overexpression, Rapamycin was not able to significantly rescue the climbing defect, although a slight tendency was present, from 1.01 cm/s to 1.11 cm/s when Rapamycin was added (red bars; Figure 24A). Since Atg8a overexpression was able to rescue the vacuolization in FRDA flies, but not the locomotor deficit, I was interested if Rapamycin might behave the same way. As expected, control flies did not show signs of vacuolization after 35d,

with or without Rapamycin treatment (Figure 24C, D). Frataxin knockdown triggered a substantial vacuolization near the outer optic chiasm (arrows; Figure 24C').

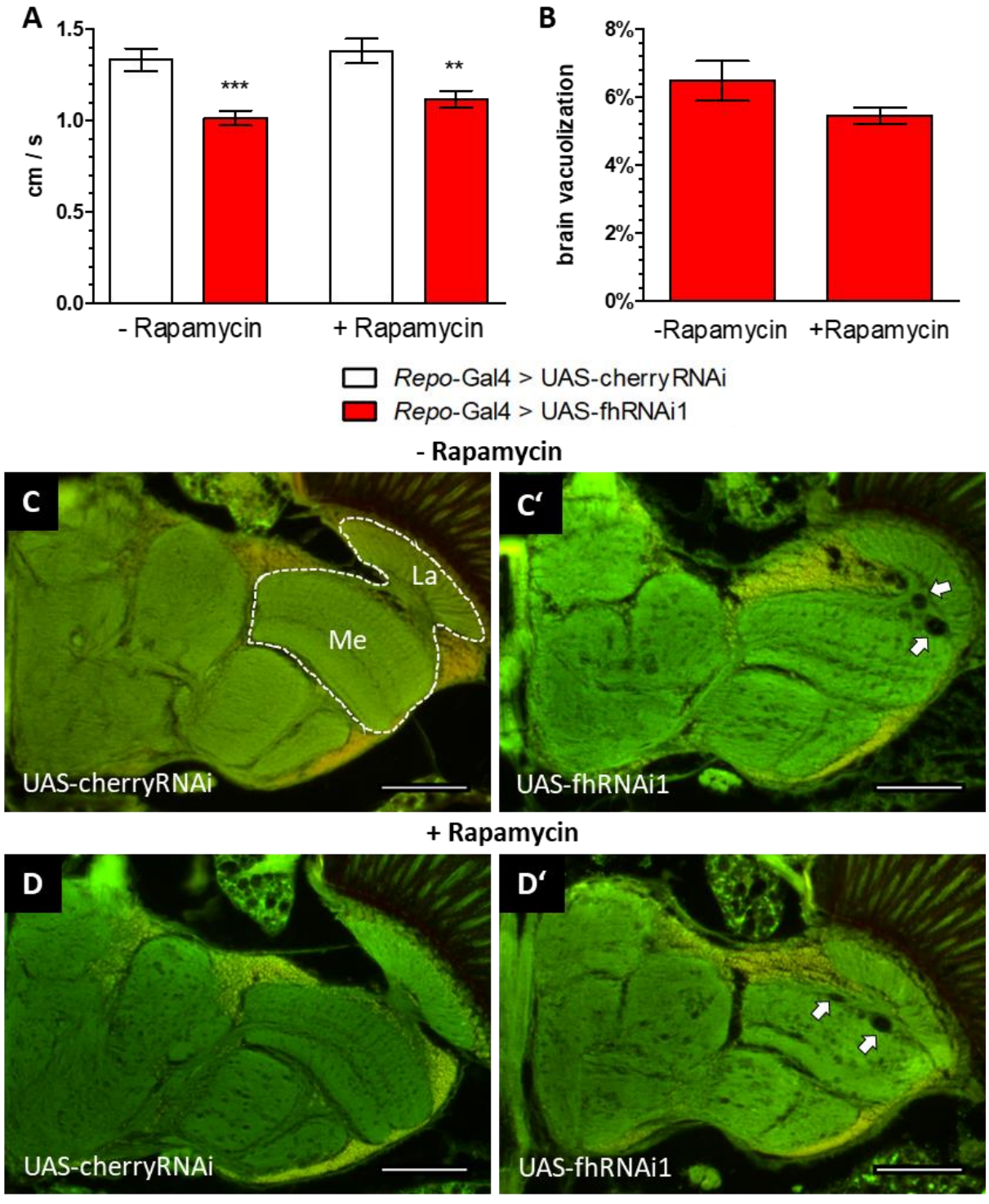

Figure 24: Rapamycin fails to ameliorate locomotion or brain vacuolization

(A) Negative geotaxis assay of 10d old flies. Rapamycin has a minor, but insignificant effect on climbing speed. n = 12. (B) Quantification of vacuolization from C' and D'. No significant reduction of vacuolization area. n = 10. The quantified region is marked in C. Me = Medulla; La = Lamina. (C-D') Representative paraffin sections of 35d old flies. Scale bars represent 50 µm. (C and D) Control flies (*Repo*-Gal4 > UAS-cherryRNAi) fed with normal food (C) or 50 µm Rapamycin (D). No apparent holes visible. (C') FRDA flies (*Repo*-Gal4 > UAS-fhRNAi1) fed with normal food. Major vacuolization occurs at the outer optic chiasm (arrows). (D') FRDA flies fed with 50 µm Rapamycin. Vacuolization is still present (arrows).

In contrast to Atg8a overexpression, Rapamycin was unable to restore brain integrity, as vacuoles were still present in this case (arrows; Figure 24D'). Again, there was a slight but insignificant tendency for a positive effect (decrease of vacuolization area from 6.5% to 5.5%; Figure 24B) In conclusion, promoting mitophagy via pharmacological means might be beneficial but the effect was insufficient to rescue locomotor ability or brain vacuolization significantly in this model.

3.4. Genetic screen reveals *Marf* as a major component of FRDA

3.4.1. *Marf* knockdown in glial cells rescues locomotor deficit

Since promoting mitophagy via genetic manipulation had a beneficial on frataxin depleted flies in glia, I conducted a forward genetic screen to find additional potential modifiers of FRDA phenotypes.

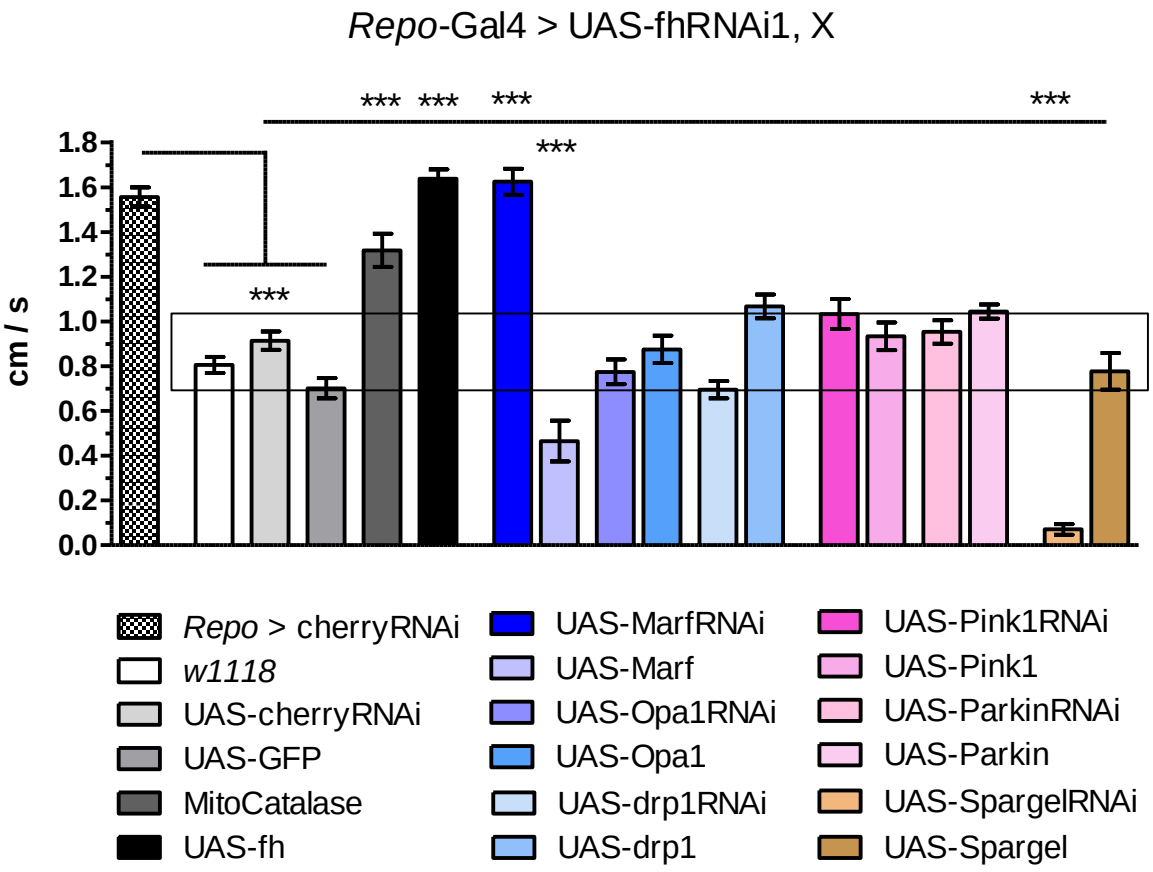

Figure 25: Genetic screen reveals *Marf* as potential modifier

Locomotor performance of 10d old flies co-expressing frataxin knockdown and an additional transgene (*Repo*-Gal4 > UAS-fhRNAi1, X), except the first bar (*Repo*-Gal4 > UAS-cherryRNAi). The black square denotes a 'base' climbing level of FRDA flies, which fluctuates slightly in different fly strains. From all tested interactions, only *Marf* knockdown was able to restore locomotion. n = 12.

As mitochondrial morphology and homeostasis were clearly disturbed in my model, I focused on relevant genes controlling mitochondrial homeostasis: Genes involved in mitochondrial fusion and fission (*Marf, Opa1* and *drp1*), mitochondrial quality control (*Pink*, *Parkin*) and mitochondrial biogenesis (*Spargel*). As an additional control to verify the reliability of the approach, a constitutively expressed mitochondrial catalase (*mitoCatalase*) was included, since it has been described to improve frataxin deficiency (Anderson et al, 2008).

I initially evaluated locomotor ability as a comparatively quick and simple readout of the genetic interactions (Figure 25).

Control flies with normal levels of frataxin (*Repo*-Gal4 > UAS-cherryRNAi) reached a speed of about 1.55 cm/s (left bar). All other bars denote frataxin knockdown flies co-expressing a second construct. As expected, FRDA flies climbed significantly slower displaying a speed of 0.8 cm/s. Importantly, co-expression of a second transgene did not alter the locomotor ability of FRDA flies significantly (ranging between 0.7 cm/s and 0.9 cm/s upon co-expression of GFP and cherryRNAi, respectively). Restoring frataxin levels rescued the locomotor deficit completely. Similarly, mitochondrial catalase successfully improved climbing speed to 1.32 cm/s. These results confirmed the reliability of the method. From all tested interactions, only *Marf* knockdown was able to rescue the locomotor deficit in a significant manner. Climbing speed was restored up to 1.63 cm/s, while *Marf* overexpression decreased climbing speed to about 0.64 cm/s. Since *Marf* promotes mitochondrial fusion (Westermann, 2010b), this result suggests that inhibition of fusion might be beneficial, while promoting fusion might be detrimental. The other two genes involved in mitochondrial dynamics should therefore elicit a similar response. Interestingly, this was not the case. Both *Opa1* and *drp1* did not alter the locomotor deficit significantly when manipulated. This suggests that *Marf's* role in mitochondrial dynamics might not be the crucial factor for the rescue. Changes in *Pink1* and *Parkin* expression also had no effect on the locomotor ability as all genotypes exhibited an equal climbing speed. Lastly, stimulating mitochondrial biogenesis via *Spargel* overexpression failed to amend the locomotor defect. Rather, inhibiting biogenesis via *Spargel* knockdown was highly detrimental for the flies and reduced climbing speed to almost zero.

3.4.2. *Marf* knockdown ameliorates brain vacuolization and lipid accumulation

The negative geotaxis assay revealed *Marf* as a promising modifier of FRDA phenotypes. Therefore I wanted to know if *Marf* knockdown would also rescue other known glial phenotypes such as brain vacuolization and lipid accumulation.

To assess brain vacuolization, I performed paraffin sections of 35d old fly brains of some of the genotypes from the screen above and quantified the area of vacuolization (Figure 26A). As expected, FRDA flies showed brain vacuolization in the region of the outer optic chiasm (about 6.2%; arrows in Figure 26B). In agreement with the results from the negative geotaxis assay, only *Marf* knockdown restored brain integrity (Figure 26C). Vacuolization was reduced to 2.2%, not significantly different from brains of healthy flies (1.3%). Marf overexpression exacerbated the phenotype and increased vacuolization to 10.1% (arrows in Figure 26D). No other gene tested had an influence on vacuolization (drp1 overexpression is pictured as an example; arrows in Figure 26E).

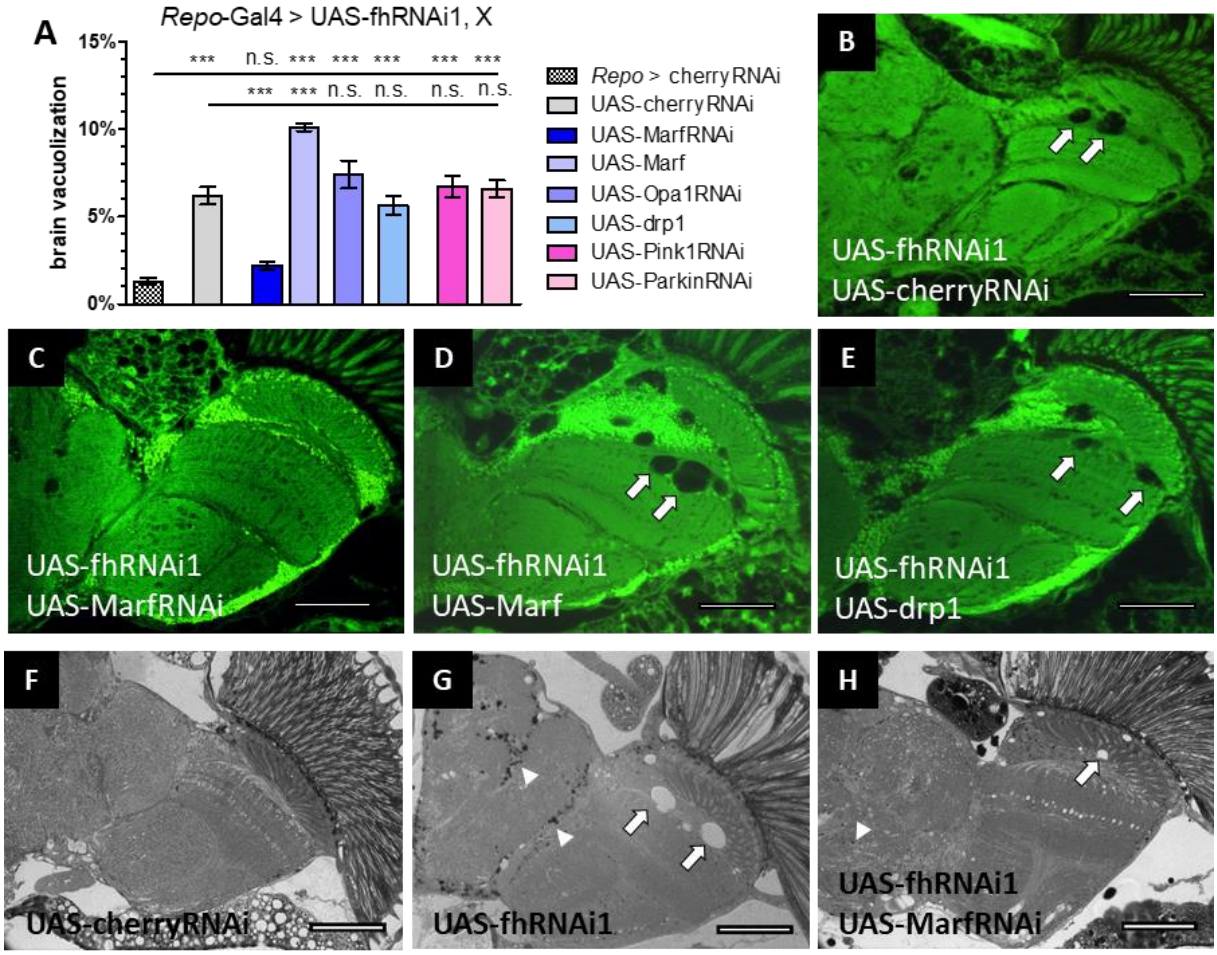

Figure 26: *Marf* knockdown improves brain vacuolization and lipid accumulation

(A) Brain vacuolization of 35d old flies co-expressing frataxin knockdown and an additional transgene (*Repo*-Gal4 > UAS-fhRNAi1, X), except the first bar (*Repo*-Gal4 > UAS-cherryRNAi). Only Marf knockdown restores brain integrity. n = 7. (B-E) Representative paraffin sections of brains quantified in A. Scale bars represent 50 µm. (B) X = UAS-cherryRNAi. Substantial vacuolization present (arrows). (C) X = UAS-MarfRNAi. Complete absence of vacuolization. (D) X = UAS-Marf. Vacuoles are enlarged compared to B (arrows). (E) X = UAS-drp1. Vacuoles present (arrow). (F-H) Representative semi-thin plastic epon sections of 35 old fly brains. Scale bars represent 50 µm. (F) Control fly (*Repo*-Gal4 > UAS-cherryRNAi). No vacuoles and lipid droplets present. (G) Frataxin deficient fly (*Repo*-Gal4 > UAS-fhRNAi1). Visible brain vacuolization (arrows) and lipid droplet accumulation (arrowheads). (H) Fly co-expressing knockdown of frataxin and Marf (*Repo*-Gal4 > UAS-fhRNAi1, UAS-MarfRNAi). Clear improvement both in the size/number of vacuoles (arrow) and size/number of lipid droplets (arrowhead).

Finally, I examined if MarfRNAi would be able to rescue the lipid accumulation as well. Semi-thin plastic epon sections revealed that *Marf* knockdown indeed not only ameliorated the brain vacuolization (arrows), but also improved the lipid accumulation considerably compared to FRDA flies (arrowheads, Figure 26I and H, respectively). Indeed, brain integrity reached almost control fly level (Figure 26G).

Altogether, *Marf* knockdown improved three important hallmarks observed upon frataxin silencing in glia cells. Therefore I decided to focus on *Marf* as the most promising modifier in order to decipher the molecular mechanism underlying the rescue described above.

3.4.3. *Marf* knockdown fails to restore mitochondrial morphology or ameliorate p62 accumulation

Above results emphasize the key importance Marf has in the pathology of FRDA. Thus, I wanted to evaluate how *Marf* knockdown facilitates the rescue of FRDA phenotypes in glia. Marf has been primarily described as a mediator of mitochondrial fusion (Westermann, 2010b), suggesting that it might act through restoration of mitochondrial morphology. Marf is also involved in mitophagy, as a substrate of the ubiquitin ligase Parkin (Pallanck, 2013).

However, other proteins involved in those pathways failed to elicit an effect: Neither drp1 and Opa1 (involved in mitochondrial dynamics) nor Pink1 and Parkin (involved in mitophagy) were able to rescue the locomotor deficit (Figure 25) or the brain vacuolization (Figure 26). Taken together, these results hint at another role of Marf in FRDA. Nevertheless, I wanted to investigate the potential influence of *Marf* silencing on the mitochondrial morphology defects and p62 accumulation described above in frataxin-deficient glia cells (Figure 13 and Figure 17, respectively).

In agreement with previous results (Figure 13), control flies generally showed small, evenly distributed mitochondria in the GGC (Figure 27A). In FRDA flies, mitochondria appeared less randomly spread out and more clustered (Figure 27B). *Marf* knockdown slightly reduced the clustering, but failed to restore control morphology (Figure 27C). The situation for p62 was comparable: Control flies displayed a faint background staining of p62, but no apparent accumulation in the GGCs (red oval, Figure 27A'). Frataxin knockdown resulted in observable p62 accumulation in the GGC (Figure 27B'). MarfRNAi was not able to abolish the p62 accumulation (Figure 27C').

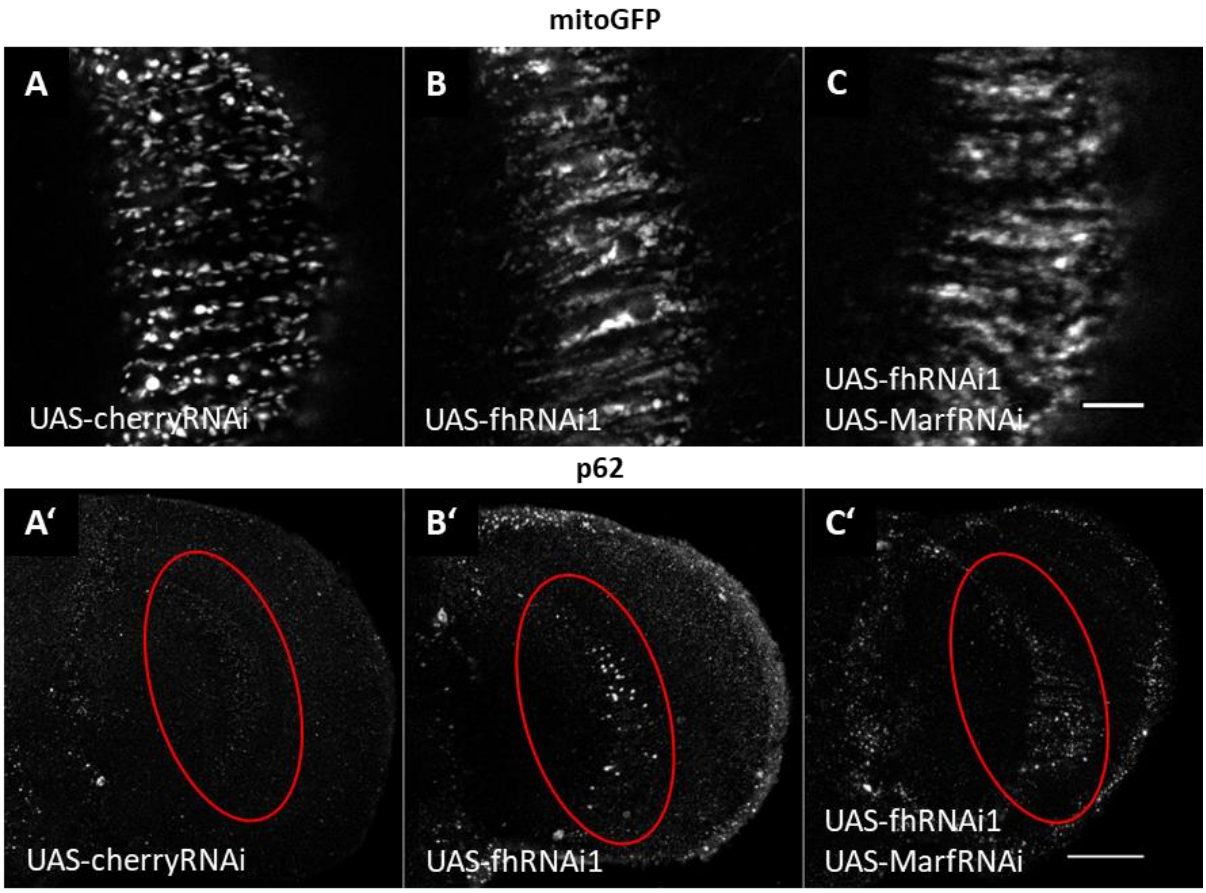

Figure 27: *Marf* knockdown fails to ameliorate mitochondrial morphology or p62 accumulation
(A-C) Representative GGC region confocal images of control (A, *Repo*-Gal4 > UAS-mitoGFP, UAS-cherryRNAi), frataxin knockdown (B, *Repo*-Gal4 > UAS-mitoGFP, UAS-fhRNAi1) and FRDA flies co-expressing frataxin and Marf knockdown (C, *Repo*-Gal4 > UAS-mitoGFP, UAS-fhRNAi1, UAS-MarfRNAi) labeled with mitoGFP. Control flies show small, discrete mitochondria, while frataxin knockdown leads to clustered mitochondria. Marf knockdown reduces clustering, but does not restore control morphology. Scale bar represents 10 µm. (A'-C') Representative optic lobes of control (A', *Repo*-Gal4 > UAS-cherryRNAi), frataxin knockdown (B', *Repo*-Gal4 > UAS-fhRNAi1) and FRDA flies co-expressing frataxin and Marf knockdown (C', *Repo*-Gal4 > UAS-fhRNAi1, UAS-MarfRNAi) stained for p62. FRDA flies display p62 accumulation in the GGC region, which is still present with additional *Marf* knockdown (red ovals). Scale bar represents 40 µm.

These results confirm that neither mitochondrial fusion nor mitophagy seem to be the key pathways by which *Marf* knockdown achieves the rescue of locomotor ability, brain vacuolization and lipid accumulation. Additionally, *Marf* knockdown does not appear to directly restore mitochondrial function.

3.4.4. Genetic screen in muscles reveals tissue-specific interaction with Marf

MarfRNAi in glia had improved locomotion, brain vacuolization and lipid accumulation considerably. Therefore, I was interested if this was a glial-specific effect or if MarfRNAi would also amend frataxin-deficient phenotypes in other tissues. For this purpose, I repeated the genetic screen of chapter 3.4.1 with the *Mef2*-Gal4 driver to test whether genetic manipulation in muscles leads to the similar results. However, the effect of targeted frataxin

silencing in muscles was so dramatic that any co-expression almost completely abolished locomotion. Thus, I decided to keep the flies at 18°C during development and post-eclosion. This lowers the effect of the UAS/Gal4 driven expression and alleviated the consequences of frataxin knockdown slightly. Flies were transferred to room temperature 1 h prior to the assay.

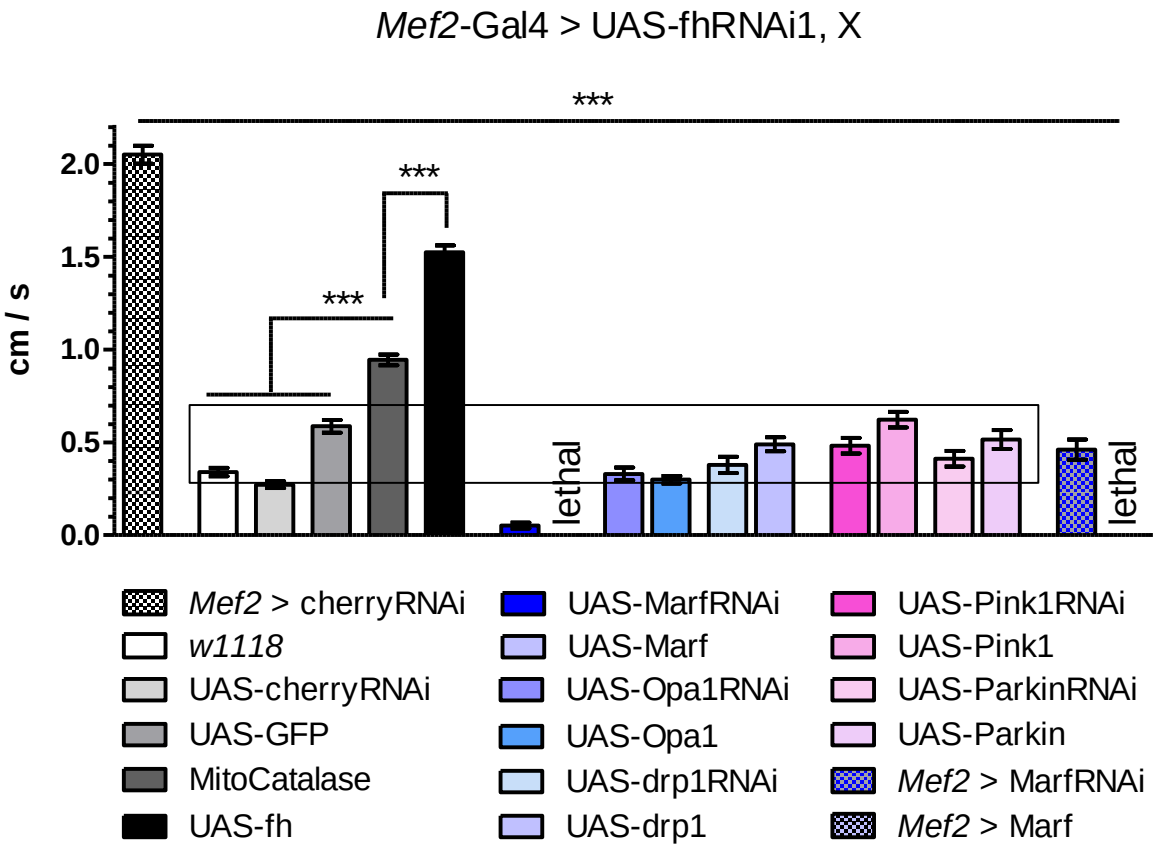

Figure 28: Genetic screen in muscles reveals no modifier for rescue

Locomotor performance of 10d old flies co-expressing frataxin knockdown and an additional transgene (Mef2-Gal4 > UAS-fhRNAi1, X), except the first bar and the last two bars (Mef2-Gal4 > X). Black square denotes a 'base' climbing level of FRDA flies, which fluctuates slightly in different fly strains. No genetic interaction improved locomotion significantly. n = 12.

Healthy control flies (*Mef2*-Gal4 > UAS-cherryRNAi) reached a speed of 2.05 cm/s after 10d (left bar; Figure 28). Frataxin knockdown in muscles strongly impaired the climbing speed even at this permissive conditions. Controls ranged from 0.27 cm/s (UAS-cherryRNAi) to 0.59 cm/s (UAS-GFP). As expected, co-expression of frataxin (UAS-fh) improved locomotion tremendously, to about 1.52 cm/s, but still significantly different from controls. Similarly, overexpression of mitochondrial catalase boosted the locomotor ability to 0.94 cm/s, but much less than *fh* overexpression. Surprisingly and in contrast to glia, *Marf* knockdown in muscles exacerbated the locomotor deficit. MarfRNAi flies were basically unable to climb and reached an average speed of only 0.05 cm/s. Since overexpression of *Marf* triggered developmental lethality, these results indicate that maintenance of optimal Marf levels is of paramount

importance in muscles. To confirm this hypothesis, I also tested the locomotion of flies in which *Marf* was knocked down or overexpressed in a control background (*Mef2*-Gal4 > UAS-MarfRNAi or UAS-Marf, respectively). Both manipulations were already harmful in that case: *Marf* knockdown flies reached about 0.46 cm/s, whereas no adult flies were obtained upon *Marf* overexpression (far right bars; Figure 28). The climbing speeds for all other genotypes were not significantly different from flies co-expressing control constructs (black square).

In contrast to glia, *Marf* knockdown was unable to rescue the locomotor defect of targeted frataxin depletion in muscles. Moreover, no additional construct was able to ameliorate the locomotor deficit, suggesting that the muscular phenotype in this model is too severe to detect improvements via genetic manipulation of mitochondrial dynamics or degradation.

3.5. ER and ER stress are pivotal elements in FRDA

Up to this point, my experiments could not resolve the mechanism underlying the protection observed by *Marf* knockdown in glia. In addition to mitochondrial fusion and degradation, Marf is also involved in ER-mitochondrial contacts. In mouse fibroblasts, Mitofusin 2 tethered mitochondria to the ER to facilitate the uptake of Ca^{2+} ions and promote lipid biosynthesis (Brito & Scorrano, 2008). More recently, *Marf* has been shown to mediate ER stress in a *Drosophila* model of Parkinson's disease (Debattisti et al, 2014; Celardo et al, 2016). Therefore, I wanted to investigate whether the ER was affected in the fly FRDA model.

3.5.1. ER structure appears intact

First, I assessed the structure of the ER in glia and muscles using an ER-GFP line. It consists of a GFP fused to a KDEL sequence, a C-terminal endoplasmic reticulum retention signal and localizes to the ER (K Irvine, personal communication, 2007). For the GGCs, ER-GFP was clustered around nuclei and extended into the cells (Figure 29A).The same ER-GFP patterning was clearly observed in FRDA flies (Figure 29B). However, I cannot rule out the possibility of subtle differences that cannot be distinguished with this method due to cell and ER size. In muscles, the ER was organized in a ladder-like structure around the actin filaments, forming the so-called sarcoplasmic reticulum (Figure 29C). Occasionally, ER-GFP aggregates were present in the IFM (arrows). In FRDA flies, the overall organization of the ER was conserved (Figure 29D). However, aggregates were both larger and more numerous (arrows). These aggregates might be caused by ER swelling, a morphological change associated with multiple cell death modalities (van Cruchten & van den Broeck, 2002).

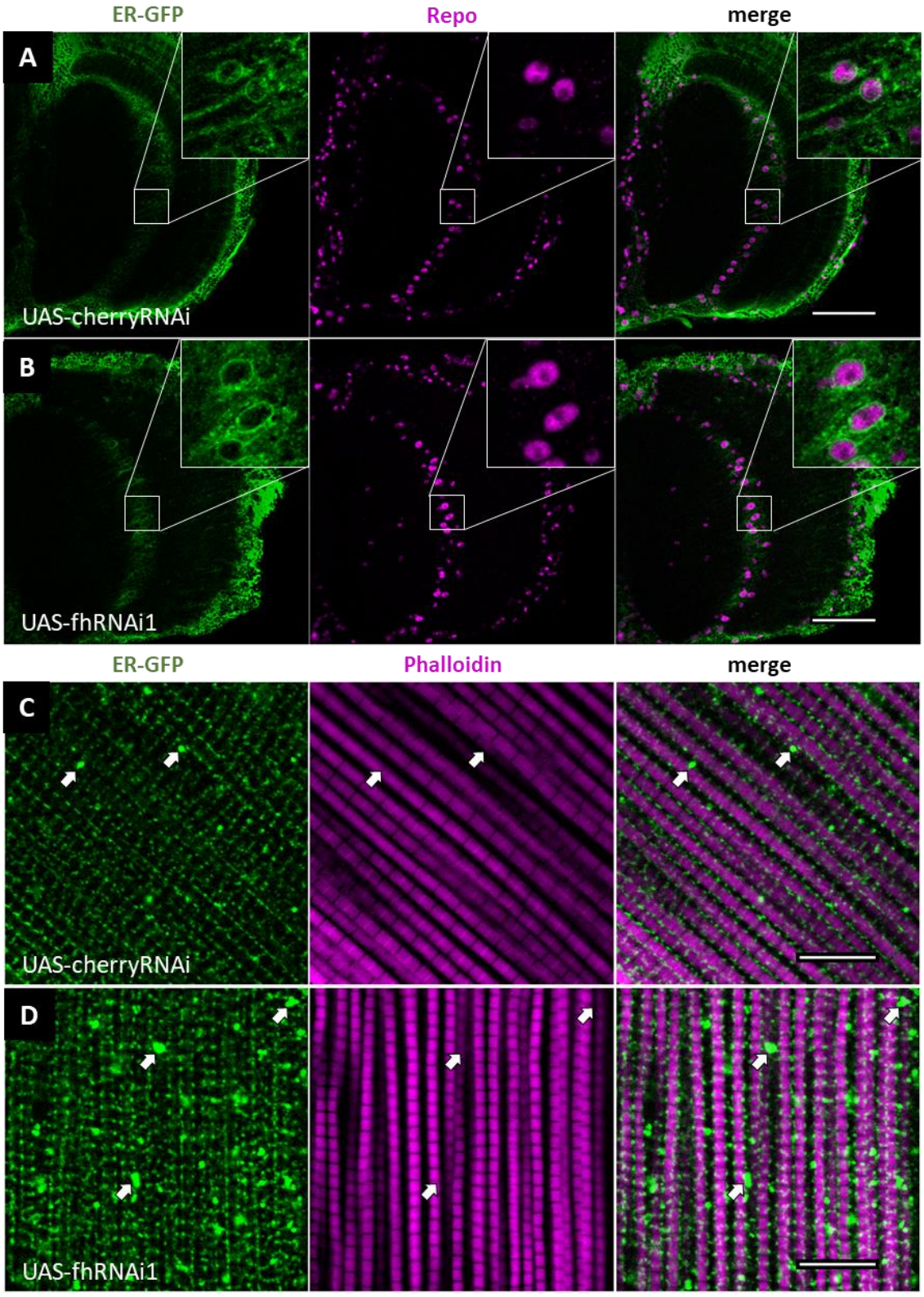

Figure 29: ER structure is intact

(A-B) Representative optic lobes of 35d old control (A; *Repo*-Gal4 > UAS-ER-GFP UAS-cherryRNAi) and frataxin knockdown flies (B; *Repo*-Gal4 > UAS-ER-GFP, UAS-fhRNAi1) labeled with ER-GFP (green) and stained for Repo (magenta). ER-GFP is clustered around nuclei and extends into the cells. No apparent difference in ER structure (insets). Scale bars represent 40 µm. (C-D) Representative IFM of 6d old control (C; *Mef2*-Gal4 > UAS-ER-GFP, UAS-cherryRNAi) and frataxin knockdown flies (D; *Mef2*-Gal4 > UAS-ER-GFP, UAS-fhRNAi1) labeled with ER-GFP (green) and stained with Phalloidin (magenta). In both cases, the ER appears as a ladder-like structure around the actin fibers. Some aggregates are present in controls (arrows), which increase in size and number in FRDA flies (arrows). Scale bars represent 10 µm.

3.5.2. ER stress response is altered

Mitochondria-ER contacts and their many roles have recently come to the forefront in neurodegenerative diseases (reviewed in Paillusson et al, 2016). One such role is linked to ER stress. ER stress in turn activates the three branches of the unfolded protein response (UPR; see chapter 1.6.1).

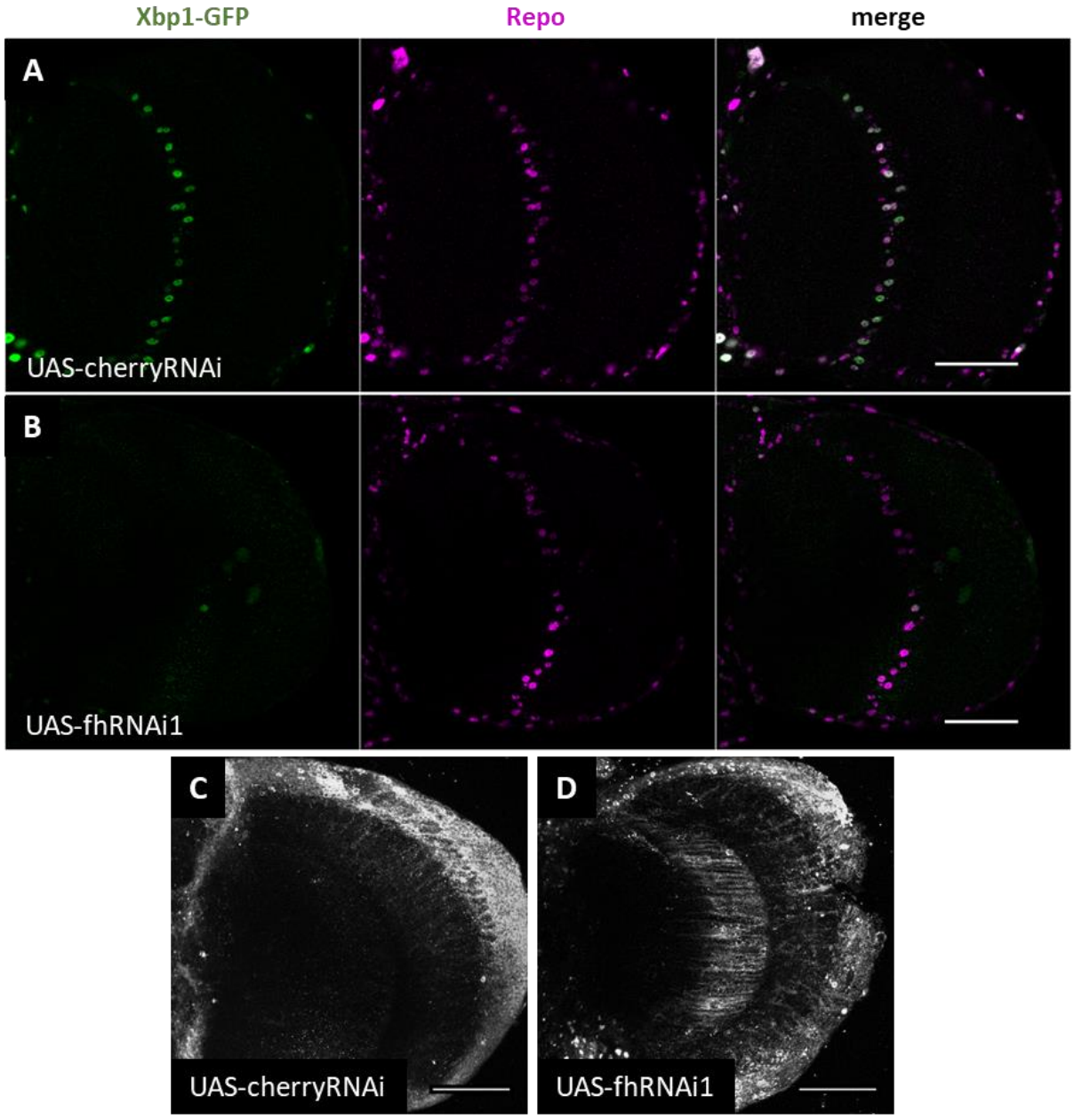

Figure 30: ER stress response is altered in frataxin deficient glia

(A-B) Representative optic lobes of 35d old control (A; *Repo*-Gal4 > UAS-Xbp1-GFP, UAS-cherryRNAi) and frataxin knockdown flies (B; *Repo*-Gal4 > UAS-Xbp1-GFP, UAS-fhRNAi1) labeled with Xbp1-GFP (green) and stained for Repo (magenta). Xbp1-GFP localizes to nuclei in controls. Nuclear localization is lost upon frataxin depletion. Scale bars represent 40 µm. (C-D) Representative optic lobes of 35d old control (C; *Repo*-Gal4 > UAS-cherryRNAi) and frataxin knockdown flies (D; *Repo*-Gal4 > UAS-fhRNAi1) stained for BiP. Accumulation of BiP in the GGC region. Scale bars represent 40 µm.

To visualize ER-stress, I utilized the Xbp1-GFP reporter. Xbp1 is a transcription factor activated by alternative splicing after ER stress and then translocates into the nucleus to activate gene transcription. The GFP-tagged reporter only expresses GFP in-frame when IRE1-mediated splicing of Xbp1 occurs (Sone et al, 2013). As a second marker, I used an antibody against the ER chaperone BiP/GRP78 (called BiP from now on).

Xbp1-GFP localized to the nucleus in the GGCs of controls, suggesting that the IRE1/Xbp1 pathway is activated by default in these cells (Figure 30A). This is in agreement with Sone et al, who also found Xbp1-GFP localized to glia, but not neurons during fly development. Interestingly, nuclear localization was abolished upon frataxin depletion (Figure 30B). In contrast, BiP levels were increased in this region after frataxin silencing (Figure 30C-D). These results clearly indicate that the ER stress response is modified in glia of FRDA flies, even though ER structure appeared to be normal.

Next, I decided to examine if the ER stress response was also altered in muscles in order to discriminate between general and tissue-specific events (Figure 31).

In contrast to glia, the Ire1/Xbp1 pathway was inactive in normal conditions, as no Xbp1-GFP signal could be detected in any control muscle (Figure 31A). In frataxin deficient flies, the pathway was activated and Xbp1-GFP could be found localized to nuclei, confirmed by counterstaining with DAPI (Figure 31B). This represents a striking difference between glia and muscles and implies that the ER stress response might vary in a tissue-dependent manner, depending on the structure and function of the ER in these tissues. In contrast to glia, qPCR can be used in this tissue to assess the transcription levels of *Xbp1* and *BiP*. Both endogenous *Xbp1* and *BiP* were upregulated about two-fold compared to controls (Figure 31C). Lastly, I assessed the third signaling pathway of the UPR by measuring the amount of phosphorylated eIF2α via Western Blot (Figure 31D-E). P-eIF2α levels were increased by about 60%. Altogether, these results indicate that all UPR branches are activated in muscles.

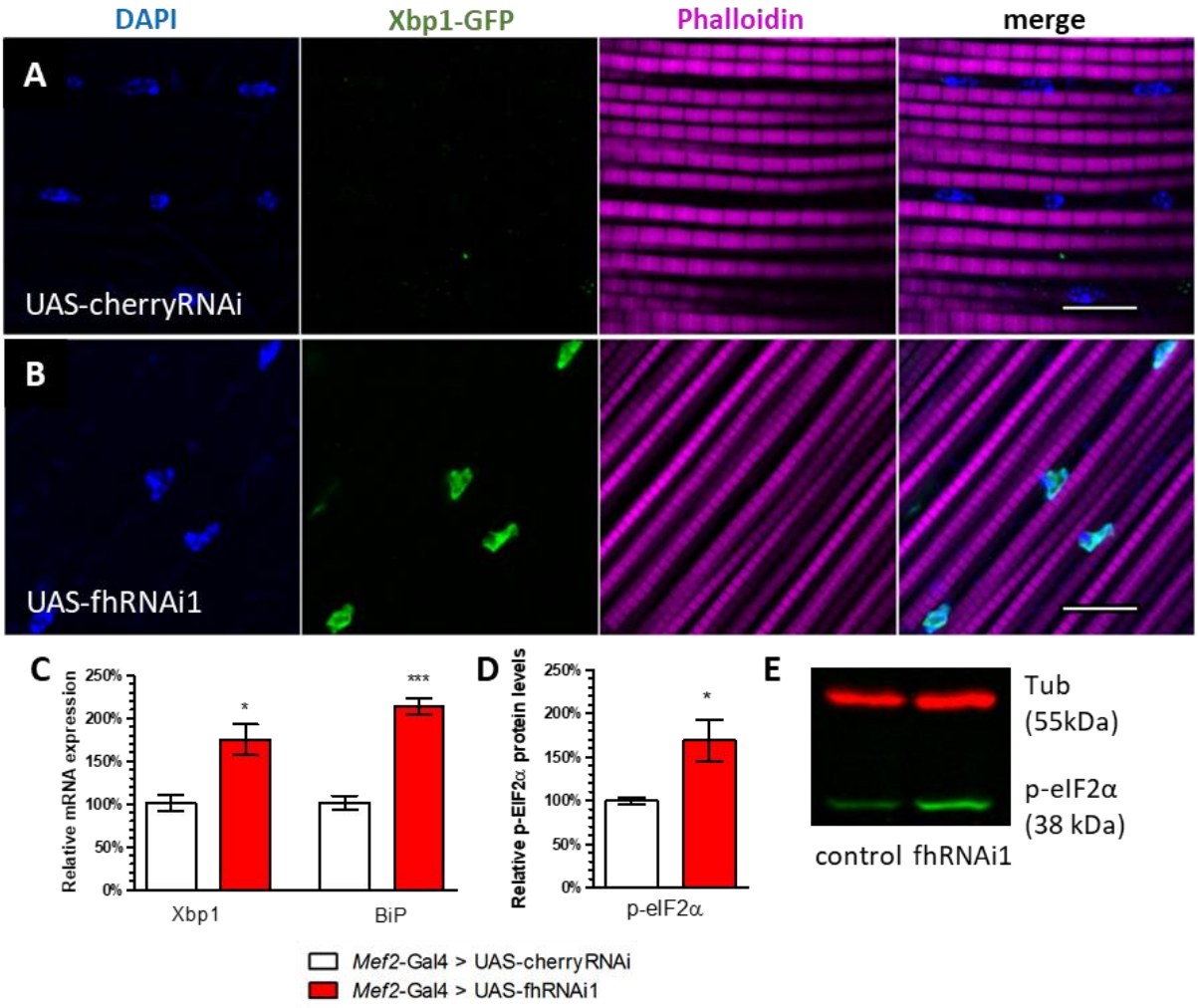

Figure 31: All UPR branches are activated in muscles

(A-B) Representative IFM of 6d old control (A; *Mef2*-Gal4 > UAS-Xbp1-GFP, UAS-cherryRNAi) and frataxin knockdown flies (B; *Mef2*-Gal4 > UAS-Xbp1-GFP, UAS-fhRNAi1) labeled with Xbp1-GFP (green) and stained with DAPI (blue) and Phalloidin (magenta). Xbp1-GFP is present only in FRDA flies and localizes to nuclei, confirmed by co-staining with DAPI. Scale bars represent 10 µm. (C) Relative gene expression levels of Xbp1 and BiP in 7d old control and FRDA flies. Both Xbp1 and BiP display increased mRNA levels. n = 4-6. (D) Quantification of p-eIF2α protein levels in FRDA flies 5 days post-eclosion compared to controls. P-eIF2α levels are increased. n = 3. (E) Representative example of a p-eIF2α Western blot from D.

In conclusion, both glia and muscles exhibited a change in the ER stress response, though they differed in the exact reaction. The distinctive demands of the ER in both tissues might be the cause for the discrepancy. Importantly, FRDA rises as another neurodegenerative disease where changes in the endoplasmic reticulum appear to be an important hallmark.

3.5.3. *Marf* knockdown reduces ER stress in glial cells

After confirming the hypothesis that frataxin knockdown induces ER stress in flies, the next step was to examine whether *Marf* knockdown would be able to restore normal ER function in the glia.

To this end, I first determined BiP levels via antibody staining in the GGCs. Compared to FRDA flies (Figure 32A), *Marf* knockdown resulted in a variable amount of BiP reduction, ranging from non-visible (Figure 32B) to significant (Figure 32B'). Importantly, about 80% of flies displayed substantial reduction (leaning towards Figure 32B'), whereas only about 20% exhibited minor reduction (leaning towards Figure 32B).

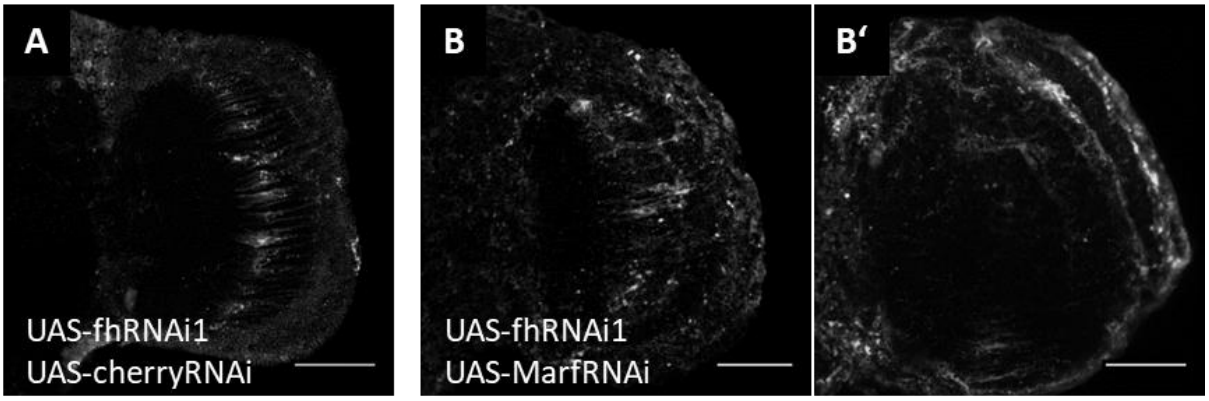

Figure 32: *Marf* knockdown reduces BiP accumulation

(A) Representative optic lobe of a 35d old frataxin depleted fly (*Repo*-Gal4 > UAS-fhRNAi1, UAS-cherryRNAi) stained for BiP. Accumulation of BiP in the GGC region. (B-B'). Representative optic lobes of 35d old FRDA flies co-expressing MarfRNAi (*Repo*-Gal4 > UAS-fhRNAi1, UAS-MarfRNAi) stained for BiP. Various levels of BiP staining are present in *Marf* knockdown flies, ranging from no (B) to substantial (B') reduction. Scale bars represent 40 μm.

Since the above result strongly implies that *Marf* knockdown suppresses ER stress in glia, I examined if *Marf* downregulation would also be able to restore nuclear Xbp1-GFP localization. As expected, Xbp1-GFP localized to nuclei in control flies, while only a basal BiP staining was detected (Figure 33A). Upon frataxin depletion, the nuclear Xbp1-GFP localization was abolished and BiP staining increased in the GGC region (Figure 33B). Remarkably, *Marf* knockdown reduced the BiP accumulation as well as restored nuclear Xbp1-GFP localization in most of the GGCs (Figure 33C).

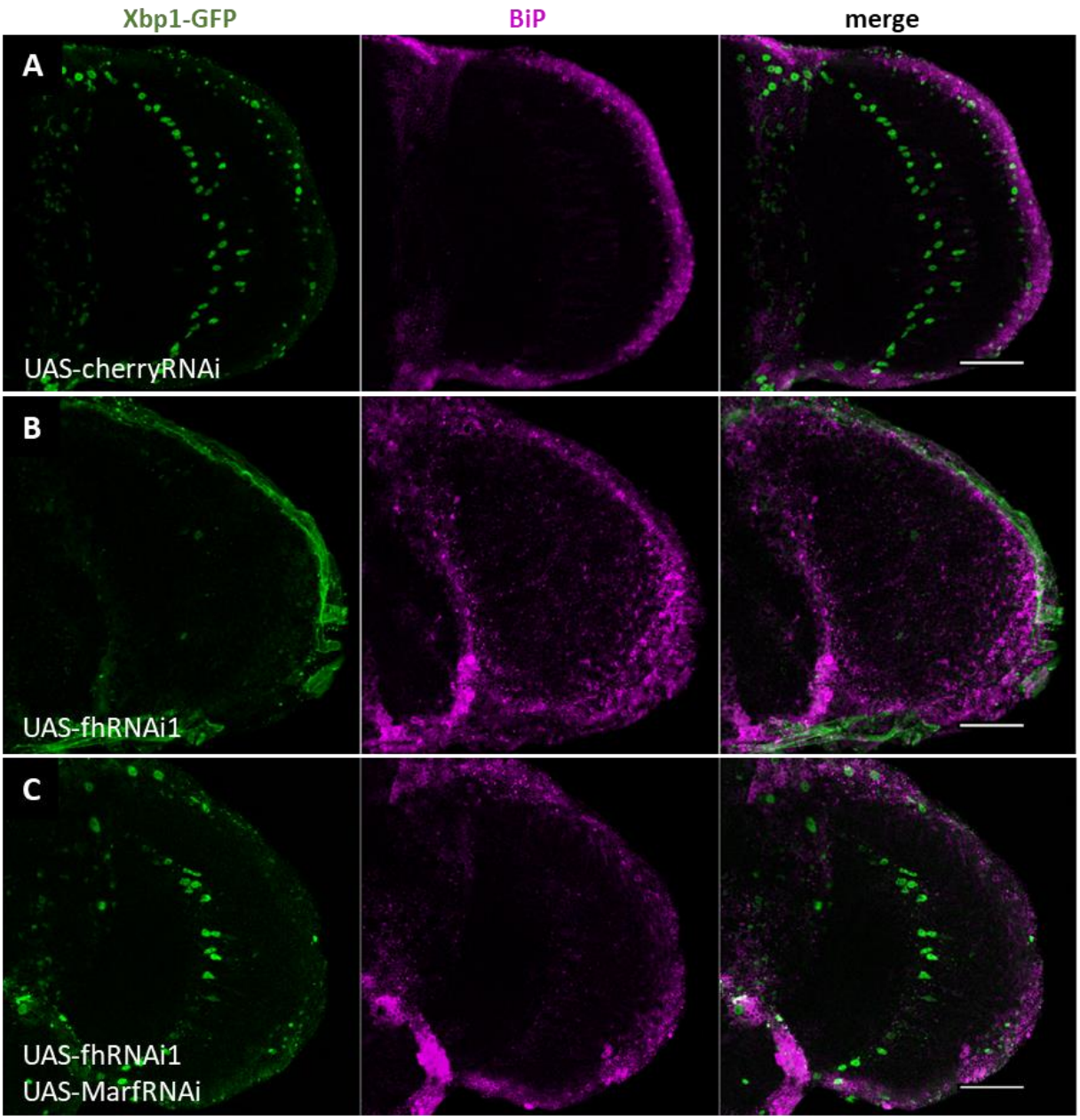

Figure 33: *Marf* knockdown restores nuclear Xbp1-GFP localization

(A-C) Representative optic lobes of 35d old flies labeled with Xbp1-GFP (green) and stained for BiP (magenta). Scale bars represent 40 µm. (A) Control fly (*Repo*-Gal4 > UAS-Xbp1-GFP, UAS-cherryRNAi). Xbp1-GFP localizes to nuclei, moderate BiP staining in the GGC region. (B) FRDA fly (*Repo*-Gal4 > UAS-Xbp1-GFP, UAS-fhRNAi1). Nuclear Xbp1-GFP localization is abolished, while BiP staining is increased. (C) FRDA fly with concomitant Marf knockdown (*Repo*-Gal4 > UAS-Xbp1-GFP, UAS-fhRNAi1, UAS-MarfRNAi). Nuclear Xbp1-GFP localization is restored in most cells; BiP staining is reduced compared to FRDA flies.

In summary, *Marf* downregulation is able to compensate the altered ER stress response and reverses the locomotor dysfunction, the brain degeneration and the lipid accumulation. More importantly, these results suggest that mitofusin indeed mediates the ER stress response in frataxin-deficient glia. Furthermore, the altered ER stress response seems to be of key importance in the pathology of the disease.

3.5.4. Chemical reduction of ER stress reduces brain vacuolization

Since above results strongly imply that the rescue of *Marf* downregulation is tied to its function in mediating ER stress, I tested whether a similar effect could be reached by chemical treatment. For this purpose I administered tauroursodeoxycholic acid (TUDCA), which has already been shown to attenuate ER stress in *Drosophila* (Debattisti et al, 2014).

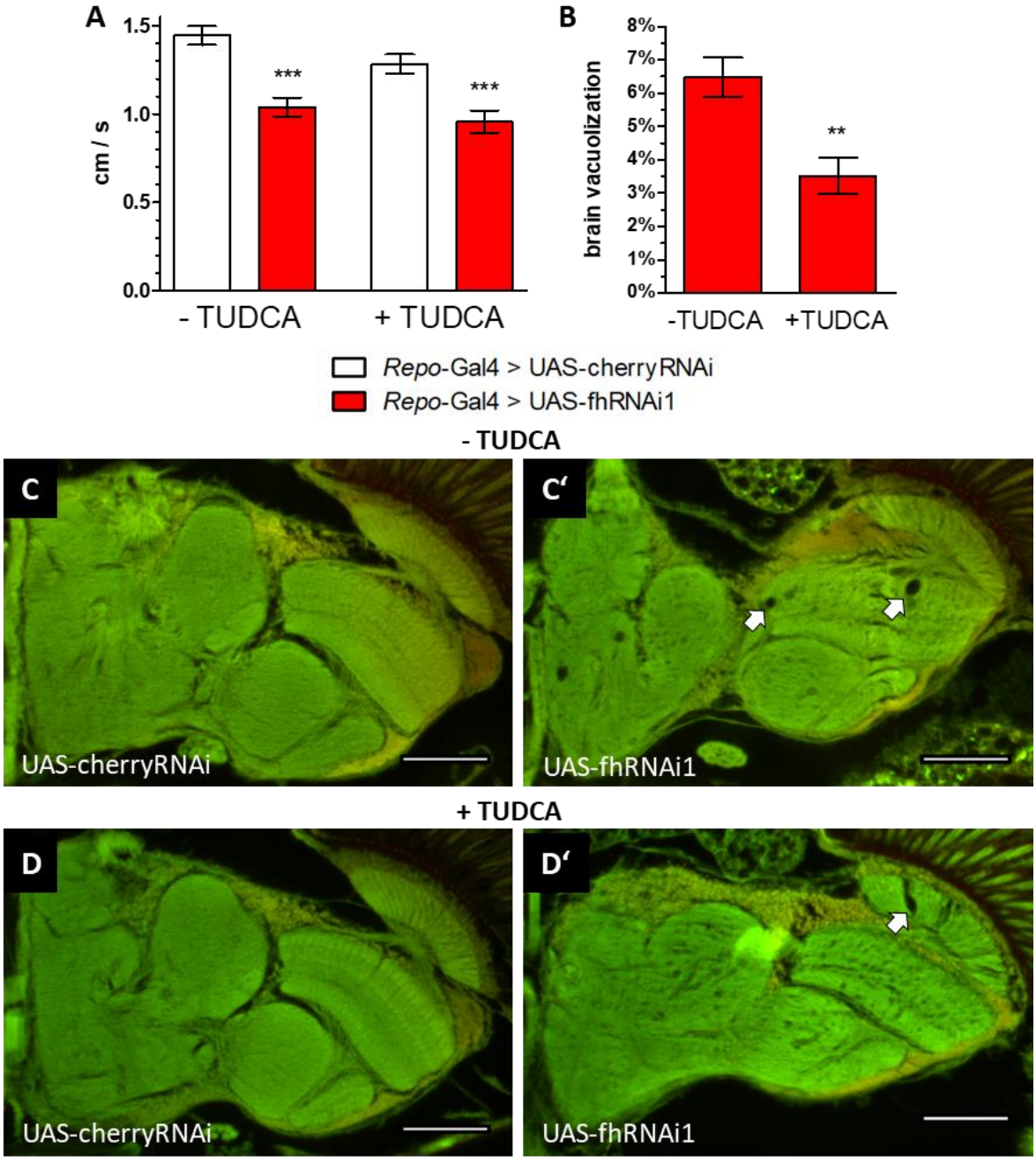

Figure 34: TUDCA ameliorates brain vacuolization

(A) Negative geotaxis assay of 10d old flies. TUDCA does not improve the locomotion in frataxin deficient flies. n = 12. (B) Quantification of vacuolization from C' and D'. n = 11. (C-D') Representative paraffin sections of 35d old flies. Scale bars represent 50 µm. (C, D) Control flies (*Repo*-Gal4 > UAS-cherryRNAi) fed with control food (C) or 15 mm TUDCA (D). No holes present. (C') FRDA flies (*Repo*-Gal4 > UAS-fhRNAi1) fed with water. Vacuolization occurs (arrows). (D') FRDA flies fed with 15 mM TUDCA. Administering the chemical reduces brain vacuolization (arrow).

In the negative geotaxis assay, TUDCA-fed FRDA flies displayed an identical locomotor deficit compared to untreated FRDA flies (Figure 34A). However, TUDCA administration was able to significantly ameliorate the brain vacuolization of frataxin depleted flies (Figure 34B-D'). The area measured was reduced from 6.5% to 3.5% in flies treated with TUDCA, a reduction of almost 50%.

In conclusion, reducing ER stress via TUDCA successfully improved one of the hallmarks of glial downregulation, but, in contrast to genetic manipulation via *Marf* knockdown, could not restore locomotion. Nevertheless, this highlights ER stress as a promising target for treatment of FRDA.

3.5.5. Genetic screen of MAM genes reveals Porin as another potential modifier of FRDA phenotypes

Next, I wanted to test if modification of other genes involved in MAMs would be able to elicit a similar effect to *Marf*. To this end, I tested *Drosophila* homologues of known tethering proteins where stocks were readily available from stock centers in a negative geotaxis assay: Bap31 and Fis1 form a tethering complex involved in Apoptosis signaling, while Itpr and Porin form a tethering complex responsible for Ca^{2+} transfer (reviewed in Paillusson et al, 2016). Moreover, I tested another putative MAM regulator, the small GTPase Sar1 (Ackema et al, 2016), which proved to be lethal when downregulated. Finally, one gene involved in mediating the ER stress response was added to the screen, PERK (reviewed in Hetz & Mollereau, 2014; Celardo et al, 2016). Altogether, seven lines were tested.

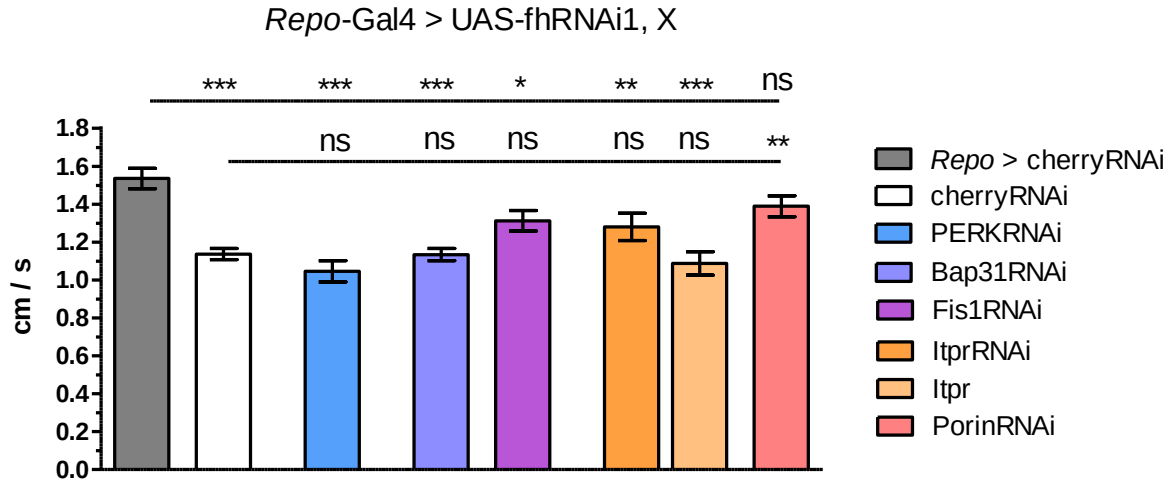

Figure 35: Porin knockdown improves locomotor deficit

Locomotor performance of 10d old flies co-expressing frataxin knockdown and an additional transgene (*Repo*-Gal4 > UAS-fhRNAi1, X), except the first bar (*Repo*-Gal4 > UAS-cherryRNAi). Only *Porin* knockdown improved locomotion significantly. n = 12.

Of all lines, only *Porin* knockdown displayed a significant increase in locomotor ability after 10d compared to FRDA flies (Figure 35). Climbing speed was increased around 22% from 1.14 cm/s to 1.39 cm/s. This result together with the MarfRNAi rescue suggests that modifying MAMs could be an interesting, novel way of ameliorating FRDA phenotypes.

3.6. Moderate frataxin knockdown as a tool for drug testing in a system-wide manner

Strong frataxin knockdown can serve as a reasonable model for unravelling downstream effects of frataxin knockdown in a tissue-specific manner (Anderson et al, 2008; Navarro et al, 2010; Navarro et al, 2015 and this work). However, the severe frataxin deficiency presents two disadvantages: First, ubiquitous silencing triggers pre-adult lethality (Anderson et al, 2005). Second, the effects induced are likely too strong to be completely rescued using pharmacological approaches (see Figure 24 and Figure 34).

Thus, I decided to use a second fly model of FRDA exhibiting a more moderate knockdown that more closely resembles the situation in patients (Llorens et al, 2007). This model has been already successfully used to test certain chemical treatments in *Drosophila* (Soriano et al, 2013; Calap-Quintana et al, 2015). This moderate knockdown line is called fhRNAi2 in this thesis.

3.6.1. Rapamycin ameliorates p62 accumulation

I first assessed whether p62 accumulation would also be present in this model. Congruent with tissue-specific knockdown, p62 accumulated when frataxin was downregulated moderately in the whole fly (Figure 36A-B). P62 levels were increased about two-fold after 7d, rising to about seven-fold after 30d. I could also confirm that oxidative stress aggravates p62 accumulation in young flies. Compared to flies kept in normal conditions, p62 accumulation increased from two-fold to four-fold.

In yeast, rapamycin is able to protect frataxin depleted cells from oxidative damage by promoting autophagy (Marobbio et al, 2012). Therefore, I tested whether rapamycin treatment would amend the p62 accumulation in this model. In agreement with the yeast study, rapamycin lowered the p62 accumulation significantly under oxidative stress conditions, from four-fold back to about two-fold (Figure 36C-D).

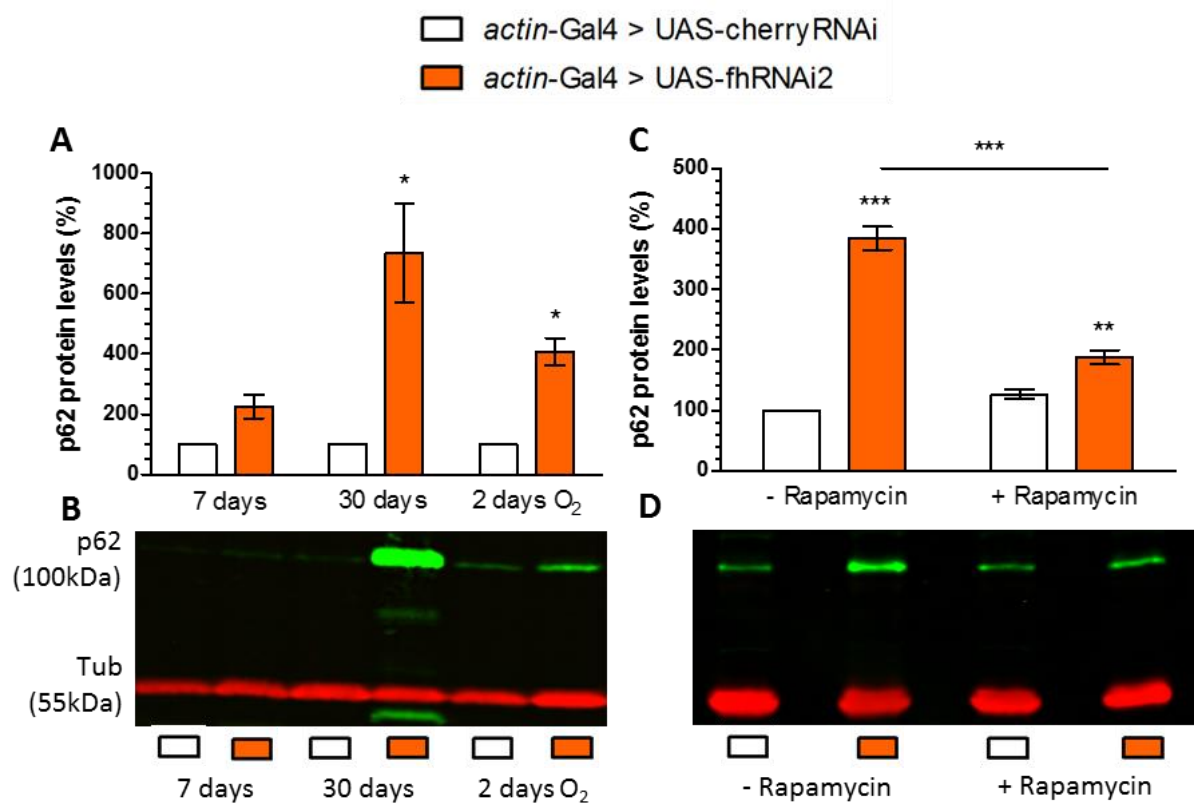

Figure 36: Rapamycin reduces p62 accumulation under oxidative stress conditions

(A) Quantification of p62 levels of control (*actin*-Gal4 > UAS-cherryRNAi) and frataxin knockdown flies (*actin*-Gal4 > UAS-fhRNAi2). Strong age-dependent accumulation. Oxidative stress exacerbates the phenotype. n = 3. (B) Representative Western Blot of A. (C) Quantification of p62 levels of control and frataxin knockdown flies fed with control food or Rapamycin and treated with 2d hyperoxia. Rapamycin significantly reduces p62 accumulation. n = 3. (D) Representative Western Blot of C.

This result is in agreement with Calap-Quintana et al, who described that under hyperoxic conditions rapamycin acts cytoprotective by enhancing autophagy.

3.6.2. TUDCA improves Aconitase activity

TUDCA had already shown a positive effect under strong glial knockdown conditions by reducing brain vacuolization (Figure 34). Naturally, it was interesting to test whether pharmacological treatment with TUDCA would also be able to restore defects upon moderate ubiquitous frataxin silencing. Thus, flies were treated with 15 mM TUDCA, subjected to 2d of hyperoxia and their aconitase activity measured (Figure 37). As expected, frataxin depletion reduced aconitase activity to 46% in control food. Importantly, TUDCA distribution did not alter aconitase activity in control flies. FRDA flies, however, benefitted from the chemical. Aconitase activity was increased by about 33% to 67% of control level. This suggests that reducing ER stress might even be beneficial for mitochondrial function.

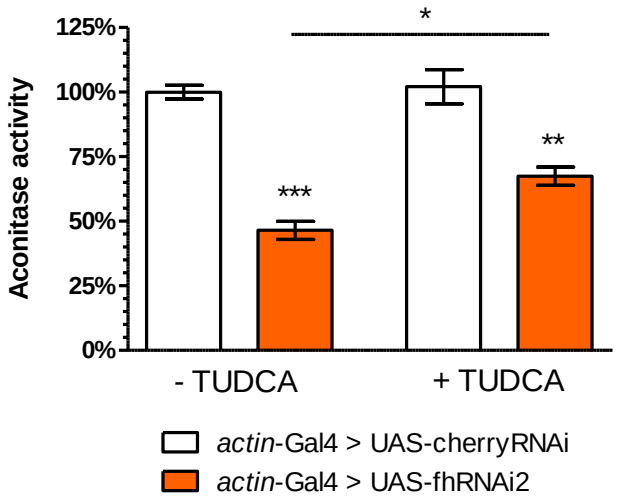

Figure 37: TUDCA improves Aconitase activity

Aconitase activity of flies exposed to 2d of hyperoxia. Frataxin knockdown reduces Aconitase activity significantly. TUDCA administration improves Aconitase activity by approx. 33%. n = 3.

In conclusion, reducing ER stress via TUDCA treatment is able to improve the flies' condition under moderate ubiquitous frataxin silencing. Thus, the ER component of the disease shows promise as a target for potential treatments.

4. Discussion

4.1. *Drosophila* IFM are suitable for studying effects of frataxin knockdown

Drosophila muscles are enriched in mitochondria and therefore appear as a promising tissue to study the effects of frataxin knockdown on mitochondrial integrity. Indeed, the IFM have been previously used to successfully investigate mitochondrial homeostasis in Parkinson's disease (Clark et al, 2006; Deng et al, 2008). Although FRDA in humans is primarily a neuronal disorder, effects of frataxin depletion on the skeletal muscles of patients have been reported but symptoms are less prominent. Investigation of the calf muscles revealed impaired mitochondrial respiration, ATP synthesis and delayed recovery of tissue oxygenation after exercise (Lodi et al, 1999; Lynch et al, 2002; Nachbauer et al, 2012). These results could not be reproduced by a study using the forearm instead of the calf (Bossie et al, 2016), but the authors speculated that the difference might be due to the size and energy demands of the muscle type. In mouse, conditional ablation of frataxin produced no defects in the skeletal muscles (Puccio et al, 2001), but differentially regulated lipogenesis has been reported in a GAA-repeat based model (Coppola et al, 2009).

Therefore, I first needed to verify that frataxin knockdown in the IFM would trigger previously established defects such as decreased energy production and reduced activity of ISC-containing enzymes. Interestingly, using the *Mef2*-Gal4 driver line with UAS-fhRNAi1 did not induce a developmental arrest as has been reported for ubiquitous or glial specific knockdown. With *actin*-Gal4, larvae failed to enter the pupal stage (Anderson et al, 2005), while *Repo*-Gal4 driven knockdown resulted in partial lethality in the pupal stage (Navarro et al, 2010). For *Mef2*-Gal4, every fly expressing UAS-fhRNAi1 was able to eclose normally without a developmental delay.

Physiological and biochemical analysis revealed that these flies share the familiar symptoms of FRDA: Loss of locomotor ability, reduced ATP levels, aconitase activity and life span (Figure 12). In agreement with the human condition, these phenotypes became more severe with age. Remarkably, despite the absence of a developmental arrest, the deterioration occurred much more rapidly than previously reported for other tissues, allowing a fast analysis in an age-dependent manner without having to age the flies for an extended period. This serves as an advantage to other tissues.

Overall, these results prove the suitability of IFM to study downstream effects of frataxin depletion. Interestingly, *Drosophila* skeletal muscles recapitulate defects reported in muscles of patients (Lodi et al, 1999; Lynch et al, 2002; Nachbauer et al, 2012), whereas the conditional

mouse model shows no phenotype (Puccio et al, 2001). A reason for that might be that the IFM in fruit flies are more sensitive to frataxin depletion than mouse skeletal muscles, suggesting that fly muscles are a better model tissue than mouse muscles for FRDA studies. Therefore, *Drosophila* also appears an interesting model organism to further study the effects of frataxin deficiency on skeletal muscles.

4.2. Mitochondrial homeostasis is impaired

As a mitochondrial protein, loss of frataxin is closely linked to a disruption to mitochondrial homeostasis (Pandolfo, 2012). However, information about pathways like mitochondrial dynamics and quality control is limited and partially contradictory in different models. Thus, I was interested in an analysis of the complete mitochondrial network to shed light into this matter.

4.2.1. Mitochondrial morphology is altered

To evaluate mitochondrial homeostasis in frataxin depleted flies, I first assessed mitochondrial morphology in glia and muscles. In glia, mitochondria appeared clustered around the nucleus, while they were more evenly distributed in control flies (Figure 13). In muscles, mitochondria normally form long chains between the muscle fibres (Figure 11B). In frataxin knockdown flies, gaps occurred within the chain and mitochondria were fragmented, with additional hollow mitochondria present (Figure 14). Interestingly, mitochondria from flies directly post-eclosion displayed mitochondrial organization still similar to controls, suggesting they are still mostly functional in this case.

In both human and rat cell culture, frataxin knockdown triggered the formation of enlarged mitochondria (Bolinches-Amoros et al, 2014; Obis et al, 2014), while increased fragmentation was observed in yeast and *C.elegans* (Lefevre et al, 2012; Schiavi et al, 2015). For *Drosophila*, the effects seemed to be tissue-dependent. In dopaminergic neurons, frataxin knockdown had triggered enlarged mitochondria under hyperoxic conditions (Edenharter, 2013). However, in both glia and muscles, mitochondria appeared fragmented. These results confirm that mitochondrial morphology and distribution are altered upon frataxin depletion. Furthermore, the mitochondrial response seems dependent on the physiology and adaptation capacity of the cell type. Enlarged mitochondria were reported for neuronal (Bolinches-Amoros et al, 2014; Edenharter, 2013) and cardiac cells (Obis et al, 2014), while fragmentation was found in muscles (Schiavi et al, 2015 and this work) and glia (this work).

An analysis of the expression profile in muscles revealed that the alterations in morphology coincide with changes in the expression levels of genes involved in mitochondrial dynamics, although a similar analysis performed in yeast revealed no significant differences (Lefevre et al, 2012). The upregulation of *Opa1* and downregulation of *drp1* and *Pink1* point towards increased mitochondrial fusion. Since this result is in contrast to the observed phenotype, these changes represent either a compensatory response or a pathological consequence. As mitochondrial fragmentation is consistent with targeted degradation (Gomes & Scorrano, 2013), this might indicate a pathological consequence instead of a cellular adaptation in this tissue.

4.2.2. Morphological changes correlate to physiological consequences

Mitochondrial fragmentation and perinuclear localization are signs of defective mitochondria (Palikaras & Tavernarakis, 2014). TMRE staining in IFM confirmed that the visible alterations correspond to a loss of mitochondrial membrane potential (Figure 15). A majority of mitochondria are still healthy in young frataxin-depleted flies, while fragmented mitochondria of older flies had lost TMRE staining and thus their membrane potential. Since mitochondrial membrane potential is important for proper energy production, this result agrees with the age-dependent reduction in ATP levels (Figure 12A), known hallmarks of FRDA (Koeppen & Mazurkiewicz, 2013). Thus, it is possible to directly correlate visible mitochondrial fragmentation to a functional deficit. Importantly, mitochondrial dysfunction precedes the morphological changes, since a significant loss of membrane potential is already found shortly post-eclosion (Figure 15), while morphology still appears mostly unaffected at this age (Figure 14).

4.2.3. Oxidative stress response is altered

Susceptibility to oxidative insult is another established feature of FRDA in patients (Pandolfo, 2012). However, various models have reported conflicting results with regard to the involvement of oxidative stress. For mouse, oxidative stress was present in models with residual frataxin expression, whereas it was absent in conditional knockout models (Perdomini et al, 2013). For *Drosophila*, increased sensitivity to oxidative stress and successful treatment with antioxidants have been reported before (Llorens et al, 2007; Anderson et al, 2008; Navarro et al, 2010; Soriano et al, 2013). Still, the role of oxidative stress in frataxin depleted flies has been challenged as well, since other studies found no increase in ROS and treatment with

antioxidants was unable to improve the flies' condition (Shidara & Hollenbeck, 2010; Tricoire et al, 2014; Chen et al, 2016).

To address this question in our tissues of interest, I investigated the redox potential of mitochondria via a redox-sensitive GFP reporter specific for the glutathione redox pool (Albrecht et al, 2011). Glutathione is a powerful cellular antioxidant capable of neutralizing reactive oxygen species. It is normally present in cells in a reduced state (GSH) and becomes oxidized (GSSG) under oxidative stress conditions by donating an electron (Kaplowitz, 1981). In a study of FRDA patients, total GSH levels were reduced in erythrocytes (Piemonte et al, 2001). The ratio of GSSG to GSH can be used to determine the level of oxidative stress within the cell and increased ROS production directly correlates to increased GSSG:GSH levels (Armstrong et al, 2010). In various FRDA models, the GSSG:GSH ratio was generally raised when frataxin was depleted. This was the case for yeast (Auchère et al, 2008; Bulteau et al, 2012) and human cell culture (Tan et al, 2003; Bulteau et al, 2012). In mouse, an increase was reported for skeletal muscles (Calatrava-Ferreras et al, 2016), while the ratio appeared unchanged in neurons (Shan et al, 2013).

Surprisingly and in contrast to most other models, glutathione was not oxidized, but instead even more reduced than in control flies (Figure 16).

One possible explanation is that the GSSG/GSH ratio was measured at time points where mitochondria are strongly affected and less ROS are produced as a byproduct of respiration. In agreement, the oxidant-sensitivity of frataxin depleted cells derives directly from a higher production of mitochondrial ROS (Tan et al, 2003). This might also partially explain the contradicting results regarding the involvement of oxidative stress. Depending on the tissue and severity of frataxin knockdown, endogenous ROS levels might be unaffected, but external oxidative stress would still elicit detrimental effects (Armstrong et al, 2010).

To further address this question, it would be interesting to determine the GSH/GSSG ratio at earlier time points. Additionally, testing total glutathione levels in the cytosol and mitochondria might provide further insight, since glutathione gets transported into mitochondria upon frataxin depletion (Auchère et al, 2008; Tan et al, 2003).

Furthermore, mitochondrial and cytosolic redox states can differ even within the same cell depending on the insult (Albrecht et al, 2011). It would also be interesting to test another roGFP specific for hydrogen peroxide (H_2O_2) levels, as H_2O_2 scavengers have been able to rescue frataxin knockdown defects in the fly (Anderson et al, 2008).

4.3. Mitophagy is activated and proceeds normally

Mitochondrial fragmentation is a known prerequisite for clearance by autophagy (Palikaras & Tavernarakis, 2014). In frataxin depleted flies, the autophagy marker p62 accumulated in both glial cells and muscles (Figure 17 and Figure 18), in agreement with increased amounts detected in a cardiac mouse model of FRDA (Huang et al, 2013). In fact, p62 levels were increased tremendously in muscle tissue in an age-dependent manner and accumulated in vesicle-like structures reminiscent of autophagosomes. These vesicles partially co-localized to mitoGFP, indicating that mitochondria might be present in them. As accumulation of p62 has been linked to a block in autophagic clearance (Bartlett et al, 2011), I was interested if there was a defect in autophagy which would prevent mitochondria from being properly degraded. Interestingly, increased numbers of autophagosomes and lysosomes were observed in dorsal root ganglia of mouse models (Simon et al, 2004; Al-Mahdawi et al, 2006). In *C.elegans*, it has been shown that autophagy is induced and autophagic flux increases upon frataxin silencing (Schiavi et al, 2015). In contrast to my results, the authors describe a decrease in p62 levels in the worm. However, frataxin depletion extends longevity in *C.elegans*, a sharp discrepancy to every other model.

To solve this inconsistency, I performed a detailed analysis of the autophagic flux in muscles (Figure 20). The marker GFP-Atg8a was properly recruited to the p62 vesicles, suggesting a functional autophagosome formation. The lysosomal marker LAMP1-GFP also co-localized to these vesicles, showing that fusion with lysosomes occurs. In addition, both proteins did not accumulate in frataxin depleted flies, further confirming a working turnover of both proteins. In fact, I could detect increased levels of free GFP, a sign for enhanced turnover of the protein and consequently autophagic flux (Mauvezin et al, 2014). The results were even more pronounced in glial cells, where reduction of GFP-Atg8a and LAMP1-GFP levels in conjunction with increased levels of free GFP hint at an increased autophagic flux, despite a slight accumulation of p62 (Figure 22).

How can this difference be explained? For glial cells, one explanation is the general age of the fly. P62 levels increase naturally with age in the brain (Nezis et al, 2008). Indeed, p62 levels in the GGC region were highly variable and could be dependent on how severely affected the individual fly is. In agreement, overexpression of Atg8a reduced p62 levels in the brain (Figure 23A). In muscles, p62 accumulation is already evident shortly after eclosion and the pathology progresses much more rapidly in this tissue. Therefore, one can speculate that the accumulation of defective mitochondria is too substantial within a short amount of time for the autophagic machinery to cope with. Even if autophagy is activated and proceeds without inhibition, the

machinery is overwhelmed with potential targets, leading to the observed increase in p62 levels, as not every organelle can be processed at the same time. Another possible explanation might be the structure of mitochondria in muscles. In contrast to glia, mitochondria are organized in tight chains, possibly limiting access for the autophagic machinery and consequently slowing down turnover.

To further ensure that the autophagic flux I measured corresponds to a mitophagic flux, I utilized the mtRosella biosensor. It has already been used as a powerful tool for visualizing mitophagy *in vivo* in yeast, *C.elegans* and mammalian cells (Rosado et al, 2008; Böckler & Westermann, 2014; Schiavi et al, 2015; Sargsyan et al, 2015). In my case, the majority of damaged organelles had lost both pHluorin and dsRed signal, further indicating a proper turnover (Figure 21).

Altogether, these results clearly show that in the fly model, mitophagy is induced, mitophagic flux enhanced and can proceed normally. This is in agreement with results from other FRDA models such as cell culture, *C.elegans* (Bolinches-Amoros et al, 2014; Schiavi et al, 2015). Moreover, lysosomes and autophagosomes accumulate in the dorsal root ganglia of FRDA mouse models (Simon et al, 2004; Al-Mahdawi et al, 2006). These results suggest that mitophagy works as a protection mechanism against mitochondrial deficiency when frataxin is depleted. Importantly, enhanced autophagic activity appears to be the first biomarker so far which is common to all models.

Unexpectedly, overexpression of GFP-Atg8a reduced p62 accumulation in glial cells while overexpression of LAMP1-GFP did not (Figure 23). Since, in contrast to LAMP1-GFP, the GFP-Atg8a construct incorporates the full-length protein, this implies that the GFP-tagged Atg8a is fully functional and able to stimulate autophagy. Indeed, mCherry-tagged Atg8a has been shown to rescue Atg8a null mutants and was able to boost autophagy (Pircs et al, 2012). This induction of autophagy by GFP-Atg8a partially ameliorated the brain vacuolization, but was unable to restore locomotion or reduce the lipid accumulation, further confirming autophagy working as a cytoprotective mechanism in Friedreich's ataxia. In line with this argument, promoting autophagy has also been shown to successfully counteract neurodegeneration in *Drosophila* models of Huntington's and Parkinson's disease (Ravikumar et al, 2004; Tain et al, 2009). However, enhancing autophagy alone is not sufficient to fully combat frataxin deficiency in the FRDA model I utilize.

4.4. Frataxin knockdown triggers ER stress

4.4.1. The UPR is activated in muscles

ER stress is now considered a hallmark of virtually every neurodegenerative disease, even in disorders not actually connected to misfolded proteins. Instead, it can be defined as a more general, indirect response to external stressors (Scheper & Hoozemans, 2015). Interestingly, increasing evidence has linked the endoplasmic reticulum to many cellular processes also disturbed in Friedreich's ataxia: energy production, lipid and calcium metabolism and apoptosis signalling (Hetz & Mollereau, 2014). Few studies have looked at ER stress in FRDA so far. An increase in expression or activity of ER stress markers such as ATF4, BiP and phosphorylated eIF2α has been described before in cell culture (Lu & Cortopassi, 2007). In another cell culture study, frataxin depleted cells were more sensitive to chemically-induced ER stress which in turn triggered accumulation of BiP (Bolinches-Amoros et al, 2014). These results suggest that frataxin depletion triggers the UPR.

A thorough investigation of the ER structure in muscles using an ER-targeted GFP revealed that the basic structure was intact, forming a ladder-like structure around the actin filaments. Interestingly, frataxin depletion resulted in the formation of GFP aggregates, a potential sign of ER swelling, which has been connected to cell death (Figure 29). In agreement with previous results, all UPR branches were activated in muscles. Xbp1 and BiP mRNA levels were increased as were protein levels of phosphorylated eIF2α. In addition, the marker Xbp1-GFP localized to nuclei in frataxin depleted flies, a sign for the activation of the Ire1-Xbp1 branch (Figure 31). These results clearly show that ER stress is present in frataxin depleted muscles, which in turn stimulates the UPR.

4.4.2. Glia as a special case?

When examining ER stress markers in glial cells, it initially was surprising that Xbp1-GFP already localized to the nucleus of the GGCs in freshly eclosed control flies (Figure 30). Interestingly, default activation of the Ire1/Xbp1 pathway has already been described in a subpopulation of larval glial cells (Sone et al, 2013). The authors speculated that this phenotype is related to the specific role of secretory glial cells in generating the components for the multi-layered membrane sheaths around neurons. Thus, it is possible that the Ire1/Xbp1-active glia protect neurons from their deterioration through this ensheathment. In agreement, the GGCs are part of this subpopulation of ensheathing glia (Awasaki et al, 2008). Besides glia, default activation of Xbp1-based reporters has also been reported for the larval intestine, fat body, certain neurons and developing photoreceptors, as well as for the adult male reproductive

system and the intestinal stem cells (Ryoo, 2015). Such activation seems to be pivotal for a proper homeostasis of certain tissues, particularly secretory ones.

In frataxin depleted flies, nuclear Xbp1-GFP staining is abrogated, meaning that this pathway is likely shut down. This might represent a pivotal element underlying or at least contributing to the brain degeneration observed in these flies. In accordance with muscles, BiP levels were increased, hinting at increased levels of ER stress in this tissue as well, even though Xbp1 was deactivated. However, BiP is a general marker whose transcription can be activated by all pathways. It would be interesting to test the other pathways in this tissue in detail to check their activation status. Interestingly, no apparent difference in ER structure could be detected and, in contrast to muscles, no GFP aggregates were visible. It cannot be ruled out that changes in ER morphology are present, but cannot be resolved with a fluorescent marker like ER-GFP.

Overall, ER stress also manifests in glia, although the different main role of the ER in both tissues may account for the differences. Indeed, skeletal muscles feature a highly specialized ER called sarcoplasmic reticulum, which serves mainly as a calcium storage depot and regulates its release for muscle contraction (Rayavarapu et al, 2012).

4.5. *Marf* knockdown ameliorates FRDA phenotypes in glia by mediating the ER stress response

4.5.1. *Marf* emerges as a key mediator of FRDA phenotypes

Since mitochondria were clearly affected, I performed a negative geotaxis assay with genes involved in mitochondrial homeostasis to potentially identify modifiers of frataxin phenotypes. Interestingly, only *Marf* knockdown proved highly beneficial. In agreement with Anderson et al, 2008, overexpression of the hydrogen peroxide scavenger mitochondrial catalase was also able to improve the locomotor deficit, albeit not as profound as *Marf*. This highlights Marf as a key mediator in the pathology. In addition, *Marf* knockdown resulted in almost complete recovery of lipid accumulation and brain vacuolization, whereas manipulation of other genes did not influence them (Figure 26).

4.5.2. Neither mitochondrial dynamics nor mitophagy are crucial for *Marf* rescue

Because of Marf's prominent role in mitochondrial fusion, it would seem likely that the inhibition of fusion is the key factor behind the Marf rescue. Importantly, *Marf* knockdown was able to suppress Pink1 and Parkin loss-of-function in *Drosophila* models of Parkinson's disease and cardiac dysfunction by preventing mitochondrial fusion (Deng et al, 2008; Liu & Lu, 2010; Bhandari et al, 2014). However, in these studies *Opa1* downregulation and *drp1* overexpression

showed a similar effect. This was not the case here: Manipulation of *Opa1* and *drp1* were unable to counteract frataxin deficiency the same way *Marf* downregulation did. *Marf* knockdown in fact changed the mitochondrial morphology, but did not restore control shape (Figure 27A-C).

Another possibility might have been Marf's role in mitophagy. Marf's position in the outer mitochondrial membrane makes it a prime target of Pink1 and Parkin for ubiquitination to mediate mitophagy (Ziviani et al, 2010). However, modification of both Pink1 and Parkin failed to modify FRDA phenotypes. In addition, *Marf* knockdown failed to abrogate the p62 accumulation in glia (Figure 27D-F).

These results imply that the rescue via *Marf* knockdown is neither a direct consequence of restored mitochondrial dynamics nor mitophagy. Interestingly, *Marf* knockdown was also able to rescue phenotypes in two *Drosophila* models of Parkinson's disease without directly improving mitochondrial function (Celardo et al, 2016).

4.5.3. *Marf* knockdown remodels the ER stress response

Interestingly, human and fly mitofusins have been described to modulate cellular responses to ER stress (Munoz et al, 2013; Debattisti et al, 2014). In frataxin depleted glial cells, *Marf* knockdown was able to both restore nuclear Xbp1-GFP localization and reduce BiP accumulation in the majority of flies (Figure 32). This clearly highlights the involvement of *Marf* in mediating ER stress and heavily implies that the rescue of FRDA phenotypes by *Marf* knockdown might be connected to resuscitating proper ER function in glia.

The question remains how *Marf* knockdown could facilitate restoration of ER function and ultimately counteract frataxin deficiency. In the fruit fly, ablating *Marf* in muscles has been shown to induce ER stress (Debattisti et al, 2014). Of particular interest is the function of mitofusins within the so called ER mitochondria-associated membranes (MAMs). MAMs connect the ER to mitochondria and regulate several essential cellular processes like calcium signaling, phospholipid exchange, apoptosis and autophagy (Rowland & Voeltz, 2012). They have recently come to the forefront as major contributors to the pathology of various neurodegenerative diseases such as Alzheimer's disease and Parkinson's disease (Zampese et al, 2011; Cali et al, 2013). Mitofusin has been described as such a tether between mitochondria an the ER based on findings in human cell culture (Brito & Scorrano, 2008). Further studies corroborated that ablation of Mitofusin results in reduced ER-mitochondrial contacts, leading to diminished mitochondrial Ca^{2+} uptake and lipid transfer (Sebastián et al, 2012; Schneeberger et al, 2013; Naon et al, 2016).

However, the role of Mitofusins as ER-mitochondrial tethers has been challenged by others (Cosson et al, 2012; Filadi et al, 2015; Leal et al, 2016). In these studies, ablation of Mitofusin entailed the loss of ER-mitochondria contacts and subsequently reduced Ca^{2+} uptake by mitochondria. Their model places Mitofusin as a tether antagonist preventing excessive proximity between the two organelles. Therefore, it remains unclear if Mitofusin serves as an agonist or antagonist for ER-mitochondria contacts and more data are needed to resolve this issue.

Importantly, a recent paper has found that increased ER stress signaling is mediated by Marf in a *Drosophila* model of Parkinson's disease. Reducing mitofusin-ER contacts proved neuroprotective independently of restoring mitochondrial function, likely by decreasing contacts between defective mitochondria and the ER (Celardo et al, 2016). This result provides a possible explanation for my phenotypes: In frataxin deficient flies, defective mitochondria accumulate and induce ER stress by tethering through Marf. When *Marf* is downregulated, these contacts are diminished and ER stress signaling is reduced, protecting the glial cells from excessive ER stress. Interestingly, it has been shown that *Marf* mutants display reduced number of lipid droplets in addition to alterations in ER and mitochondrial structure (Sandoval et al, 2014). Furthermore, loss of frataxin induces abnormal sphingolipid synthesis, which are synthesized in the ER (Chen et al, 2016). These findings connect the ER stress to altered lipid metabolism and provide an explanation how *Marf* knockdown in glia is able to reduce the lipid accumulation and brain vacuolization (Figure 26).

4.5.4. *Marf* knockdown is detrimental in muscle tissue

Because *Marf* knockdown in glial cells displayed a striking benefit for frataxin depleted flies, it seemed likely that reducing Marf levels in the IFM would also prove favorable. However, *Marf* knockdown in muscles not only failed to ameliorate the locomotion of frataxin deficient flies, but resulted in diminished locomotor ability (Figure 28). This result can be explained by the fact that manipulation of Marf in IFM adversely affects even control flies. While *Marf* knockdown reduced locomotion drastically, overexpression proved developmentally lethal. This suggests that maintenance of a specific mitochondrial network is of paramount importance in muscles. More specifically, previous results in IFM show that *Marf* downregulation is able to suppress *Pink1* and *Parkin* mutants and this rescue can also be obtained by *Opa1* downregulation or *drp1* overexpression (Deng et al, 2008). By contrast, *Opa1* downregulation or *drp1* overexpression are not equivalent to *Marf* knockdown in my glial model of FRDA (Figure 25). It is conceivable that tight regulation of mitochondrial dynamics

is more important in muscles than in glia. In agreement with this idea, *Marf* overexpression in glia was viable, in contrast to muscles.

4.6. *Drosophila* as a model for testing pharmacological treatments

4.6.1. ER stress appears a promising, novel target

As mentioned above, from my tested genetic manipulations, only *Marf* downregulation ameliorated locomotion, brain vacuolization and lipid accumulation (Figure 25 and Figure 26). Interestingly, *Marf* knockdown neither reduced the p62 accumulation nor restored mitochondrial morphology (Figure 27). In addition to its role in mitochondrial dynamics and mitophagy, Marf is also a putative ER-mitochondria tether and mediates ER stress (Celardo et al, 2016).

The chemical TUDCA is a known attenuator of ER stress and has been able to ameliorate defects of *Marf* mutants in *Drosophila* (Debattisti et al, 2014). Importantly, TUDCA reduced the brain vacuolization of frataxin depleted flies (Figure 34B), further supporting the hypothesis that reduction of ER stress is the mechanism behind the influence of *Marf* on the glial phenotypes. In addition, the aconitase activity of FRDA flies could be improved with TUDCA when tested in a system-wide manner under moderate knockdown conditions (Figure 37), However, TUDCA was not able to amend the locomotor deficit of the flies upon strong downregulation in glia (Figure 34A). A possible explanation is the strong knockdown of the fhRNAi1 model described in Anderson et al, 2005. So far, drug treatment has only been carried out successfully in moderate knockdown conditions. Two studies that showed a beneficial effect of deferiprone, idebenone and rapamycin utilized the moderate fhRNAi2 line (Soriano et al, 2013; Calap-Quintana et al, 2015). One study, in which flies were treated with methylene blue to rescue heart deficiency, applies the strong line fhRNAi1, but use an inducible geneswitch driver to downregulate frataxin to about 40%, similar to the moderate line fhRNAi2 (Tricoire et al, 2014). In the new mutant model, application of myriocin, an inhibitor of sphingolipid synthesis, partially suppressed photoreceptor degeneration (Chen et al, 2016). It is conceivable that chemical administration alone is not sufficient to completely abolish FRDA phenotypes after substantial frataxin depletion. To my knowledge, TUDCA provides the first pharmacological treatment that benefits the fly under strong knockdown conditions.

Overall, these results highlight ER stress as a major contributor to FRDA phenotypes and targeting ER stress emerges as a novel therapeutic approach in the treatment of the disease. Of course, additional phenotypes will have to be tested to fully grasp the effect of lowering ER

stress might have on the fly. In addition, the role of ER stress in other models will have to be examined.

4.6.2. Targeting autophagy shows limited success

Genetic manipulation of the autophagy pathway in glia had provided beneficial effects on FRDA phenotypes in my model, as overexpressing Atg8a reduced brain vacuolization (Figure 23). Atg8a is involved in autophagosome formation by linking selected cargo to the phagophore (Nixon, 2013). Enhancing Atg8a expression has been described to promote basal autophagy and in turn enhance longevity and resistance to oxidative stress in *Drosophila* neurons (Simonsen et al, 2008). Therefore, the drug rapamycin as an activator of autophagy was an obvious target to test the effect of chemically induced autophagy on glial phenotypes.

Unfortunately, rapamycin failed to restore brain vacuolization in addition to locomotion (Figure 24). This result stands in contrast to previous data, which showed an effect of rapamycin in the fruit fly by promoting antioxidant defenses (Calap-Quintana et al, 2015). In their work, rapamycin improved locomotion and increased ATP levels. As mentioned above, the most striking difference is the use of the moderate fhRNAi2 line for their experiments. Keeping in mind that Atg8a overexpression was only able to reduce brain vacuolization while it had no effect on locomotion or lipid accumulation, it is reasonable to speculate that chemical activation of autophagy is not sufficient to rescue the strong frataxin deficiency in my model. Interestingly, Calap-Quintana et al described that rapamycin is able to protect the flies from frataxin deficiency by promoting antioxidant defenses, independently of the autophagy induction ability of rapamycin. In contrast, my data suggest an involvement of autophagy, since mitophagic flux was enhanced in glia and overexpression of Atg8a was sufficient to improve brain vacuolization (Figure 22 and Figure 23). However, I cannot exclude that rapamycin reduces the number of mitochondria targeted for degradation by increasing antioxidant enzymes that might improve mitochondrial condition. When administered in moderate downregulation conditions (fhRNAi2 line), rapamycin reduced the p62 accumulation under hyperoxia (Figure 36). This seems in agreement with Calap-Quintana et al, as they described that autophagy induction by rapamycin becomes relevant under external oxidative stress. However, it has not been examined if rapamycin would also prevent the age-dependent p62 accumulation.

4.6.3. Are muscle phenotypes too severe to be rescued by targeting downstream effects?

In contrast to glia, genetic manipulation of both autophagy and mitochondrial dynamics in muscles failed to improve frataxin phenotypes. Whereas overexpressing GFP-Atg8a abrogated

the p62 accumulation in glia (Figure 22A-A'), the amount of p62 vesicles in muscles was unaffected compared to controls (Figure 20C and Figure 18D, respectively). In addition, *Marf* knockdown was detrimental instead of beneficial for locomotion (Figure 28). Since phenotypes in the IFM generally were much more severe in muscles than in glia, it becomes conceivable that the knockdown might be too strong to suppress frataxin deficiency by targeting downstream effects. A noteworthy exception was overexpression of a mitochondrial catalase (Figure 28). To address this challenge, it might be interesting to target the iron metabolism, since mitochondrial overload is likely one of the first steps of frataxin depletion. In fact, mitoferrin downregulation was able to prevent mitochondrial iron overload and subsequent deficiency in the moderate fhRNAi2 line (Navarro et al, 2015).

However, as skeletal muscles are not primarily disturbed in FRDA, affected tissues like glia or a system-wide approach appear more suitable for identifying potential treatments.

4.7. Is the endoplasmic reticulum the master mediator of FRDA phenotypes?

The endoplasmic reticulum is an important organelle within the cell and its interaction with mitochondria through the MAMs is likely a major contributor to several neurodegenerative diseases such as Alzheimer's disease or Parkinson's disease (Paillusson et al, 2016). Could it also be of similar importance in FRDA? Certainly, many of the intracellular responses from ER-mitochondria axis disruption are present in various models of the disease: Mitochondrial damage, disrupted Ca^{2+} homeostasis and lipid metabolism, axonal transport damage and autophagy induction (Navarro et al, 2010; Shidara & Hollenbeck, 2010; Huang et al, 2013; Bolinches-Amoros et al, 2014; Mincheva-Tasheva et al, 2014; Chen et al, 2016 and this work).

Disruptions to the ER-mitochondria axis provide a mechanism by which these different features might arise. Indeed, my results provide evidence that ER stress is present and the UPR is activated upon frataxin depletion in fruit flies (Figure 29-Figure 31). In addition, *Marf* downregulation in glial cells restored locomotion and abrogated the lipid accumulation and brain vacuolization of FRDA flies. This rescue is likely caused by influencing the ER stress response, since other pathways appeared unaffected and TUDCA successfully counteracted the brain vacuolization in glia (Figure 34), similar to *Marf* knockdown. TUDCA also improved aconitase activity under moderate knockdown conditions (Figure 37). It is reasonable to speculate that Marf is able to mediate such a response since it has been described as an ER-mitochondria tether (Brito & Scorrano, 2008) and has been implicated in calcium and lipid transfer between the ER and mitochondria (Sebastián et al, 2012; Schneeberger et al, 2013). In

agreement, mitofusin-mediated ER stress has recently been described to trigger neurodegeneration in a *Drosophila* model of Parkinson's disease (Celardo et al, 2016).

Based on frataxin's role in ISC biogenesis, altered cellular iron metabolism and mitochondrial dysfunction resulting from iron overload are likely the primary symptoms of frataxin depletion (Pandolfo, 2012). Therefore mitochondrial damage, which manifests as loss of membrane potential and energy production, probably results directly from disturbance in frataxin levels. Altered ER-mitochondria contacts, mediated through Marf, might then be pivotal in causing the other known hallmarks of FRDA. In line with this argument, a genetic screen of MAM genes revealed that *Porin* knockdown was also able to significantly rescue negative geotaxis (Figure 35). Interestingly, Porin is located in the mitochondrial membrane and promotes Ca^{2+} exchange with the ER, similar to Marf (Szabadkai et al, 2006).

To provide conclusive evidence for this hypothesis, it will also be necessary to utilize methods that reliably quantify ER-mitochondrial distance using electron microscopy techniques. Unfortunately, it is not possible to apply them to glia due to their electron-density (see Appendix, Figure 39).

5. References

Ackema KB, Prescianotto-Baschong C, Hench J, Wang SC, Chia ZH, Mergentaler H, Bard F, Frank S & Spang A (2016) Sar1, a Novel Regulator of ER-Mitochondrial Contact Sites. *PLoS One* **11:** e0154280

Adamec J, Rusnak F, Owen WG, Naylor S, Benson LM, Gacy AM & Isaya G (2000) Iron-dependent self-assembly of recombinant yeast frataxin: implications for Friedreich ataxia. *Am J Hum Genet* **67:** 549–562

Adinolfi S, Iannuzzi C, Prischi F, Pastore C, Iametti S, Martin SR, Bonomi F & Pastore A (2009) Bacterial frataxin CyaY is the gatekeeper of iron-sulfur cluster formation catalyzed by IscS. *Nat Struct Mol Biol* **16:** 390–396

Albrecht SC, Barata AG, Grosshans J, Teleman AA & Dick TP (2011) In vivo mapping of hydrogen peroxide and oxidized glutathione reveals chemical and regional specificity of redox homeostasis. *Cell Metab* **14:** 819–829

Al-Mahdawi S, Pinto RM, Varshney D, Lawrence L, Lowrie MB, Hughes S, Webster Z, Blake J, Cooper JM, King R & Pook MA (2006) GAA repeat expansion mutation mouse models of Friedreich ataxia exhibit oxidative stress leading to progressive neuronal and cardiac pathology. *Genomics* **88:** 580–590

Altmann K, Frank M, Neumann D, Jakobs S & Westermann B (2008) The class V myosin motor protein, Myo2, plays a major role in mitochondrial motility in Saccharomyces cerevisiae. *J Cell Biol* **181:** 119–130

Anderson PR, Kirby K, Hilliker AJ & Phillips JP (2005) RNAi-mediated suppression of the mitochondrial iron chaperone, frataxin, in Drosophila. *Hum Mol Genet* **14:** 3397–3405

Anderson PR, Kirby K, Orr WC, Hilliker AJ & Phillips JP (2008) Hydrogen peroxide scavenging rescues frataxin deficiency in a Drosophila model of Friedreich's ataxia. *Proc Natl Acad Sci U S A* **105:** 611–616

Armstrong JS, Khdour O & Hecht SM (2010) Does oxidative stress contribute to the pathology of Friedreich's ataxia? A radical question. *FASEB J* **24:** 2152–2163

Auchère F, Santos R, Planamente S, Lesuisse E & Camadro J-M (2008) Glutathione-dependent redox status of frataxin-deficient cells in a yeast model of Friedreich's ataxia. *Hum Mol Genet* **17:** 2790–2802

Awasaki T, Lai S-L, Ito K & Lee T (2008) Organization and postembryonic development of glial cells in the adult central brain of Drosophila. *J Neurosci* **28:** 13742–13753

Bartlett BJ, Isakson P, Lewerenz J, Sanchez H, Kotzebue RW, Cumming RC, Harris GL, Nezis IP, Schubert DR, Simonsen A & Finley KD (2011) p62, Ref(2)P and ubiquitinated proteins are conserved markers of neuronal aging, aggregate formation and progressive autophagic defects. *Autophagy* **7:** 572–583

Barupala DP, Dzul SP, Riggs-Gelasco PJ & Stemmler TL (2016) Synthesis, delivery and regulation of eukaryotic heme and Fe-S cluster cofactors. *Arch Biochem Biophys* **592:** 60–75

Beauchamp M, Labelle H, Duhaime M & Joncas J (1995) Natural history of muscle weakness in Friedreich's Ataxia and its relation to loss of ambulation. *Clin Orthop Relat Res:* 270–275

Bereiter-Hahn J (1990) Behavior of mitochondria in the living cell. *Int Rev Cytol* **122:** 1–63

Bhandari P, Song M, Chen Y, Burelle Y & Dorn GW2 (2014) Mitochondrial contagion induced by Parkin deficiency in Drosophila hearts and its containment by suppressing mitofusin. *Circ Res* **114:** 257–265

Böckler S & Westermann B (2014) Mitochondrial ER contacts are crucial for mitophagy in yeast. *Dev Cell* **28:** 450–458

Bolinches-Amoros A, Molla B, Pla-Martin D, Palau F & Gonzalez-Cabo P (2014) Mitochondrial dysfunction induced by frataxin deficiency is associated with cellular senescence and abnormal calcium metabolism. *Front Cell Neurosci* **8:** 124

Bossie HM, Willingham TB, van Schoick RA, O'Connor PJ & McCully KK (2016) Mitochondrial capacity, muscle endurance, and low energy in friedreich ataxia. *Muscle Nerve*

Botella JA, Ulschmid JK, Gruenewald C, Moehle C, Kretzschmar D, Becker K & Schneuwly S (2004) The Drosophila carbonyl reductase sniffer prevents oxidative stress-induced neurodegeneration. *Curr Biol* **14:** 782–786

Brito OM de & **Scorrano L (**2008) Mitofusin 2 tethers endoplasmic reticulum to mitochondria. *Nature* **456:** 605–610

Bulteau AL, Planamente S, Jornea L, Dur A, Lesuisse E, Camadro JM & Auchère F (2012) Changes in mitochondrial glutathione levels and protein thiol oxidation in Δyfh1 yeast cells and the lymphoblasts of patients with Friedreich's ataxia. *Biochim Biophys Acta* **1822:** 212–225

Bulteau A-L, O'Neill HA, Kennedy MC, Ikeda-Saito M, Isaya G & Szweda LI (2004) Frataxin acts as an iron chaperone protein to modulate mitochondrial aconitase activity. *Science* **305:** 242–245

Calap-Quintana P, Soriano S, Llorens JV, Al-Ramahi I, Botas J, Molto MD & Martinez-Sebastian MJ (2015) TORC1 Inhibition by Rapamycin Promotes Antioxidant Defences in a Drosophila Model of Friedreich's Ataxia. *PLoS One* **10:** e0132376

Calatrava-Ferreras L, Gonzalo-Gobernado R, Reimers D, Herranz AS, Casarejos MJ, Jiménez-Escrig A, Regadera J, Velasco-Martín J, Vallejo-Muñoz M, Díaz-Gil JJ & Bazán E (2016) Liver Growth Factor (LGF) Upregulates Frataxin Protein Expression and Reduces Oxidative Stress in Friedreich's Ataxia Transgenic Mice. *Int J Mol Sci* **17**

Cali T, Ottolini D, Negro A & Brini M (2013) Enhanced parkin levels favor ER-mitochondria crosstalk and guarantee Ca(2+) transfer to sustain cell bioenergetics. *Biochim Biophys Acta* **1832:** 495–508

Campanella A, Rovelli E, Santambrogio P, Cozzi A, Taroni F & Levi S (2009) Mitochondrial ferritin limits oxidative damage regulating mitochondrial iron availability: hypothesis for a protective role in Friedreich ataxia. *Hum Mol Genet* **18:** 1–11

Campuzano V, Montermini L, Lutz Y, Cova L, Hindelang C, Jiralerspong S, Trottier Y, Kish SJ, Faucheux B, Trouillas P, Authier FJ, Durr A, Mandel JL, Vescovi A, Pandolfo M & Koenig M (1997) Frataxin is reduced in Friedreich ataxia patients and is associated with mitochondrial membranes. *Hum Mol Genet* **6:** 1771–1780

Campuzano V, Montermini L, Molto MD, Pianese L, Cossee M, Cavalcanti F, Monros E, Rodius F, Duclos F, Monticelli A, Zara F, Canizares J, Koutnikova H, Bidichandani SI, Gellera C, Brice A, Trouillas P, Michele G de, **Filla A & Frutos R** de et al (1996) Friedreich's ataxia: Autosomal recessive disease caused by an intronic GAA triplet repeat expansion. *Science* **271:** 1423–1427

Canizares J, Blanca JM, Navarro JA, Monros E, Palau F & Molto MD (2000) dfh is a Drosophila homolog of the Friedreich's ataxia disease gene. *Gene* **256:** 35–42

Celardo I, Costa AC, Lehmann S, Jones C, Wood N, Mencacci NE, Mallucci GR, Loh SHY & Martins LM (2016) Mitofusin-mediated ER stress triggers neurodegeneration in pink1/parkin models of Parkinson's disease. *Cell Death Dis* **7:** e2271

Chen H, Vermulst M, Wang YE, Chomyn A, Prolla TA, McCaffery JM & Chan DC (2010) Mitochondrial fusion is required for mtDNA stability in skeletal muscle and tolerance of mtDNA mutations. *Cell* **141:** 280–289

Chen K, Lin G, Haelterman NA, Ho TS-Y, Li T, Li Z, Duraine L, Graham BH, Jaiswal M, Yamamoto S, Rasband MN & Bellen HJ (2016) Loss of Frataxin induces iron toxicity, sphingolipid synthesis, and Pdk1/Mef2 activation, leading to neurodegeneration. *Elife* **5**

Chiang S, Kovacevic Z, Sahni S, Lane DJR, Merlot AM, Kalinowski DS, Huang ML-H & Des Richardson R (2016) Frataxin and the molecular mechanism of mitochondrial iron-loading in Friedreich's ataxia. *Clin Sci (Lond)* **130:** 853–870

Cho SJ, Lee MG, Yang JK, Lee JY, Song HK & Suh SW (2000) Crystal structure of Escherichia coli CyaY protein reveals a previously unidentified fold for the evolutionarily conserved frataxin family. *Proc Natl Acad Sci U S A* **97:** 8932–8937

Clark IE, Dodson MW, Jiang C, Cao JH, Huh JR, Seol JH, Yoo SJ, Hay BA & Guo M (2006) Drosophila pink1 is required for mitochondrial function and interacts genetically with parkin. *Nature* **441:** 1162–1166

Coppola G, Marmolino D, Lu D, Wang Q, Cnop M, Rai M, Acquaviva F, Cocozza S, Pandolfo M & Geschwind DH (2009) Functional genomic analysis of frataxin deficiency reveals tissue-specific alterations and identifies the PPARgamma pathway as a therapeutic target in Friedreich's ataxia. *Hum Mol Genet* **18:** 2452–2461

Cossee M, Durr A, Schmitt M, Dahl N, Trouillas P, Allinson P, Kostrzewa M, Nivelon-Chevallier A, Gustavson KH, Kohlschutter A, Muller U, Mandel JL, Brice A, Koenig M, Cavalcanti F, Tammaro A, Michele G de, **Filla A, Cocozza S & Labuda M et al (**1999) Friedreich's ataxia: Point mutations and clinical presentation of compound heterozygotes. *Ann Neurol* **45:** 200–206

Cossee M, Puccio H, Gansmuller A, Koutnikova H, Dierich A, LeMeur M, Fischbeck K, Dolle P & Koenig M (2000) Inactivation of the Friedreich ataxia mouse gene leads to early embryonic lethality without iron accumulation. *Hum Mol Genet* **9:** 1219–1226

Cossee M, Schmitt M, Campuzano V, Reutenauer L, Moutou C, Mandel JL & Koenig M (1997) Evolution of the Friedreich's ataxia trinucleotide repeat expansion: Founder effect and premutations. *Proc Natl Acad Sci U S A* **94:** 7452–7457

Cosson P, Marchetti A, Ravazzola M & Orci L (2012) Mitofusin-2 independent juxtaposition of endoplasmic reticulum and mitochondria: an ultrastructural study. *PLoS One* **7:** e46293

Debattisti V, Pendin D, Ziviani E, Daga A & Scorrano L (2014) Reduction of endoplasmic reticulum stress attenuates the defects caused by Drosophila mitofusin depletion. *J Cell Biol* **204:** 303–312

Delatycki MB, Williamson R & Forrest SM (2000) Friedreich ataxia: an overview. *J Med Genet* **37:** 1–8

Deng H, Dodson MW, Huang H & Guo M (2008) The Parkinson's disease genes pink1 and parkin promote mitochondrial fission and/or inhibit fusion in Drosophila. *Proc Natl Acad Sci U S A* **105:** 14503–14508

Dhe-Paganon S, Shigeta R, Chi YI, Ristow M & Shoelson SE (2000) Crystal structure of human frataxin. *J Biol Chem* **275:** 30753–30756

Dürr A, Cossee M, Agid Y, Campuzano V, Mignard C, Penet C, Mandel JL, Brice A & Koenig M (1996) Clinical and genetic abnormalities in patients with Friedreich's ataxia. *N Engl J Med* **335:** 1169–1175

Edenharter O (2013) *Study of the Mitochondrial Dynamics in a Drosophila model of Friedreich's ataxia.* Masterarbeit, Universität Regensburg

Edwards TN & Meinertzhagen IA (2010) The functional organisation of glia in the adult brain of Drosophila and other insects. *Prog Neurobiol* **90:** 471–497

Eisenstein RS (2000) Iron regulatory proteins and the molecular control of mammalian iron metabolism. *Annu Rev Nutr* **20:** 627–662

Emond M, Lepage G, Vanasse M & Pandolfo M (2000) Increased levels of plasma malondialdehyde in Friedreich ataxia. *Neurology* **55:** 1752–1753

Exner N, Lutz AK, Haass C & Winklhofer KF (2012) Mitochondrial dysfunction in Parkinson's disease: Molecular mechanisms and pathophysiological consequences. *EMBO J* **31:** 3038–3062

Faraj SE, Gonzalez-Lebrero RM, Roman EA & Santos J (2016) Human Frataxin Folds Via an Intermediate State. Role of the C-Terminal Region. *Sci Rep* **6:** 20782

Fecto F, Yan J, Vemula SP, Liu E, Yang Y, Chen W, Zheng JG, Shi Y, Siddique N, Arrat H, Donkervoort S, Ajroud-Driss S, Sufit RL, Heller SL, Deng H-X & Siddique T (2011) SQSTM1 mutations in familial and sporadic amyotrophic lateral sclerosis. *Arch Neurol* **68:** 1440–1446

Filadi R, Greotti E, Turacchio G, Luini A, Pozzan T & Pizzo P (2015) Mitofusin 2 ablation increases endoplasmic reticulum-mitochondria coupling. *Proc Natl Acad Sci U S A* **112:** E2174-81

Filla A, Michele G de, **Cavalcanti F, Pianese L, Monticelli A, Campanella G & Cocozza S (**1996) The relationship between trinucleotide (GAA) repeat length and clinical features in Friedreich ataxia. *Am J Hum Genet* **59:** 554–560

Foury F & Cazzalini O (1997) Deletion of the yeast homologue of the human gene associated with Friedreich's ataxia elicits iron accumulation in mitochondria. *FEBS Lett* **411:** 373–377

Friedreich N (1863) Über degenerative Atrophie der spinalen Hinterstränge. *Virchows Arch Pathol Anat Physiol Klin Med* **26:** 391–419

Gandre-Babbe S & van der Bliek AM (2008) The novel tail-anchored membrane protein Mff controls mitochondrial and peroxisomal fission in mammalian cells. *Mol Biol Cell* **19:** 2402–2412

Gatchel JR & Zoghbi HY (2005) Diseases of unstable repeat expansion: mechanisms and common principles. *Nat Rev Genet* **6:** 743–755

Gibson TJ, Koonin EV, Musco G, Pastore A & Bork P (1996) Friedreich's ataxia protein: Phylogenetic evidence for mitochondrial dysfunction. *Trends Neurosci* **19:** 465–468

Gomes LC & Scorrano L (2013) Mitochondrial morphology in mitophagy and macroautophagy. *Biochim Biophys Acta* **1833:** 205–212

Gonzalez-Cabo P & Palau F (2013) Mitochondrial pathophysiology in Friedreich's ataxia. *J Neurochem* **126 Suppl 1:** 53–64

Gonzalez-Cabo P, Vazquez-Manrique RP, Garcia-Gimeno MA, Sanz P & Palau F (2005) Frataxin interacts functionally with mitochondrial electron transport chain proteins. *Hum Mol Genet* **14:** 2091–2098

Greene E, Mahishi L, Entezam A, Kumari D & Usdin K (2007) Repeat-induced epigenetic changes in intron 1 of the frataxin gene and its consequences in Friedreich ataxia. *Nucleic Acids Res* **35:** 3383–3390

Gutscher M, Pauleau A-L, Marty L, Brach T, Wabnitz GH, Samstag Y, Meyer AJ & Dick TP (2008) Real-time imaging of the intracellular glutathione redox potential. *Nat Methods* **5:** 553–559

Hales KG & Fuller MT (1997) Developmentally regulated mitochondrial fusion mediated by a conserved, novel, predicted GTPase. *Cell* **90:** 121–129

Hanson GT, Aggeler R, Oglesbee D, Cannon M, Capaldi RA, Tsien RY & Remington SJ (2004) Investigating mitochondrial redox potential with redox-sensitive green fluorescent protein indicators. *J Biol Chem* **279:** 13044–13053

Harding AE (1981) Friedreich's ataxia: a clinical and genetic study of 90 families with an analysis of early diagnostic criteria and intrafamilial clustering of clinical features. *Brain* **104:** 589–620

Hartenstein V (2011) Morphological diversity and development of glia in Drosophila. *Glia* **59:** 1237–1252

Hayashi T, Rizzuto R, Hajnoczky G & Su T-P (2009) MAM: more than just a housekeeper. *Trends Cell Biol* **19:** 81–88

He Y, Alam SL, Proteasa SV, Zhang Y, Lesuisse E, Dancis A & Stemmler TL (2004) Yeast frataxin solution structure, iron binding, and ferrochelatase interaction. *Biochemistry* **43:** 16254–16262

Hetz C & Mollereau B (2014) Disturbance of endoplasmic reticulum proteostasis in neurodegenerative diseases. *Nat Rev Neurosci* **15:** 233–249

Hick A, Wattenhofer-Donze M, Chintawar S, Tropel P, Simard JP, Vaucamps N, Gall D, Lambot L, Andre C, Reutenauer L, Rai M, Teletin M, Messaddeq N, Schiffmann SN, Viville S, Pearson CE, Pandolfo M & Puccio H (2013) Neurons and cardiomyocytes derived from induced pluripotent stem cells as a model for mitochondrial defects in Friedreich's ataxia. *Dis Model Mech* **6:** 608–621

Hoozemans JJM, van Haastert ES, Eikelenboom P, Vos RAI de, **Rozemuller JM & Scheper W (**2007) Activation of the unfolded protein response in Parkinson's disease. *Biochem Biophys Res Commun* **354:** 707–711

Huang ML-H, Becker EM, Whitnall M, Suryo Rahmanto Y, Ponka P & Des Richardson R (2009) Elucidation of the mechanism of mitochondrial iron loading in Friedreich's ataxia by analysis of a mouse mutant. *Proc Natl Acad Sci U S A* **106:** 16381–16386

Huang ML-H, Sivagurunathan S, Ting S, Jansson PJ, Austin CJD, Kelly M, Semsarian C, Zhang D & Des Richardson R (2013) Molecular and functional alterations in a mouse cardiac model of Friedreich ataxia: activation of the integrated stress response, eIF2alpha phosphorylation, and the induction of downstream targets. *Am J Pathol* **183:** 745–757

Iannuzzi C, Adinolfi S, Howes BD, Garcia-Serres R, Clémancey M, Latour J-M, Smulevich G & Pastore A (2011) The role of CyaY in iron sulfur cluster assembly on the E. coli IscU scaffold protein. *PLoS One* **6:** e21992

Irvine K (2007) *P{UAS-GFP.KDEL} construct and insertions*

Islam R, Yang L, Sah M, Kannan K, Anamani D, Vijayan C, Kwok J, Cantino ME, Beal MF & Fridell Y-WC (2012) A neuroprotective role of the human uncoupling protein 2 (hUCP2) in a Drosophila Parkinson's disease model. *Neurobiol Dis* **46:** 137–146

Itoh K, Nakamura K, Iijima M & Sesaki H (2013) Mitochondrial dynamics in neurodegeneration. *Trends Cell Biol* **23:** 64–71

Jin SM, Lazarou M, Wang C, Kane LA, Narendra DP & Youle RJ (2010) Mitochondrial membrane potential regulates PINK1 import and proteolytic destabilization by PARL. *J Cell Biol* **191:** 933–942

Johansen T & Lamark T (2011) Selective autophagy mediated by autophagic adapter proteins. *Autophagy* **7:** 279–296

Juhasz G, Hill JH, Yan Y, Sass M, Baehrecke EH, Backer JM & Neufeld TP (2008) The class III PI(3)K Vps34 promotes autophagy and endocytosis but not TOR signaling in Drosophila. *J Cell Biol* **181:** 655–666

Kaplowitz N (1981) The importance and regulation of hepatic glutathione. *Yale J Biol Med* **54:** 497–502

Kim I, Rodriguez-Enriquez S & Lemasters JJ (2007) Selective degradation of mitochondria by mitophagy. *Arch Biochem Biophys* **462:** 245–253

Kiriyama Y & Nochi H (2015) The Function of Autophagy in Neurodegenerative Diseases. *Int J Mol Sci* **16:** 26797–26812

Koeppen AH (2011) Friedreich's ataxia: pathology, pathogenesis, and molecular genetics. *J Neurol Sci* **303:** 1–12

Koeppen AH & Mazurkiewicz JE (2013) Friedreich ataxia: Neuropathology revised. *J Neuropathol Exp Neurol* **72:** 78–90

Kondapalli KC, Kok NM, Dancis A & Stemmler TL (2008) Drosophila frataxin: an iron chaperone during cellular Fe-S cluster bioassembly. *Biochemistry* **47:** 6917–6927

Korennykh A & Walter P (2012) Structural basis of the unfolded protein response. *Annu Rev Cell Dev Biol* **28:** 251–277

Kornmann B, Currie E, Collins SR, Schuldiner M, Nunnari J, Weissman JS & Walter P (2009) An ER-mitochondria tethering complex revealed by a synthetic biology screen. *Science* **325:** 477–481

Koshiba T, Detmer SA, Kaiser JT, Chen H, McCaffery JM & Chan DC (2004) Structural basis of mitochondrial tethering by mitofusin complexes. *Science* **305:** 858–862

Koutnikova H, Campuzano V, Foury F, Dolle P, Cazzalini O & Koenig M (1997) Studies of human, mouse and yeast homologues indicate a mitochondrial function for frataxin. *Nat Genet* **16:** 345–351

Lagedrost SJ, Sutton MSJ, Cohen MS, Satou GM, Kaufman BD, Perlman SL, Rummey C, Meier T & Lynch DR (2011) Idebenone in Friedreich ataxia cardiomyopathy-results from a 6-month phase III study (IONIA). *Am Heart J* **161:** 639-645.e1

Lamarche JB, Cote M & Lemieux B (1980) The cardiomyopathy of Friedreich's ataxia morphological observations in 3 cases. *Can J Neurol Sci* **7:** 389–396

Layer G, Ollagnier-de Choudens S, Sanakis Y & Fontecave M (2006) Iron-sulfur cluster biosynthesis: characterization of Escherichia coli CYaY as an iron donor for the assembly of 2Fe-2S clusters in the scaffold IscU. *J Biol Chem* **281:** 16256–16263

Lazarou M, Jin SM, Kane LA & Youle RJ (2012) Role of PINK1 binding to the TOM complex and alternate intracellular membranes in recruitment and activation of the E3 ligase Parkin. *Dev Cell* **22:** 320–333

Lazarou M, Sliter DA, Kane LA, Sarraf SA, Wang C, Burman JL, Sideris DP, Fogel AI & Youle RJ (2015) The ubiquitin kinase PINK1 recruits autophagy receptors to induce mitophagy. *Nature* **524:** 309–314

Leal NS, Schreiner B, Pinho CM, Filadi R, Wiehager B, Karlström H, Pizzo P & Ankarcrona M (2016) Mitofusin-2 knockdown increases ER-mitochondria contact and decreases amyloid β-peptide production. *J Cell Mol Med* **20:** 1686–1695

Lee H & Yoon Y (2016) Mitochondrial fission and fusion. *Biochem Soc Trans* **44:** 1725–1735

Lee J-H, Yu WH, Kumar A, Lee S, Mohan PS, Peterhoff CM, Wolfe DM, Martinez-Vicente M, Massey AC, Sovak G, Uchiyama Y, Westaway D, Cuervo AM & Nixon RA (2010) Lysosomal proteolysis and autophagy require presenilin 1 and are disrupted by Alzheimer-related PS1 mutations. *Cell* **141:** 1146–1158

Lee S, Lee K-S, Huh S, Liu S, Lee D-Y, Hong SH, Yu K & Lu B (2016) Polo Kinase Phosphorylates Miro to Control ER-Mitochondria Contact Sites and Mitochondrial Ca(2+) Homeostasis in Neural Stem Cell Development. *Dev Cell* **37:** 174–189

Lefevre S, Sliwa D, Rustin P, Camadro J-M & Santos R (2012) Oxidative stress induces mitochondrial fragmentation in frataxin-deficient cells. *Biochem Biophys Res Commun* **418:** 336–341

Legesse-Miller A, Massol RH & Kirchhausen T (2003) Constriction and Dnm1p recruitment are distinct processes in mitochondrial fission. *Mol Biol Cell* **14:** 1953–1963

Li Y, Lu Y, Polak U, Lin K, Shen J, Farmer J, Seyer L, Bhalla AD, Rozwadowska N, Lynch DR, Butler JS & Napierala M (2015) Expanded GAA repeats impede transcription elongation through the FXN gene and induce transcriptional silencing that is restricted to the FXN locus. *Hum Mol Genet* **24:** 6932–6943

Lill R (2009) Function and biogenesis of iron-sulphur proteins. *Nature* **460:** 831–838

Liu L, Zhang K, Sandoval H, Yamamoto S, Jaiswal M, Sanz E, Li Z, Hui J, Graham BH, Quintana A & Bellen HJ (2015) Glial lipid droplets and ROS induced by mitochondrial defects promote neurodegeneration. *Cell* **160:** 177–190

Liu S & Lu B (2010) Reduction of protein translation and activation of autophagy protect against PINK1 pathogenesis in Drosophila melanogaster. *PLoS Genet* **6:** e1001237

Liu X & Hajnoczky G (2011) Altered fusion dynamics underlie unique morphological changes in mitochondria during hypoxia-reoxygenation stress. *Cell Death Differ* **18:** 1561–1572

Llorens JV, Navarro JA, Martinez-Sebastian MJ, Baylies MK, Schneuwly S, Botella JA & Molto MD (2007) Causative role of oxidative stress in a Drosophila model of Friedreich ataxia. *FASEB J* **21:** 333–344

Lodi R, Cooper JM, Bradley JL, Manners D, Styles P, Taylor DJ & Schapira AH (1999) Deficit of in vivo mitochondrial ATP production in patients with Friedreich ataxia. *Proc Natl Acad Sci U S A* **96:** 11492–11495

Loria F & Diaz-Nido J (2015) Frataxin knockdown in human astrocytes triggers cell death and the release of factors that cause neuronal toxicity. *Neurobiol Dis* **76:** 1–12

Loson OC, Song Z, Chen H & Chan DC (2013) Fis1, Mff, MiD49, and MiD51 mediate Drp1 recruitment in mitochondrial fission. *Mol Biol Cell* **24:** 659–667

Lu C & Cortopassi G (2007) Frataxin knockdown causes loss of cytoplasmic iron-sulfur cluster functions, redox alterations and induction of heme transcripts. *Arch Biochem Biophys* **457:** 111–122

Lu C, Schoenfeld R, Shan Y, Tsai H-J, Hammock B & Cortopassi G (2009) Frataxin deficiency induces Schwann cell inflammation and death. *Biochim Biophys Acta* **1792:** 1052–1061

Lutz AK, Exner N, Fett ME, Schlehe JS, Kloos K, Lammermann K, Brunner B, Kurz-Drexler A, Vogel F, Reichert AS, Bouman L, Vogt-Weisenhorn D, Wurst W, Tatzelt J, Haass C & Winklhofer KF (2009) Loss of parkin or PINK1 function increases Drp1-dependent mitochondrial fragmentation. *J Biol Chem* **284:** 22938–22951

Luz AL, Rooney JP, Kubik LL, Gonzalez CP, Song DH & Meyer JN (2015) Mitochondrial Morphology and Fundamental Parameters of the Mitochondrial Respiratory Chain Are Altered in Caenorhabditis elegans Strains Deficient in Mitochondrial Dynamics and Homeostasis Processes. *PLoS One* **10:** e0130940

Lynch DR, Lech G, Farmer JM, Balcer LJ, Bank W, Chance B & Wilson RB (2002) Near infrared muscle spectroscopy in patients with Friedreich's ataxia. *Muscle Nerve* **25:** 664–673

Marobbio CMT, Pisano I, Porcelli V, Lasorsa FM & Palmieri L (2012) Rapamycin reduces oxidative stress in frataxin-deficient yeast cells. *Mitochondrion* **12:** 156–161

Martelli A, Friedman LS, Reutenauer L, Messaddeq N, Perlman SL, Lynch DR, Fedosov K, Schulz JB, Pandolfo M & Puccio H (2012a) Clinical data and characterization of the liver conditional mouse model exclude neoplasia as a non-neurological manifestation associated with Friedreich's ataxia. *Dis Model Mech* **5:** 860–869

Martelli A, Napierala M & Puccio H (2012b) Understanding the genetic and molecular pathogenesis of Friedreich's ataxia through animal and cellular models. *Dis Model Mech* **5:** 165–176

Martinou J-C & Youle RJ (2011) Mitochondria in apoptosis: Bcl-2 family members and mitochondrial dynamics. *Dev Cell* **21:** 92–101

Mauvezin C, Ayala C, Braden CR, Kim J & Neufeld TP (2014) Assays to monitor autophagy in Drosophila. *Methods* **68:** 134–139

McWilliams TG & Muqit MM (2017) PINK1 and Parkin: Emerging themes in mitochondrial homeostasis. *Curr Opin Cell Biol* **45:** 83–91

Meeusen S, DeVay R, Block J, Cassidy-Stone A, Wayson S, McCaffery JM & Nunnari J (2006) Mitochondrial inner-membrane fusion and crista maintenance requires the dynamin-related GTPase Mgm1. *Cell* **127:** 383–395

Meier T, Perlman SL, Rummey C, Coppard NJ & Lynch DR (2012) Assessment of neurological efficacy of idebenone in pediatric patients with Friedreich's ataxia: data from a 6-month controlled study followed by a 12-month open-label extension study. *J Neurol* **259:** 284–291

Melendez A & Levine B (2009) Autophagy in C. elegans. *WormBook:* 1–26

Mincheva-Tasheva S, Obis E, Tamarit J & Ros J (2014) Apoptotic cell death and altered calcium homeostasis caused by frataxin depletion in dorsal root ganglia neurons can be prevented by BH4 domain of Bcl-xL protein. *Hum Mol Genet* **23:** 1829–1841

Mishra P & Chan DC (2014) Mitochondrial dynamics and inheritance during cell division, development and disease. *Nat Rev Mol Cell Biol* **15:** 634–646

Montermini L, Richter A, Morgan K, Justice CM, Julien D, Castellotti B, Mercier J, Poirier J, Capozzoli F, Bouchard JP, Lemieux B, Mathieu J, Vanasse M, Seni MH, Graham G, Andermann F, Andermann E, Melancon SB, Keats BJ & Di Donato S et al (1997) Phenotypic variability in Friedreich ataxia: role of the associated GAA triplet repeat expansion. *Ann Neurol* **41:** 675–682

Morral JA, Davis AN, Qian J, Gelman BB & Koeppen AH (2010) Pathology and pathogenesis of sensory neuropathy in Friedreich's ataxia. *Acta Neuropathol* **120:** 97–108

Mulakkal NC, Nagy P, Takats S, Tusco R, Juhasz G & Nezis IP (2014) Autophagy in Drosophila: From historical studies to current knowledge. *Biomed Res Int* **2014:** 273473

Munoz JP, Ivanova S, Sanchez-Wandelmer J, Martinez-Cristobal P, Noguera E, Sancho A, Diaz-Ramos A, Hernandez-Alvarez MI, Sebastian D, Mauvezin C, Palacin M & Zorzano A (2013) Mfn2 modulates the UPR and mitochondrial function via repression of PERK. *EMBO J* **32:** 2348–2361

Nachbauer W, Boesch S, Reindl M, Eigentler A, Hufler K, Poewe W, Löscher W & Wanschitz J (2012) Skeletal muscle involvement in friedreich ataxia and potential effects of recombinant human erythropoietin administration on muscle regeneration and neovascularization. *J Neuropathol Exp Neurol* **71:** 708–715

Naon D, Zaninello M, Giacomello M, Varanita T, Grespi F, Lakshminaranayan S, Serafini A, Semenzato M, Herkenne S, Hernández-Alvarez MI, Zorzano A, Stefani D de, **Dorn GW & Scorrano L (**2016) Critical reappraisal confirms that Mitofusin 2 is an endoplasmic reticulum-mitochondria tether. *Proc Natl Acad Sci U S A* **113:** 11249–11254

Navarro JA, Botella JA, Metzendorf C, Lind MI & Schneuwly S (2015) Mitoferrin modulates iron toxicity in a Drosophila model of Friedreich's ataxia. *Free Radic Biol Med* **85:** 71–82

Navarro JA, Llorens JV, Soriano S, Botella JA, Schneuwly S, Martinez-Sebastian MJ & Molto MD (2011) Overexpression of human and fly frataxins in Drosophila provokes deleterious effects at biochemical, physiological and developmental levels. *PLoS One* **6:** e21017

Navarro JA, Ohmann E, Sanchez D, Botella JA, Liebisch G, Molto MD, Ganfornina MD, Schmitz G & Schneuwly S (2010) Altered lipid metabolism in a Drosophila model of Friedreich's ataxia. *Hum Mol Genet* **19:** 2828–2840

Nezis IP, Simonsen A, Sagona AP, Finley K, Gaumer S, Contamine D, Rusten TE, Stenmark H & Brech A (2008) Ref(2)P, the Drosophila melanogaster homologue of mammalian p62, is required for the formation of protein aggregates in adult brain. *J Cell Biol* **180:** 1065–1071

Ngoh GA, Papanicolaou KN & Walsh K (2012) Loss of mitofusin 2 promotes endoplasmic reticulum stress. *J Biol Chem* **287:** 20321–20332

Nguyen TN, Padman BS & Lazarou M (2016) Deciphering the Molecular Signals of PINK1/Parkin Mitophagy. *Trends Cell Biol* **26:** 733–744

Nixon RA (2013) The role of autophagy in neurodegenerative disease. *Nat Med* **19:** 983–997

Noda T & Ohsumi Y (1998) Tor, a phosphatidylinositol kinase homologue, controls autophagy in yeast. *J Biol Chem* **273:** 3963–3966

Obis E, Irazusta V, Sanchis D, Ros J & Tamarit J (2014) Frataxin deficiency in neonatal rat ventricular myocytes targets mitochondria and lipid metabolism. *Free Radic Biol Med* **73:** 21–33

Okatsu K, Saisho K, Shimanuki M, Nakada K, Shitara H, Sou Y-S, Kimura M, Sato S, Hattori N, Komatsu M, Tanaka K & Matsuda N (2010) p62/SQSTM1 cooperates with Parkin for perinuclear clustering of depolarized mitochondria. *Genes Cells* **15:** 887–900

Ono T, Isobe K, Nakada K & Hayashi JI (2001) Human cells are protected from mitochondrial dysfunction by complementation of DNA products in fused mitochondria. *Nat Genet* **28:** 272–275

Paillusson S, Stoica R, Gomez-Suaga P, Lau DHW, Mueller S, Miller T & Miller CCJ (2016) There's Something Wrong with my MAM; the ER-Mitochondria Axis and Neurodegenerative Diseases. *Trends Neurosci* **39:** 146–157

Palikaras K & Tavernarakis N (2014) Mitochondrial homeostasis: the interplay between mitophagy and mitochondrial biogenesis. *Exp Gerontol* **56:** 182–188

Pallanck L (2013) Mitophagy: mitofusin recruits a mitochondrial killer. *Curr Biol* **23:** R570-2

Pandey A, Gordon DM, Pain J, Stemmler TL, Dancis A & Pain D (2013) Frataxin directly stimulates mitochondrial cysteine desulfurase by exposing substrate-binding sites, and a mutant Fe-S cluster scaffold protein with frataxin-bypassing ability acts similarly. *J Biol Chem* **288:** 36773–36786

Pandolfo M (2003) Friedreich ataxia. *Semin Pediatr Neurol* **10:** 163–172

Pandolfo M (2012) Friedreich ataxia: new pathways. *J Child Neurol* **27:** 1204–1211

Pandolfo M & Hausmann L (2013) Deferiprone for the treatment of Friedreich's ataxia. *J Neurochem* **126 Suppl 1:** 142–146

Pastore A, Tozzi G, Gaeta LM, Bertini E, Serafini V, Di Cesare S, Bonetto V, Casoni F, Carrozzo R, Federici G & Piemonte F (2003) Actin glutathionylation increases in fibroblasts of patients with Friedreich's ataxia: a potential role in the pathogenesis of the disease. *J Biol Chem* **278:** 42588–42595

Patel M, Isaacs CJ, Seyer L, Brigatti K, Gelbard S, Strawser C, Foerster D, Shinnick J, Schadt K, Yiu EM, Delatycki MB, Perlman S, Wilmot GR, Zesiewicz T, Mathews K, Gomez CM, Yoon G, Subramony SH, Brocht A & Farmer J et al (2016) Progression of Friedreich ataxia: quantitative characterization over 5 years. *Ann Clin Transl Neurol* **3:** 684–694

Perdomini M, Hick A, Puccio H & Pook MA (2013) Animal and cellular models of Friedreich ataxia. *J Neurochem* **126 Suppl 1:** 65–79

Pesah Y, Pham T, Burgess H, Middlebrooks B, Verstreken P, Zhou Y, Harding M, Bellen H & Mardon G (2004) Drosophila parkin mutants have decreased mass and cell size and increased sensitivity to oxygen radical stress. *Development* **131:** 2183–2194

Phillips MJ & Voeltz GK (2016) Structure and function of ER membrane contact sites with other organelles. *Nat Rev Mol Cell Biol* **17:** 69–82

Pickrell AM & Youle RJ (2015) The roles of PINK1, parkin, and mitochondrial fidelity in Parkinson's disease. *Neuron* **85:** 257–273

Piemonte F, Pastore A, Tozzi G, Tagliacozzi D, Santorelli FM, Carrozzo R, Casali C, Damiano M, Federici G & Bertini E (2001) Glutathione in blood of patients with Friedreich's ataxia. *Eur J Clin Invest* **31:** 1007–1011

Pircs K, Nagy P, Varga A, Venkei Z, Erdi B, Hegedus K & Juhasz G (2012) Advantages and limitations of different p62-based assays for estimating autophagic activity in Drosophila. *PLoS One* **7:** e44214

Pogson JH, Ivatt RM, Sanchez-Martinez A, Tufi R, Wilson E, Mortiboys H & Whitworth AJ (2014) The complex I subunit NDUFA10 selectively rescues Drosophila pink1 mutants through a mechanism independent of mitophagy. *PLoS Genet* **10:** e1004815

Potaman VN, Oussatcheva EA, Lyubchenko YL, Shlyakhtenko LS, Bidichandani SI, Ashizawa T & Sinden RR (2004) Length-dependent structure formation in Friedreich ataxia (GAA)n*(TTC)n repeats at neutral pH. *Nucleic Acids Res* **32:** 1224–1231

Puccio H, Simon D, Cossee M, Criqui-Filipe P, Tiziano F, Melki J, Hindelang C, Matyas R, Rustin P & Koenig M (2001) Mouse models for Friedreich ataxia exhibit cardiomyopathy, sensory nerve defect and Fe-S enzyme deficiency followed by intramitochondrial iron deposits. *Nat Genet* **27:** 181–186

Pulipparacharuvil S, Akbar MA, Ray S, Sevrioukov EA, Haberman AS, Rohrer J & Kramer H (2005) Drosophila Vps16A is required for trafficking to lysosomes and biogenesis of pigment granules. *J Cell Sci* **118:** 3663–3673

Ravikumar B, Vacher C, Berger Z, Davies JE, Luo S, Oroz LG, Scaravilli F, Easton DF, Duden R, O'Kane CJ & Rubinsztein DC (2004) Inhibition of mTOR induces autophagy and reduces toxicity of polyglutamine expansions in fly and mouse models of Huntington disease. *Nat Genet* **36:** 585–595

Rayavarapu S, Coley W & Nagaraju K (2012) Endoplasmic reticulum stress in skeletal muscle homeostasis and disease. *Curr Rheumatol Rep* **14:** 238–243

Reddy PH (2008) Mitochondrial medicine for aging and neurodegenerative diseases. *Neuromolecular Med* **10:** 291–315

Rosado CJ, Mijaljica D, Hatzinisiriou I, Prescott M & Devenish RJ (2008) Rosella: a fluorescent pH-biosensor for reporting vacuolar turnover of cytosol and organelles in yeast. *Autophagy* **4:** 205–213

Rötig A, Lonlay P de, **Chretien D, Foury F, Koenig M, Sidi D, Munnich A & Rustin P (**1997) Aconitase and mitochondrial iron-sulphur protein deficiency in Friedreich ataxia. *Nat Genet* **17:** 215–217

Rowland AA & Voeltz GK (2012) Endoplasmic reticulum-mitochondria contacts: function of the junction. *Nat Rev Mol Cell Biol* **13:** 607–625

Rozpedek W, Markiewicz L, Diehl JA, Pytel D & Majsterek I (2015) Unfolded Protein Response and PERK Kinase as a New Therapeutic Target in the Pathogenesis of Alzheimer's Disease. *Curr Med Chem* **22:** 3169–3184

Ryoo HD (2015) Drosophila as a model for unfolded protein response research. *BMB Rep* **48:** 445–453

Sandi C, Al-Mahdawi S & Pook MA (2013) Epigenetics in Friedreich's Ataxia: Challenges and Opportunities for Therapy. *Genet Res Int* **2013:** 852080

Sandoval H, Yao C-K, Chen K, Jaiswal M, Donti T, Lin YQ, Bayat V, Xiong B, Zhang K, David G, Charng W-L, Yamamoto S, Duraine L, Graham BH & Bellen HJ (2014) Mitochondrial fusion but not fission regulates larval growth and synaptic development through steroid hormone production. *Elife* **3**

Sargsyan A, Cai J, Fandino LB, Labasky ME, Forostyan T, Colosimo LK, Thompson SJ & Graham TE (2015) Rapid parallel measurements of macroautophagy and mitophagy in mammalian cells using a single fluorescent biosensor. *Sci Rep* **5:** 12397

Scheper W & Hoozemans JJM (2015) The unfolded protein response in neurodegenerative diseases: a neuropathological perspective. *Acta Neuropathol* **130:** 315–331

Schiavi A, Maglioni S, Palikaras K, Shaik A, Strappazzon F, Brinkmann V, Torgovnick A, Castelein N, Henau S de, **Braeckman BP, Cecconi F, Tavernarakis N & Ventura N (**2015) Iron-Starvation-Induced Mitophagy Mediates Lifespan Extension upon Mitochondrial Stress in C. elegans. *Curr Biol* **25:** 1810–1822

Schiavi A, Torgovnick A, Kell A, Megalou E, Castelein N, Guccini I, Marzocchella L, Gelino S, Hansen M, Malisan F, Condo I, Bei R, Rea SL, Braeckman BP, Tavernarakis N, Testi R & Ventura N (2013) Autophagy induction extends lifespan and reduces lipid content in response to frataxin silencing in C. elegans. *Exp Gerontol* **48:** 191–201

Schindelin J, Arganda-Carreras I, Frise E, Kaynig V, Longair M, Pietzsch T, Preibisch S, Rueden C, Saalfeld S, Schmid B, Tinevez J-Y, White DJ, Hartenstein V, Eliceiri K, Tomancak P & Cardona A (2012) Fiji: an open-source platform for biological-image analysis. *Nat Methods* **9:** 676–682

Schmucker S, Argentini M, Carelle-Calmels N, Martelli A & Puccio H (2008) The in vivo mitochondrial two-step maturation of human frataxin. *Hum Mol Genet* **17:** 3521–3531

Schmucker S, Martelli A, Colin F, Page A, Wattenhofer-Donze M, Reutenauer L & Puccio H (2011) Mammalian frataxin: An essential function for cellular viability through an interaction with a preformed ISCU/NFS1/ISD11 iron-sulfur assembly complex. *PLoS One* **6:** e16199

Schneeberger M, Dietrich MO, Sebastián D, Imbernón M, Castaño C, Garcia A, Esteban Y, Gonzalez-Franquesa A, Rodríguez IC, Bortolozzi A, Garcia-Roves PM, Gomis R, Nogueiras R, Horvath TL, Zorzano A & Claret M (2013) Mitofusin 2 in POMC neurons connects ER stress with leptin resistance and energy imbalance. *Cell* **155:** 172–187

Schulz JB, Dehmer T, Schöls L, Mende H, Hardt C, Vorgerd M, Bürk K, Matson W, Dichgans J, Beal MF & Bogdanov MB (2000) Oxidative stress in patients with Friedreich ataxia. *Neurology* **55:** 1719–1721

Scott RC, Schuldiner O & Neufeld TP (2004) Role and regulation of starvation-induced autophagy in the Drosophila fat body. *Dev Cell* **7:** 167–178

Sebastián D, Hernández-Alvarez MI, Segalés J, Sorianello E, Muñoz JP, Sala D, Waget A, Liesa M, Paz JC, Gopalacharyulu P, Orešič M, Pich S, Burcelin R, Palacín M & Zorzano A (2012) Mitofusin 2 (Mfn2) links mitochondrial and endoplasmic reticulum function with insulin signaling and is essential for normal glucose homeostasis. *Proc Natl Acad Sci U S A* **109:** 5523–5528

Shan Y, Schoenfeld RA, Hayashi G, Napoli E, Akiyama T, Iodi Carstens M, Carstens EE, Pook MA & Cortopassi GA (2013) Frataxin deficiency leads to defects in expression of antioxidants and Nrf2 expression in dorsal root ganglia of the Friedreich's ataxia YG8R mouse model. *Antioxid Redox Signal* **19:** 1481–1493

Shidara Y & Hollenbeck PJ (2010) Defects in mitochondrial axonal transport and membrane potential without increased reactive oxygen species production in a Drosophila model of Friedreich ataxia. *J Neurosci* **30:** 11369–11378

Simon D, Seznec H, Gansmuller A, Carelle N, Weber P, Metzger D, Rustin P, Koenig M & Puccio H (2004) Friedreich ataxia mouse models with progressive cerebellar and sensory ataxia reveal autophagic neurodegeneration in dorsal root ganglia. *J Neurosci* **24:** 1987–1995

Simonsen A, Cumming RC, Brech A, Isakson P, Schubert DR & Finley KD (2008) Promoting basal levels of autophagy in the nervous system enhances longevity and oxidant resistance in adult Drosophila. *Autophagy* **4:** 176–184

Sone M, Zeng X, Larese J & Ryoo HD (2013) A modified UPR stress sensing system reveals a novel tissue distribution of IRE1/XBP1 activity during normal Drosophila development. *Cell Stress Chaperones* **18:** 307–319

Soriano S, Calap-Quintana P, Llorens JV, Al-Ramahi I, Gutierrez L, Martinez-Sebastian MJ, Botas J & Molto MD (2016) Metal Homeostasis Regulators Suppress FRDA Phenotypes in a Drosophila Model of the Disease. *PLoS One* **11:** e0159209

Soriano S, Llorens JV, Blanco-Sobero L, Gutierrez L, Calap-Quintana P, Morales MP, Molto MD & Martinez-Sebastian MJ (2013) Deferiprone and idebenone rescue frataxin depletion phenotypes in a Drosophila model of Friedreich's ataxia. *Gene* **521:** 274–281

Stogsdill JA & Eroglu C (2017) The interplay between neurons and glia in synapse development and plasticity. *Curr Opin Neurobiol* **42:** 1–8

Stork T, Bernardos R & Freeman MR (2012) Analysis of glial cell development and function in Drosophila. *Cold Spring Harb Protoc* **2012:** 1–17

Stork T, Engelen D, Krudewig A, Silies M, Bainton RJ & Klambt C (2008) Organization and function of the blood-brain barrier in Drosophila. *J Neurosci* **28:** 587–597

Swarup V, Srivastava AK, Padma MV & Rajeswari MR (2013) Quantitative profiling and identification of differentially expressed plasma proteins in Friedreich's ataxia. *J Neurosci Res* **91:** 1483–1491

Swerdlow RH (2009) The neurodegenerative mitochondriopathies. *J Alzheimers Dis* **17:** 737–751

Szabadkai G, Bianchi K, Várnai P, Stefani D de, **Wieckowski MR, Cavagna D, Nagy AI, Balla T & Rizzuto R (**2006) Chaperone-mediated coupling of endoplasmic reticulum and mitochondrial Ca2+ channels. *J Cell Biol* **175:** 901–911

Tain LS, Mortiboys H, Tao RN, Ziviani E, Bandmann O & Whitworth AJ (2009) Rapamycin activation of 4E-BP prevents parkinsonian dopaminergic neuron loss. *Nat Neurosci* **12:** 1129–1135

Tamarit J, Obis E & Ros J (2016) Oxidative stress and altered lipid metabolism in Friedreich ataxia. *Free Radic Biol Med* **100:** 138–146

Tan G, Napoli E, Taroni F & Cortopassi G (2003) Decreased expression of genes involved in sulfur amino acid metabolism in frataxin-deficient cells. *Hum Mol Genet* **12:** 1699–1711

Tiefenbock SK, Baltzer C, Egli NA & Frei C (2010) The Drosophila PGC-1 homologue Spargel coordinates mitochondrial activity to insulin signalling. *EMBO J* **29:** 171–183

Tix S, Eule E, Fischbach KF & Benzer S (1997) Glia in the chiasms and medulla of the Drosophila melanogaster optic lobes. *Cell Tissue Res* **289:** 397–409

Tricoire H, Palandri A, Bourdais A, Camadro J-M & Monnier V (2014) Methylene blue rescues heart defects in a Drosophila model of Friedreich's ataxia. *Hum Mol Genet* **23:** 968–979

Tsai C-L & Barondeau DP (2010) Human frataxin is an allosteric switch that activates the Fe-S cluster biosynthetic complex. *Biochemistry* **49:** 9132–9139

van Cruchten S & van den Broeck W (2002) Morphological and biochemical aspects of apoptosis, oncosis and necrosis. *Anat Histol Embryol* **31:** 214–223

Vankan P (2013) Prevalence gradients of Friedreich's ataxia and R1b haplotype in Europe co-localize, suggesting a common Palaeolithic origin in the Franco-Cantabrian ice age refuge. *J Neurochem* **126 Suppl 1:** 11–20

Vazquez-Manrique RP, Gonzalez-Cabo P, Ros S, Aziz H, Baylis HA & Palau F (2006) Reduction of Caenorhabditis elegans frataxin increases sensitivity to oxidative stress, reduces lifespan, and causes lethality in a mitochondrial complex II mutant. *FASEB J* **20:** 172–174

Ventura N, Rea S, Henderson ST, Condo I, Johnson TE & Testi R (2005) Reduced expression of frataxin extends the lifespan of Caenorhabditis elegans. *Aging Cell* **4:** 109–112

Westermann B (2010a) Mitochondrial dynamics in model organisms: What yeasts, worms and flies have taught us about fusion and fission of mitochondria. *Semin Cell Dev Biol* **21:** 542–549

Westermann B (2010b) Mitochondrial fusion and fission in cell life and death. *Nat Rev Mol Cell Biol* **11:** 872–884

Westermann B (2012) Bioenergetic role of mitochondrial fusion and fission. *Biochim Biophys Acta* **1817:** 1833–1838

Whitnall M, Suryo Rahmanto Y, Sutak R, Xu X, Becker EM, Mikhael MR, Ponka P & Des Richardson R (2008) The MCK mouse heart model of Friedreich's ataxia: Alterations in iron-regulated proteins and cardiac hypertrophy are limited by iron chelation. *Proc Natl Acad Sci U S A* **105:** 9757–9762

Wong A, Yang J, Cavadini P, Gellera C, Lonnerdal B, Taroni F & Cortopassi G (1999) The Friedreich's ataxia mutation confers cellular sensitivity to oxidant stress which is rescued by chelators of iron and calcium and inhibitors of apoptosis. *Hum Mol Genet* **8:** 425–430

Wu J & Kaufman RJ (2006) From acute ER stress to physiological roles of the Unfolded Protein Response. *Cell Death Differ* **13:** 374–384

Xiang C, Wang Y, Zhang H & Han F (2017) The role of endoplasmic reticulum stress in neurodegenerative disease. *Apoptosis* **22:** 1–26

Yang Y, Ouyang Y, Yang L, Beal MF, McQuibban A, Vogel H & Lu B (2008) Pink1 regulates mitochondrial dynamics through interaction with the fission/fusion machinery. *Proc Natl Acad Sci U S A* **105:** 7070–7075

Yoon T & Cowan JA (2003) Iron-sulfur cluster biosynthesis. Characterization of frataxin as an iron donor for assembly of 2Fe-2S clusters in ISU-type proteins. *J Am Chem Soc* **125:** 6078–6084

Yoon T & Cowan JA (2004) Frataxin-mediated iron delivery to ferrochelatase in the final step of heme biosynthesis. *J Biol Chem* **279:** 25943–25946

Zampese E, Fasolato C, Kipanyula MJ, Bortolozzi M, Pozzan T & Pizzo P (2011) Presenilin 2 modulates endoplasmic reticulum (ER)-mitochondria interactions and Ca2+ cross-talk. *Proc Natl Acad Sci U S A* **108:** 2777–2782

Ziviani E, Tao RN & Whitworth AJ (2010) Drosophila parkin requires PINK1 for mitochondrial translocation and ubiquitinates mitofusin. *Proc Natl Acad Sci U S A* **107:** 5018–5023

6. Appendix

6.1. Supplemental figures

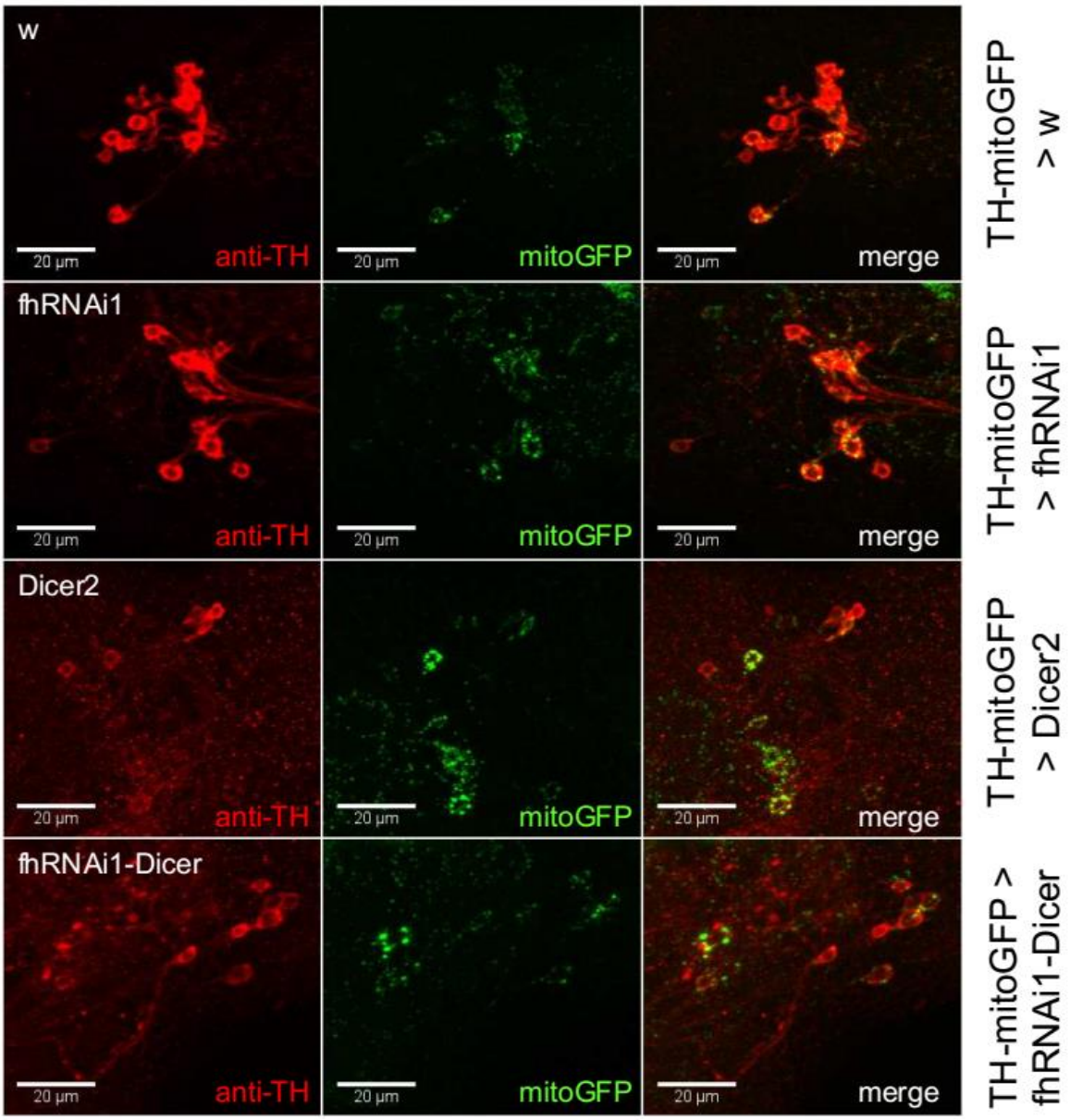

Figure 38: Dicer2 expression in dopaminergic neurons influences mitochondrial morphology

Representative images of dopaminergic neurons stained with anti-TH (marks nuclei; red channel) and labelled with mitoGFP (green channel). Dicer2 expression alone results in enlarged mitochondria, while frataxin knockdown has a minor effect (reprinted from Edenharter, 2013).

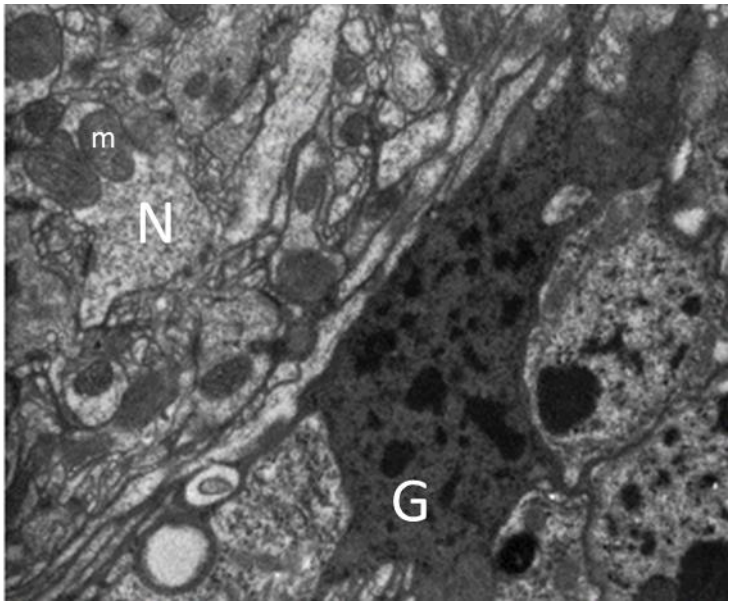

Figure 39: Glia show high electron-density

Transmission electron microscopy image of a *Drosophila* brain. Glial cells (G) show a high electron-density compared to neurons (N), which makes identifying subcellular structures like mitochondria (m) difficult (adapted from Navarro et al, 2010).

6.2. List of figures

6.3. List of tables

6.4. Abbreviations

ATF6: activating transcription factor 6

Atg1: autophagy related 1

Atg8:	autophagy related 8
BiP:	Binding immunoglobulin protein
BSA:	bovine serum albumin
cDNA:	complementary DNA
CNS:	central nervous system
DMSO:	Dimethyl sulfoxide
Drp1:	dynamin-related protein 1
eIF2α:	α subunit of eukaryotic translation initiation factor 2
ER:	endoplasmic reticulum
Fh:	frataxin homologue
Fis1:	Mitochondrial fission 1 protein
FRDA:	Friedreich's ataxia
FXN:	human frataxin
GCC:	giant glial cell
GFP:	green fluorescent protein
GSH:	reduced glutathione
GSSG:	oxidized glutathione
gDNA:	genomic DNA
IFM	indirect flight muscles
IM:	inner mitochondrial membrane
Ire1:	inositol-requiring enzyme 1
IRP2:	iron regulatory protein 2
ISC:	iron-sulphur cluster
kDa:	kilodalton
MAM:	mitochondria-associated ER membranes
Marf:	Mitochondrial assembly regulatory factor
Mff:	mitochondrial fission factor
Mfn:	Mitofusin
mitoGFP:	mitochondrial-localized GFP
mtDNA:	mitochondrial DNA
NGS:	normal goat serum
OBB:	Odyssey blocking buffer
OM:	outer mitochondrial membrane
Opa1:	optic atrophy 1

PAGE: Polyacrylamide gel electrophoresis
PBS: phosphate buffered saline
PBST: PBS with *Triton X-100*
PERK: pancreatic ER kinase
Pink1: PTEN-induced putative kinase 1
qPCR: quantitative polymerase chain reaction
RIPA: Radioimmunoprecipitation assay
RNAi: RNA interference
roGFP: redox sensitive GFP
ROS: reactive oxygen species
RT: room temperature
TBS: tris buffered saline
TBST: TBS with *Tween 20*
Tfam: mitochondrial transcription factor A
TMRE: tetramethylrhodamine ethyl ester
Tor: target of rapamycin
TUDCA: Tauroursodeoxycholic acid
UPR: unfolded protein response
vATPase: Vacuolar-type H^+-ATPase
Xbp1: X-box binding protein 1

Danksagung

Mein besonderer Dank gilt den folgenden Personen:

- Prof. Stephan Schneuwly für die Betreuung und die Möglichkeit, meine Doktorarbeit am Lehrstuhl für Entwicklungsbiologie durchzuführen.
- meinen Mentoren Prof. Michael Krahn und Prof. Benedikt Westermann für das Feedback zur Arbeit und die Bereitstellung des mtRosella-Klons.
- Dr. Juan A. Navarro for the excellent supervision. It was a great pleasure working with you during my thesis! Extra thanks for all the work you invested in me! I will miss our football conversations very much!
- den Doktoranden, die gleichzeitig mit mir am Lehrstuhl ihre Promotion durchgeführt haben: Sabina, Eva, Mathias und Matthias für die gegenseitige Unterstützung, sowohl praktisch als auch moralisch, falls die Experimente mal wieder nicht funktioniert haben.
- den weiteren Mitarbeitern: Gudrun (fleißige Arbeitsbiene der AG Navarro), Anneliese, Renate (Mikroinjektion), Uschi (Eponschnitte), Evi (die gute Seele des Lehrstuhls) und Susi für die Unterstützung bei den Experimenten und ein offenes Ohr bei Schwierigkeiten.
- meinen Studenten Carina, Florian, Jan, Katrin, Matthias, Tobias und Janik für die geleisteten Dienste ;-)
- allen anderen, die während meiner Promotion am Lehrstuhl tätig waren, für die angenehme Atmosphäre und den Spaß, den wir zusammen hatten.
- meinen Freunden Andreas, Thomas, Bille und Chris für die notwendige Ablenkung vom Arbeitsstress.
- meinem Bruder und seiner Familie für die zahlreichen Einladungen zum Essen.
- und last but not least meinen Eltern dafür, dass ihr immer für mich da wart und mich immer unterstützt habt!